

Studies on metal complexes of some tridentate acylhydrazones

Thesis submitted to
Cochin University of Science and Technology
in partial fulfillment of the requirements
for the award of the degree of
DOCTOR OF PHILOSOPHY

in
CHEMISTRY

By
NANCY MATHEW



Department of Applied Chemistry
Cochin University of Science and Technology
Kochi - 682 022

June 2011

Studies on metal complexes of some tridentate acylhydrazones

Ph. D. Thesis under the Faculty of Science

Author:

Nancy Mathew
Research Scholar, Department of Applied Chemistry
Cochin University of Science and Technology
Kochi, India 682 022
Email: nancymathew1@gmail.com

Research Advisor:

Dr. M. R. Prathapachandra Kurup
Professor
Department of Applied Chemistry
Cochin University of Science and Technology
Kochi, India 682 022
Email: mrp@cusat.ac.in

Department of Applied Chemistry
Cochin University of Science and Technology
Kochi, India 682 022

June 2011

Front cover: Crystal structure of [Fe(Hhmab)Cl₂(C₂H₅OH)]

*.....to my beloved
Amma & Appa*



DEPARTMENT OF APPLIED CHEMISTRY
COCHIN UNIVERSITY OF SCIENCE AND TECHNOLOGY
KOCHI - 682 022, INDIA



Dr. M.R. Prathapachandra Kurup
Professor

Phone Off. : 0484-2575804
Phone Res. : 0484-2576904
Telex : 885-5019 CUIIN
Fax : 0484-2577595
Email : mrp@cusat.ac.in
mrp_k@yahoo.com

16-06-2011

Certificate

*This is to certify that the thesis entitled “**Studies on metal complexes of some tridentate acylhydrazones**” submitted by Ms. Nancy Mathew, in partial fulfillment of the requirements for the degree of Doctor of Philosophy, to the Cochin University of Science and Technology, Kochi-22, is an authentic record of the original research work carried out by her under my guidance and supervision. The results embodied in this thesis, in full or in part, have not been submitted for the award of any other degree.*

M.R. Prathapachandra Kurup
(Supervising guide)

Declaration

I hereby declare that the work presented in this thesis entitled **“Studies on metal complexes of some tridentate acylhydrazones”** is entirely original and was carried out independently under the supervision of Professor M.R. Prathapachandra Kurup, Department of Applied Chemistry, Cochin University of Science and Technology and has not been included in any other thesis submitted previously for the award of any other degree.

Kochi-22

16-06-2011

Nancy Mathew

« Preface »

Coordination chemistry is a fascinating branch in inorganic chemistry, and its beauty lies in the fact that minute changes in a metal ion environment induce dramatic changes in the properties of the compounds. Studies on transition metal complexes have achieved a great interest due to their versatile applications. The convenient route for synthesis, the nature of ligands and stability of metal complexes has significant contributions in their applications in medicine, biology, catalysis and photonics.

The work embodied in the thesis was carried out by the author in the Department of Applied Chemistry during the period 2007-2011. The present work deals with the synthesis and characterization of metal complexes of some tridentate acylhydrazones. Hydrazones are promising ligands in coordination chemistry with interesting binding modes and applications. The acylhydrazones chosen for the current study are capable of forming complexes in different forms through tautomerism.

The work done is presented in seven chapters and Chapter 1 provides an introduction on acylhydrazones and their metal complexes with an extensive literature survey revealing their binding modes, applications and recent developments. Chapter 2 deals with the syntheses and characterization of four ONO donor acylhydrazones derived from substituted salicylaldehyde and acetophenone. Chapters 3-7 describe the syntheses and characterization of different metal complexes with the synthesized acylhydrazones. The present study reveals that the coordination modes of the ligands differ with different metal ions. We could isolate single crystals of some compounds and their XRD studies successfully explained their structures. A brief summary and conclusions of the work is also included in the last part of the thesis.

««« Acknowledgment »»»

This thesis would not have been possible without the assistance of a number of helping hands around me. So I take this opportunity with much pleasure to thank all the people who have helped me throughout my journey towards bringing this thesis into completion.

First, I want to express my deeply-felt thanks to my supervising guide Prof. M.R. Prathapachandra Kurup, who introduced me in to the magic world of research. His patience, enthusiasm, immense knowledge, positive attitude and encouragement act as motive forces behind this thesis.

I am grateful to Prof. K.K. Mohammed Yusuff for his encouragement and support as my doctoral committee member. I express my sincere gratitude to Prof. K. Sreekumar, Head, and Prof. K. Girish Kumar, former Head, Department of Applied Chemistry, CUSAT for the support and help during the period of this work. I am thankful for the support received from all the teaching and non-teaching staff of the Dept. of Applied Chemistry, CUSAT.

I deeply acknowledge the University Grants Commission and Kerala State Council for Science, Technology and Environment, for the financial support offered. I thank heads of the institutions of SAIK Kochi, IISc Bangalore, IIT Bombay and School of Chemistry, University of Hyderabad for services and help they had given during my research studies.

I would like to extend my gratitude to my seniors Dr. P.F. Raphael, Dr. Leji Lathief, Dr. Mini Kuriakose, Dr. Bessy Raj, Dr. Sreeshia Sasi, Dr. E. Manoj, Dr. Binu Varghese, Dr. U.L. Kala and Dr. Suja Krishnan for their help and encouragement. It is a pleasure to thank Dr. Seena E. B. for her valuable suggestions, inspiring words and support offered throughout my research period.

God showered his blessings on me in the form of friends. I am especially thankful to my dearest friend Laigi, to whom I am indebted for my research life in CUSAT. I am so fortunate to have a friend like Manju, who alone can make the world of friendship unique. I know no words of gratitude are enough for all the moments of help, care and support offered by you during my CUSAT days. I would like to say a special word of thanks to Sheeja for a nice friendship, timely help and suggestions from the beginning of my research. Really I cherish the friendly moments spent with Manju and Sheeja in Room No. 55 at Athulya hostel as well as in the Department. I sincerely appreciate the friendship and encouragement offered by Neema and I always enjoyed the fun filled moments shared with Neema and Digna during my research period. I wish to express special thanks to all my labmates Laly miss, Jessy miss, Annie miss, Jayakumar sir, Ashokan sir, Reenachechi, Renjusha, Roji, Easan sir, Jinsa, Bibitha, Nisha and Reshma for providing a friendly work atmosphere. I would like to say thanks to Dhanya, Sarika, Ananya, Shimi, Anju and all my friends in Department of Applied Chemistry to make my research days memorable.

I express my sincere thanks to all my teachers especially teachers of Newman College, for their inspiring words and blessings. I would like to say special thanks to Dr. Lissy Jose, HOD, Newman College for awakening my research interest. Starvin sir deserves a special mention; it was his excellent classes that boost up my interest in chemistry,

My family deserves special mention as I know; words are insufficient to express the depth of my love and gratitude to my parents and brother. The immense love, care and encouragement they showered on me throughout my life could only help to reach me here. I express my extreme gratitude to my in-laws for the love and support extended to me. I happily say thanks to my sisters-in-law for their well wishes and support.

With great pleasure I would like to give special thanks to my husband Eldhose for his love, patience and encouragement. Without his wholehearted support it would not have been possible me to complete this work. My special thanks to my little daughter Sarangi, who missed me, a lot during these days.

Above all, I bow before God Almighty for his countless blessings throughout my life.

Nancy

contents

Page No

Chapter 1

AN INTRODUCTION TO ACYLHYDRAZONES, THEIR BONDING MODES AND APPLICATIONS.....	1-18
1.1 Introduction	1
1.2 Acylhydrazones	2
1.3 Coordination modes of hydrazones	3
1.4 Applications of hydrazones	6
1.4.1 Biological and medicinal applications	7
1.4.2 Analytical applications	8
1.4.3 Hydrazones in nonlinear optics	8
1.4.4 Catalytic applications	9
1.4.5 Other applications	10
1.5 Scope and objectives of the work	10
1.6 Physical measurements	12
1.6.1 Elemental analyses	12
1.6.2 Conductivity measurements	12
1.6.3 Magnetic susceptibility measurements	12
1.6.4 Thermogravimetric analysis	13
1.6.5 Infrared spectroscopy	13
1.6.6 Electronic spectroscopy	13
1.6.7 NMR spectroscopy	13
1.6.8 EPR spectroscopy	14
1.6.9 Single crystal XRD	14
References	15

Chapter 2

SYNTHESES AND CHARACTERIZATION OF ACYLHYDRAZONES.....19-36

2.1	Introduction	19
2.2	Experimental	20
2.2.1	Materials	20
2.2.2	Syntheses of acylhydrazones	21
2.3	Results and discussion	22
2.3.1	Crystal structure of H ₂ hmbn·H ₂ O	22
2.3.2	NMR spectral studies	26
2.3.3	Infrared spectral studies	30
2.3.4	Electronic spectral studies	33
	References	34

Chapter 3

SYNTHESES, SPECTRAL AND STRUCTURAL STUDIES OF OXOVANADIUM(IV/V) COMPLEXES DERIVED FROM TRIDENTATE ACYLHYDRAZONES.....37-70

3.1	Introduction	37
3.2	Experimental	38
3.2.1	Materials	38
3.2.2	Syntheses of the acylhydrazones	39
3.2.3	Syntheses of vanadium complexes	39
3.3	Results and discussion	42
3.3.1	Crystal structure of the compound [VO(hman)(OCH ₃) ₂] (5)	43
3.3.2	EPR spectra	48
3.3.3	Infrared spectra	63
3.3.4	Electronic spectra	65
3.3.5	Thermal analyses	67
	References	68

Chapter 4

SYNTHESES AND CHARACTERIZATION OF Mn(II) AND Fe(III)	
COMPLEXES OF ONO DONOR ACYLHYDRAZONES.....71-97	
4.1	Introduction 71
4.2	Experimental 73
4.2.1	Materials 73
4.2.2	Syntheses of the acylhydrazones 73
4.2.3	Syntheses of manganese(II) complexes 73
4.2.4	Syntheses of iron(III) complexes 74
4.3	Results and discussion 75
4.3.1	Spectral characterization of Mn(II) complexes 76
4.3.1a	<i>EPR spectral studies</i> 76
4.3.1b	<i>Infrared spectra</i> 78
4.3.1c	<i>Electronic spectra</i> 79
4.3.2	Thermal analyses 81
4.3.3	Crystal structure of the compound [Fe(Hhmab)Cl ₂ (C ₂ H ₅ OH)] (19) 81
4.3.4	Spectral characterization of Fe(III) complexes 87
4.3.4a	<i>EPR spectral studies</i> 87
4.3.4b	<i>IR spectral studies</i> 90
4.3.4c	<i>Electronic spectral studies</i> 92
4.3.5	Thermal analyses 93
	References 94

Chapter 5

SYNTHESES AND CHARACTERIZATION OF Cu(II) COMPLEXES OF	
TRIDENTATE ACYLHYDRAZONES.....98-133	
5.1	Introduction 98
5.2	Experimental 99
5.2.1	Materials 99
5.2.2	Syntheses of the acylhydrazones 100
5.2.3	Syntheses of copper(II) complexes 100

5.3	Results and discussion	101
5.3.1	Crystal structure of the compound [Cu(hmab)phen] (25)	102
5.3.2	EPR spectra	108
5.3.3	Infrared spectra	122
5.3.4	Electronic spectra	126
5.3.5	Thermal analyses	130
	References	131

Chapter 6

SYNTHESES AND CHARACTERIZATION OF Zn(II) COMPLEXES DERIVED FROM ONO DONOR ACYLHYDRAZONES.....134-146

6.1	Introduction	134
6.2	Experimental	135
6.2.1	Materials	135
6.2.2	Syntheses of the acylhydrazones	135
6.2.3	Syntheses of Zn(II) complexes	136
6.3	Results and discussion	136
6.3.1	¹ H NMR spectral studies	137
6.3.2	Infrared spectra	139
6.3.3	Electronic spectra	143
6.3.4	Thermal analyses	144
	References	145

Chapter 7

SYNTHESES AND CHARACTERIZATION OF Mo(VI) COMPLEXES DERIVED FROM ONO DONOR ACYLHYDRAZONES.....147-161

7.1	Introduction	147
7.2	Experimental	148
7.2.1	Materials	148
7.2.2	Syntheses of the acylhydrazones	148
7.2.3	Syntheses of Mo(VI) complexes	148
7.3	Results and discussion	149

7.3.1	¹ H NMR spectral studies	150
7.3.2	Infrared spectral studies	153
7.3.3	Electronic spectral studies	157
7.3.4	Thermal studies	158
	References	160
	SUMMARY AND CONCLUSIONS.....	162-165

AN INTRODUCTION TO ACYLHYDRAZONES, THEIR BONDING MODES AND APPLICATIONS

- 1.1 Introduction
 - 1.2 Acylhydrazones
 - 1.3 Coordination modes of hydrazones
 - 1.4 Applications of hydrazones
 - 1.5 Scope and objectives of the work
 - 1.6 Physical measurements
 - References
-

1.1 Introduction

Over the past few decades inorganic chemistry has been greatly enriched by the continuing development in the area of coordination chemistry. The motive forces behind this evolution have come from the versatile applications of coordination compounds in different areas such as catalysis, bioinorganic, biomimetic and medicinal chemistry. The growing interest in coordination compounds is fueled by the search for new materials. Coordination chemistry will continue to strengthen its role as a central expertise and authority for material science. Nowadays coordination chemistry comprises a major portion of current inorganic research. It provides many new directions in research such as, in molecular magnetism, supramolecular chemistry, non-silicon-based devices, precursors for vapor phase deposition, and single molecule-based photonic devices and sensors [1].

Diverse coordination compounds arise from interesting ligand systems containing different donor sites. So the selection of ligands is most important in determining the properties of coordination compounds. A ligand system having electronegative atoms like nitrogen and oxygen increases the denticity and thus enhances the coordination possibilities. Among nitrogen-oxygen donor ligands, hydrazones possess a special place due to their widespread applications and interesting coordination capability with transition metal ions [2-4].

1.2 Acylhydrazones

Hydrazones are a class of azomethines having the group $-C=N-N-$, are interesting ligands in coordination chemistry. They are distinguished by other members of this family by the presence of two interlinking nitrogen atoms and obtained by the condensation reaction between a hydrazide which is a derivative of hydrazine with a carbonyl compound. Introduction of a $-C=O$ group in the hydrazide part increases the electron delocalization and denticity of the hydrazone and the resulting compound is known as an acylhydrazone. Fig. 1.1 represents the general formulae of a hydrazone and an acylhydrazone.

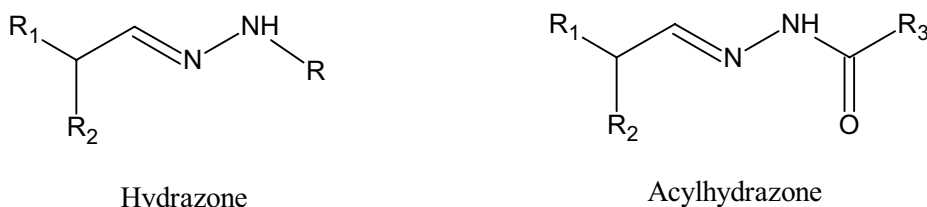


Fig. 1.1. General formulae of a substituted hydrazone and acylhydrazone.

In an acylhydrazone the basic coordination sites are carbonyl oxygen and the azomethine nitrogen. Denticity of the hydrazones can further improved by the introduction of a suitable substituent. Another interesting feature of hydrazones is

their tautomeric ability. They can exhibit *amido-iminol* tautomerism. In solid state *amido* form predominates while in solution state *iminol* form (Fig. 1.2).

This property offer the possibility for the formation of different types of complexes, *ie.* the hydrazones can coordinate to the metal either in neutral *amido* form or in deprotonated *iminolate* form. Effective conjugation over the hydrazone moiety is increased by the enolization of the ligand and thus improves the electron delocalization.

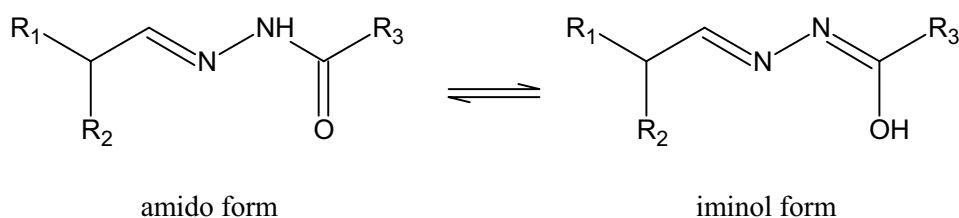
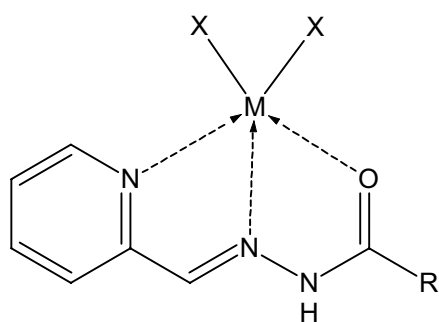


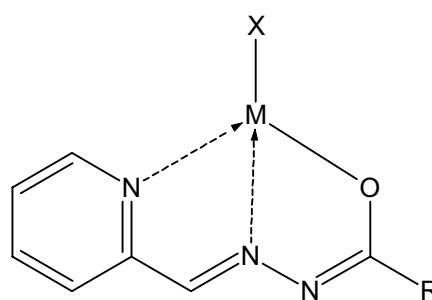
Fig. 1.2. Tautomerism of a substituted acylhydrazone.

1.3 Coordination modes of hydrazones

Hydrazones are versatile ligands and have been studied for a long time as potential multifunctional ligands with interesting coordination modes. The coordination mode adopted by a hydrazone depends on different factors like tautomerism, reaction conditions, stability of the complex formed, number and nature of the substituent on hydrazone skeleton. Coordination sites can be further improved by suitable substituents on hydrazide part as well as on carbonyl part. For example if we take a hydrazone having a pyridine group on the carbonyl part, it can coordinate to the central metal by adopting an *NNO* coordination mode, either through neutral *amido* form (Structure I) or through the deprotonated *iminolate* form (Structure II) [5-7].

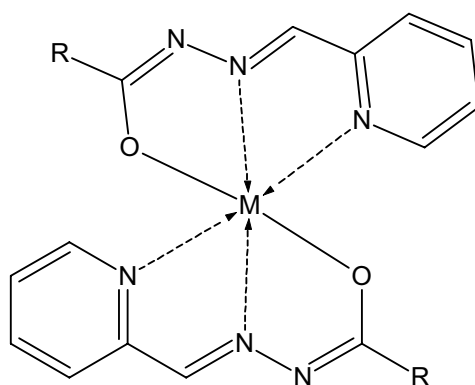


Structure I



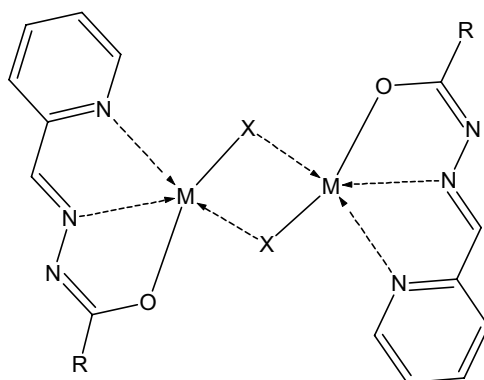
Structure II

Another possibility is the formation of a six coordinated metal complex with two deprotonated ligands (Structure III) [8-10].



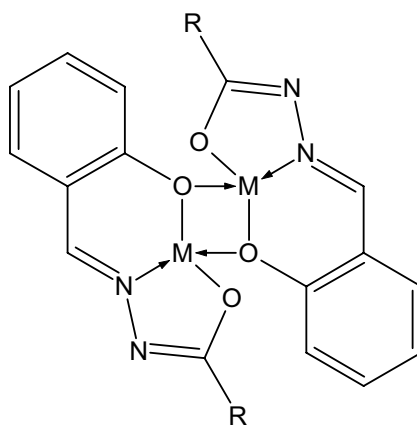
Structure III

Anions present in the metal salt or ions like azide and thiocyanate can act as a bridging ligand results the formation of a dimeric structure (Structure IV) [11,12].



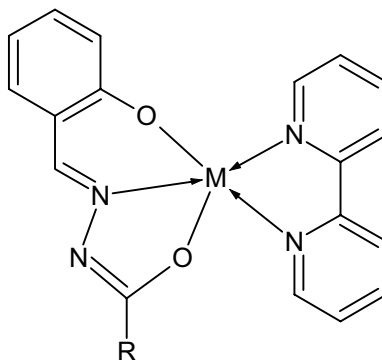
Structure IV

If the hydrazone possesses a phenolic group in the aldehyde/ketone part which is in suitable position for coordination leads to an *ONO* coordination mode, results in the formation of dimeric complexes with phenolate oxygen bridges (Structure V) [13].



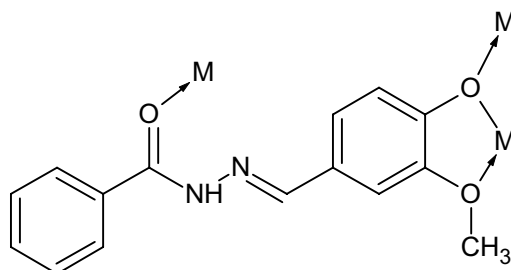
Structure V

In the case of complexes with *ONO* donor hydrazones we can incorporate heterocyclic bases to the central metal (Structure VI) [14].



Structure VI

If the hydrazone possesses an electron donating group like methoxy group in the carbonyl part it may also take part in coordination to the central metal (Structure VII) [15].



Structure VII

1.4 Applications of hydrazones

The interest in the design, syntheses and characterization of hydrazones and their metal complexes has come from their applications in various fields. Their ease of syntheses, easily tunable steric and electronic properties and good solubility in common solvents enhances research interest in this area. They have wide applications in biology, medicine, optics, catalysis and analytical chemistry.

1.4.1 Biological and medicinal applications

Metal complexes of hydrazones have been found to have biological and therapeutic activity and this is one practical reason for the continuing interest in these materials. Biological activity of hydrazones can be influenced by linking a hydrazide with pharmacologically active carbonyl compounds during condensation reactions. Many of the arylhydrazone complexes of transition metal ions are known to be effective models for elucidation of the mechanisms of enzyme inhibition [16-18]. Antitubercular activities shown by some hydrazones are comparable to that of the drugs available for the treatment of tuberculosis [19,20]. Many hydrazone derivatives have been found to possess antimicrobial [21,22] and anti-inflammatory activities [23]. Salicylaldehyde benzoylhydrazone was a potent inhibitor of DNA syntheses and cell growth in a variety of human and rodent cell lines. Further studies revealed that the copper(II) complexes of salicylaldehyde benzoylhydrazone exhibits appreciably greater inhibitory activity than the free ligand itself, suggests that the metal complexes are more biologically active than the free ligands [24-26]. Epilepsy is a common neurological disorder and a collective term given to a group of syndromes that involve spontaneous, irregular, abnormal electrical activity in the brain. The biological results revealed that some of the hydrazones have prominent anti-convulsant activity [27,28]. 3-Phenyl-5-sulfonamidoindole-2-carboxylic acid 3,4-methylenedioxy/4-methyl/4-nitrobenzylidene-hydrazide showed antidepressant activity [27].

Iron is an essential element in living kingdom and it involved in various biological processes, though in excess it is highly toxic. This condition is referred to as iron overload, leads to many diseases like β thalassemia. Nowadays chelation therapy is one of the most useful therapeutic methods for the treatment of iron overload. Some hydrazone analogues are found to be potential oral iron chelating drugs for the treatment of thalassemia and have also been suggested as possible metal chelating agents for treating neurodegenerative disorders such as

Alzheimer disease. 2-Pyridinecarbaldehyde isonicotinoylhydrazone (HPCIH) and di-2-pyridylketone isonicotinoylhydrazone (HPKIH) are two iron chelators with contrasting biological behavior. HPCIH is a well-tolerated iron chelator with limited antiproliferative activity that has potential applications in the treatment of iron overload diseases while HPKIH has significant antiproliferative activity against cancer cells [29-31].

1.4.2 Analytical applications

According to the review of Singh *et al.* hydrazones can act as selective metal extracting agents as well as in spectroscopic determination of certain transition metals [32]. Sasaki studied the spectroscopic determination of iron and vanadium using 2,6-diacetylpyridine bis(benzoylhydrazone) and 2,6-diacetylpyridine bis(2-hydroxybenzoylhydrazone) [33]. Nickel(II) ions present in edible oils, plant materials and in alloy samples can be analyzed using cinnamaldehyde-4-hydroxybenzoylhydrazones [34]. Gravimetric determinations of metal ions can be effectively done with the help of different hydrazones. Salicylaldehyde phenylhydrazone was found to be the best gravimetric reagent for the determination of copper. Metal complexes of pyridine-2-carbaldehyde-2-pyridylhydrazone have been used as acid-base indicators. Due to the high stability and readily observable color changes some of the *p*-nitrophenylhydrazones were proved to be better acid-base indicators. Some of the hydrazones can also be used as spot test reagents for the determination of transition metals [32]. Metal complexes of hydrazones have been used as luminescent probes as well as molecular sensors [35,36].

1.4.3 Hydrazones in nonlinear optics

Recently studies on the nonlinear optical properties of materials gathered considerable attention because they provide valuable information regarding the structural analysis of these materials and for their practical use in various

optoelectronic devices. Compounds which are noncentrosymmetric, planar and properly functionalized with strong electron donating and electron withdrawing groups at the terminal position of a π bridge could exhibit large molecular nonlinearity. Serbutoviez *et al.* established the relevance of push-pull hydrazones for quadratic nonlinear optics by the measurement of the molecular hyperpolarizabilities of some phenyl hydrazone derivatives [37]. Hydrazones possess the ability to exhibit *amido-iminol* tautomerism, so upon coordination to metal centre through the *iminol* form improves the conjugation and thus enhances the non linearity. Second-order nonlinear optical properties of copper and palladium complexes of *N*-salicylidene-*N'*-aroylhydrazines were studied by Cariati *et al.* and the results showed that the complexes have considerable nonlinearity [38]. Optical power limiting, a nonlinear optical effect, is interesting due to its application to the protection of eyes and sensitive optical devices from high power laser pulses. Naseema *et al.* investigated the third-order nonlinear optical properties of some hydrazones derived from *p*-tolylloxy acetohydrazide, and found that the compounds show optical limiting behaviour at a particular wavelength [39].

1.4.4 Catalytic applications

In metal complexes of hydrazones, the environment at the coordination center can be modified by attaching different substituents to the hydrazone moiety and a useful range of steric and electronic properties essential for the fine-tuning of structure and reactivity can thus be provided. Many of the hydrazone complexes show remarkable catalytic activity in various organic reactions. Monfared *et al.* studied the catalytic abilities of some oxo- and dioxovanadium(V) complexes of tridentate hydrazones towards the oxidation of various hydrocarbons and found that the complexes are effective catalysts [40]. Coordination complexes of VO^{3+} with tridentate naphthohydrazone derivatives are found to be a new class of VO^{3+} catalysts for the oxidation of olefins [41].

One of the *cis*-dioxomolybdenum(VI) complexes based on amino acid functionalized N-salicylidene hydrazide is an efficient catalyst for the peroxidic oxidation of sulfides [42]. According to Mahmudov *et al.*, a copper(II) dimer with 3-(2-hydroxy-4-nitrophenylhydrazo)pentane-2,4-dione exhibits a good catalytic activity in the peroxidative oxidation of cyclohexane by aqueous H₂O₂, under mild conditions, to afford cyclohexanol, cyclohexanone and cyclohexyl hydroperoxide [43]. Pouralimardan *et al.* demonstrated that some of the dissymmetric hydrazone manganese(II) complexes are highly selective catalysts for oxidation of cyclohexene by PhIO under mild conditions [44].

1.4.5 Other applications

Some of the arylhydrazones can act as herbicides, insecticides, nematocides, rodenticides and plant-growth regulators. Hydramethylnon is an amidinohydrazone insecticide has the trade name Amdro for control of the red imported fire ant and for use against cockroaches [45]. Hydrazones of 2-methylphthalazone are effective sterilants for houseflies [32]. Many hydrazones are found to be effective corrosion inhibitors of metals. Fouda *et al.* studied the effect of 2-hydroxyacetophenone-aryl hydrazone derivatives on the inhibition of copper and found that the corrosion is significantly decreased in presence of the investigated compounds [46].

1.5 Scope and objectives of the work

In view of their applications in various fields including biology, pharmacology, catalysis, analytical chemistry and optics, hydrazones, a member of the Schiff base family with triatomic >C=N–N< linkage, takes the forefront position in the development of coordination chemistry. Hydrazones derived from the condensation of *o*-hydroxy aromatic aldehydes and ketones with acyl-, aryl- and pyridoylhydrazines possess a third potent coordination site, makes them

tridentate ligands. This class of potential polyfunctional ligands containing amide and phenolic groups in their molecular skeleton has attracted research interest due to their vital role in the biological systems.

In order to pursue the interesting coordination properties of hydrazones, complexes with different types of ligand environments are essential. So in the present work we chose four different *ONO* donor hydrazones as principal ligands. Introduction of heterocyclic bases like 1,10-phenanthroline and 2,2'-bipyridine, the classical *N,N* donor ligands leads to the syntheses of mixed-ligand complexes, can cause different bonding, spectral properties and geometries in coordination compounds. All the above said facts stimulate our interest in the study of transition metal complexes with *ONO* donor hydrazones and as an extension of our work on hydrazones [8,10,14,47-51] with the following objectives.

- To synthesize some *ONO* donor acylhydrazones by the condensation of 2-hydroxy-4-methoxybenzaldehyde and 2-hydroxy-4-methoxyacetophenone with nicotinic acid hydrazide and benzhydrazide.
- To characterize the synthesized hydrazones by different physicochemical techniques.
- To synthesize different transition metal complexes using the synthesized hydrazones as principal ligands and some heterocyclic bases as coligands.
- To study the coordination modes of different hydrazones in metal complexes by using different physicochemical methods like partial elemental analysis, thermogravimetry and by different spectroscopic techniques.
- To establish the structure of the compounds by isolating single crystals of the compounds and collecting and refining single crystal X-ray diffraction data.

In the present work four different hydrazones were synthesized and characterized. The molecular structure of one of the hydrazones was established by single crystal X-ray diffraction studies. The metals selected for the preparation of the complexes are vanadium, manganese, iron, copper, zinc and molybdenum. The crystal structures of three of the complexes were studied through single crystal XRD.

1.6 Physical measurements

Details of physicochemical techniques employed for the present study is discussed below.

1.6.1 Elemental analyses

Microanalysis for carbon, hydrogen and nitrogen in the synthesized acylhydrazones and in their metal complexes were carried out on an Elementar model Vario EL III CHNS analyzer at the Sophisticated Analytical Instrument Facility (SAIF), Sophisticated Test and Instrumentation Centre (STIC), Kochi.

1.6.2 Conductivity measurements

Molar conductivities of the complexes in dimethylformamide (DMF) solutions (10^{-3} M) were measured at room temperature using a Systronic model 303 direct-reading conductivity bridge at the Department of Applied Chemistry, CUSAT, Kochi, India.

1.6.3 Magnetic susceptibility measurements

The magnetic susceptibility measurements of the powdered samples were done at room temperature using a Sherwood Scientific Magnetic Susceptibility Balance (M.S.B.) at the Department of Applied Chemistry, CUSAT, Kochi, India. The compound used as calibrant was $\text{HgCo}(\text{SCN})_4$.

1.6.4 Thermogravimetric analysis

TG-DTG analyses of the complexes were carried out in a Perkin Elmer Pyris Diamond TG / DTA analyzer at a heating rate of 10 °C per minute in an atmosphere of nitrogen, at the Department of Applied Chemistry, CUSAT, Kochi, India.

1.6.5 Infrared spectroscopy

Infrared spectra of the compounds were recorded on a JASCO FT IR-4100 Fourier Transform Infrared Spectrometer using KBr pellets in the range of 4000-400 cm^{-1} at the Department of Applied Chemistry, CUSAT, Kochi, India and also on a Thermo Nicolet AVATAR 370 DTGS model FT IR Spectrometer using KBr pellets in the range of 4000-400 cm^{-1} and ATR technique at Sophisticated Analytical Instrument Facility (SAIF), Sophisticated Test and Instrumentation Centre (STIC), Kochi.

1.6.6 Electronic spectroscopy

Electronic spectra of all the compounds were taken on a Spectro UV-vis Double Beam UVD-3500 spectrometer in the 200-900 nm range at the Department of Applied Chemistry, CUSAT, Kochi, India. The solvents used are dimethylformamide and acetonitrile.

1.6.7 NMR spectroscopy

^1H NMR spectra of the hydrazones and some complexes were recorded using Bruker AMX 400 FT-NMR Spectrometer with DMSO-d_6 as the solvent and TMS as internal standard at the Sophisticated Analytical Instrument Facility (SAIF), Indian Institute of Science, Bangalore, India and also on a Bruker Avance DPX-300 MHz NMR Spectrometer at NIIST Trivandrum.

1.6.8 EPR spectroscopy

The EPR spectra of the complexes in the solid state at 298 K, in DMF at 298 K and at 77 K were recorded on a Varian E-112 spectrometer using TCNE as the standard, with 100 kHz modulation frequency, modulation amplitude 2 G and 9.1 GHz microwave frequency at the SAIF, IIT Bombay, India.

1.6.9 Single crystal XRD

Single crystal X-ray diffraction data of one acylhydrazone 2-hydroxy-4-methoxybenzaldehyde nicotinoylhydrazone monohydrate (**H₂hmbn·H₂O**), and two complexes were collected on a CrysAlis CCD, Oxford Diffraction Ltd. diffractometer, equipped with a graphite crystal, incident-beam monochromator, and a fine focus sealed tube, Mo K α ($\lambda = 0.71073 \text{ \AA}$) X-ray source at the National Single Crystal X-ray diffraction Facility, IIT, Bombay, India. The trial structure was solved using SHELXS-97 and refinement was carried out by full-matrix least squares on F^2 using SHELXL-97 [52], and all the hydrogen atoms were fixed in calculated positions.

X-ray crystal structure determination of another complex was performed with a Bruker SMART APEX CCD X-ray diffractometer at the University of Hyderabad, using graphite monochromated Mo K α radiation ($\lambda=0.71073 \text{ \AA}$, φ and ω scans). The data was reduced using SAINTPLUS [53]. The structure was solved using SHELXS-97 and full matrix least squares refinement against F^2 was carried out using SHELXL-97 in anisotropic approximation for non-hydrogen atoms [54]. All hydrogen atoms were assigned on the basis of geometrical considerations and were allowed to ride upon the respective carbon atoms.

References

1. A.B.P. Lever, *Comprehensive Coordination Chemistry II* (1987).
2. F.H. Case, A.A. Schilt, N. Simonzadeh, *Anal. Chem.* 56 (1984) 2860-2862.
3. M.R. Maurya, S. Agarwal, M. Abid, A. Azam, C. Bader, M. Ebel, D. Rehder, *Dalton Trans.* (2006) 937–947.
4. R.C. Maurya, S. Rajput, *J. Mol. Struct.* 833 (2007) 133-144.
5. A.A.R. Despaigne, J.G. Da Silva, A.C.M. do Carmo, O.E. Piro, E.E. Castellano, H. Beraldo, *Inorg. Chim. Acta* 362 (2009) 2117–2122.
6. A.A.R. Despaigne, J.G. Da Silva, A.C.M. do Carmo, F. Sieves, O.E. Piro, E.E. Castellano, H. Beraldo, *Polyhedron* 28 (2009) 3797–3803.
7. P. Barbazán, R. Carballo, E.M. Vázquez-López, *Cryst. Eng. Comm.* 9 (2007) 668–675.
8. M. Kuriakose, M.R.P. Kurup, E. Suresh, *Struct. Chem.* 18 (2007) 579–584.
9. A. Ray, S. Banerjee, S. Sen, R.J. Butcher, G.M. Rosair, M.T. Garland, S. Mitra, *Struct. Chem.* 19 (2008) 209-217.
10. N.A. Mangalam, S.R. Sheeja, M.R.P. Kurup, *Polyhedron* 29 (2010) 3318-3323.
11. S. Sen, S. Mitra, D.L. Hughes, G. Rosair, C. Desplanches, *Polyhedron* 26 (2007) 1740–1744.
12. A. Datta, K. Das, Y.-M. Jhou, J.-H. Huang, H. M. Lee, *Acta Cryst.* E66 (2010) m1271.
13. L.L. Koh, O.L. Kon, K.W. Loh, Y.C. Long, J.D. Ranford, A.L.C. Tan, Y.Y. Tjan, *J. Inorg. Biochem.* 72 (1998) 155-162.
14. P.B. Sreeja, M.R.P. Kurup, A. Kishore, C. Jasmin, *Polyhedron* 23 (2004) 575–581.

15. S. Li, S. Gao, S. Liu, Y. Guo, *Cryst. Growth Des.* 10 (2010) 495-503.
16. J.C. Craig, D. Willis, S.D. Rubbo, J. Edger, *Nature* 176 (1955) 34-35.
17. S. Siemann, D.P. Evanoff, L. Marrone, A.J. Clarke, T. Viswanatha, G.I. Dmitrienko, *Antimicro. Agents Chemother.* 46 (2002) 2450-2457.
18. G. Tamasi, L. Chiasserini, L. Savini, A. Sega, R. Cini, *J. Inorg. Biochem.* 99 (2005) 1347-1359.
19. P.P.T. Sah, S.A. Peoples, *J. Pharm. Sci.* 42 (1953) 612-613.
20. J. Patole, U. Sandbhor, S. Padhye, D.N. Deobagkar, C.E. Anson, A. Powell, *Bioorg. Med. Chem. Lett.* 13 (2003) 51-55.
21. A.A. El-Sherif, *Inorg. Chim. Acta* 362 (2009) 4991-5000.
22. N. Filipović, H. Borrmann, T. Todorović, M. Borna, V. Spasojević, D. Sladić, I. Novaković, K. Andjelković, *Inorg. Chim. Acta* 362 (2009) 1996-2000.
23. A.R. Todeschini, A.L. Miranda, C.M. Silva, S.C. Parrini, E.J. Barreiro, *Eur. J. Med. Chem.* 33 (1998) 189-199.
24. D.K. Johnson, T.B. Murphy, N.J. Rose, W.H. Goodwin, L. Pickart, *Inorg. Chim. Acta* 67 (1982) 159-165.
25. L. Pickart, W.H. Goodwin, W. Burgua, T.B. Murphy, D.K. Johnson, *Biochem. Pharmacol.* 32 (1983) 3868-3871.
26. E.W. Ainscough, A.M. Brodie, A.J. Dobbs, J.D. Ranford, J.M. Waters, *Inorg. Chim. Acta* 267 (1998) 27-38.
27. S. Rollas, Ş. Güniz Küçükgülzel, *Molecules* 12 (2007) 1910-1939.
28. S.K. Sridhar, S.N. Pandeya, J.P. Stables, A. Ramesh, *Eur. J. Pharm. Sci.* 16 (2002) 129-132.

29. P.V. Bernhardt, G.J. Wilson, P.C. Sharpe, D.S. Kalinowski, D. R. Richardson, *J. Biol. Inorg. Chem.* 13 (2008) 107–119.
30. P.V. Bernhardt, *Dalton Trans.* (2007) 3214–3220.
31. E. Becker, D.R. Richardson, *J. Lab. Clin. Med.* 134 (1999) 510–521.
32. R.B. Singh, P. Jain, R.P. Singh, *Talanta* 29 (1982) 77–84.
33. Y. Sasaki, *Bull. Inst. Chem. Res.* 64 (1984) 140–149.
34. D.G. Krishna, N. Devanna, K.B. Chandrasekhar, *J. P. B. M. S.* 1 (2010) 1–5.
35. M.R. Ganjali, M. Rezapour, S. Rasoolipour, P. Norouzi, M. Adib, *J. Braz. Chem. Soc.* 18 (2007) 352–358.
36. C. Basu, S. Chowdhury, R. Banerjee, H.S. Evans, S. Mukherjee, *Polyhedron* 26 (2007) 3617–3624.
37. C. Serbutoviez, C. Bosshard, G. Knöpfle, P. Wyss, P. Prêtre, P. Günter, K. Schenk, E. Solari, G. Chapu, *Chem. Mater.* 7 (1995) 1198–1206.
38. F. Cariati, U. Caruso, R. Centore, W. Marcolli, A. De Maria, B. Panunzi, A. Roviello, A. Tuzi, *Inorg. Chem.* 41 (2002) 6597–6603.
39. K. Naseema, K.V. Sujith, K.B. Manjunatha, B. Kalluraya, G. Umesh, V. Rao, *Optic. Laser Tech.* 42 (2010) 741–748.
40. H.H. Monfared, S. Kheirabadi, N.A. Lalami, P. Mayer, *Polyhedron* 30 (2011) 1375–1384.
41. H.H. Monfared, R. Bikas, P. Mayer, *Inorg. Chim. Acta* 363 (2010) 2574–2583.
42. M. Mancka, W. Plass, *Inorg. Chem. Commun.* 10 (2007) 677–680.
43. K.T. Mahmudov, M.N. Kopylovich, M.F.C. Guedes da Silva, P.J. Figiel, Y.Yu. Karabach, A.J.L. Pombeiro, *J. Mol. Cat. A Chem.* 318 (2010) 44–50.

44. O. Pouralimardan, A.C. Chamayou, C. Janiak, H.H. Monfared, *Inorg. Chim. Acta* 360 (2007) 1599–1608.
45. J. G. Hollingshaus, *Pest. Biochem. Physiol.* 27 (1987) 61-70.
46. A.S. Fouda, M.M. Gouda, S.I. Abd El-Rahman, *Bull. Korean Chem. Soc.* 21 (2000) 1085-1089.
47. P.B. Sreeja, M.R.P. Kurup, *Spectrochim. Acta A* 61 (2005) 331-336.
48. B.N.B. Raj, M.R.P. Kurup, E. Suresh, *Spectrochim. Acta A* 71 (2008) 1253-1260.
49. N.A. Mangalam, S. Sivakumar, S.R. Sheeja, M.R.P. Kurup, E.R.T. Tiekink, *Inorg. Chim. Acta* 362 (2009) 4191- 4197.
50. S.R. Sheeja, N.A. Mangalam, M.R.P. Kurup, Y.S. Mary, K. Raju, H.T. Varghese, C.Y. Panicker, *J. Mol. Struct.* 973 (2010) 36-46.
51. M. Kuriakose, M. R. P. Kurup, E. Suresh, *Spectrochim. Acta A* 66 (2007) 353-358).
52. G.M. Sheldrick, *Acta Cryst. A* 64 (2008) 112-122.
53. *SAINTPLUS*, Bruker AXS Inc., Madison, USA (2003).
54. G.M. Sheldrick, *Acta Cryst. A* 64 (2008) 112-122.

**********

2.1	Introduction
2.2	Experimental
2.3	Results and discussion
	References

2.1 Introduction

Schiff bases, the compounds containing $-C=N-$ group have gained special attention owing to their facile synthesis and wide variety of applications. A large number of Schiff bases are often used as ligands in coordination chemistry because of their excellent metal binding capability [1-5]. Hydrazones, a subdivision of azomethine family, in which, the nitrogen in $-C=N-$ group is attached to another nitrogen atom instead of carbon in simple Schiff bases, acts as very promising ligands in coordination chemistry. Introduction of heteroatom like oxygen increases the denticity of hydrazones in metal complexes. Chemistry of hydrazones containing N and O donors and their metal complexes are particularly interesting because of their biological activity and their ability to act as potential inhibitors for many enzymes [6-10]. These ligands can coordinate with metal ions to produce stable metal complexes owing to their facile *amido-iminol* tautomerism. Nowadays the remarkable biological activity of acid hydrazides ($R-CO-NH-NH_2$) and their corresponding acyl hydrazones ($R-CO-NH-N=CH-R'$) and the dependence of their mode of chelation with transition metal ions present in living system have been of significant interest.

The presence of heterocyclic rings in the hydrazones plays a major role in deciding the extent of their pharmacological properties [11,12]. Many of the hydrazones show analytical applications such as metal extracting agents, sensors etc. [13,14]. Nonlinear optical properties shown by some hydrazones and their metal complexes offer their use in optoelectronic devices [15,16].

Increasing interest in the study of acylhydrazone complexes are based on their structural versatility offered by the hydrazone part, due to their various coordination modes. There are a large number of reports regarding the studies on isonicotinoyl hydrazones due to their iron chelating efficiency for the treatment of iron overload diseases [17-20]. The above said facts prompted us to synthesize and characterize some metal complexes using hydrazones as the ligand system. Four hydrazones were synthesized using nicotinic acid hydrazide, benzhydrazide, 2-hydroxy-4-methoxybenzaldehyde and 2-hydroxy-4-methoxyacetophenone as starting materials and they are characterized by various physicochemical techniques. The hydrazones chosen as ligands for the preparation of metal complexes are of ONO donor type and they are

1. 2-hydroxy-4-methoxybenzaldehyde nicotinoylhydrazone monohydrate (**H₂hmbn·H₂O**)
2. 2-hydroxy-4-methoxyacetophenone nicotinoylhydrazone (**H₂hman**)
3. 2-hydroxy-4-methoxybenzaldehyde benzoylhydrazone (**H₂hmhb**)
4. 2-hydroxy-4-methoxyacetophenone benzoylhydrazone (**H₂hmab**).

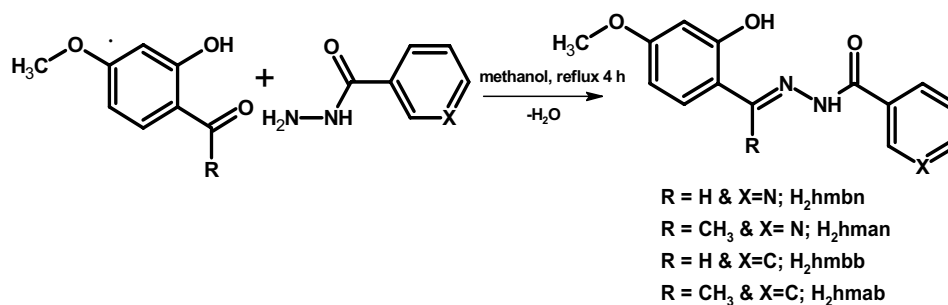
2.2 Experimental

2.2.1 Materials

2-Hydroxy-4-methoxyacetophenone (Aldrich), 2-hydroxy-4-methoxybenzaldehyde (Aldrich), nicotinic acid hydrazide (Aldrich) and benzhydrazide (Aldrich) were used without further purification. Solvent used was methanol.

2.2.2 Syntheses of acylhydrazones

The scheme for the syntheses of acylhydrazones is shown in scheme 1.



Scheme 1. Syntheses of acylhydrazones.

H₂hmbn·H₂O: Nicotinic acid hydrazide (0.137 g, 1 mmol) dissolved in methanol was refluxed with 2-hydroxy-4-methoxybenzaldehyde (0.152 g, 1 mmol) in methanol in presence of a few drops of glacial acetic acid for 4 hours. The compound was separated as pale yellow colored crystalline solid. Single crystals suitable for X-ray diffraction were obtained by recrystallization from ethanol. Yield 75%. Elemental Anal. Found (Calcd.) (%) C, 57.79 (58.13); H, 5.54 (5.23); N, 14.49 (14.53).

H₂hman: Nicotinic acid hydrazide (0.137 g, 1 mmol) dissolved in methanol was refluxed with 2-hydroxy-4-methoxyacetophenone (0.166 g, 1 mmol) in methanol in presence of a few drops of glacial acetic acid for 4 hours. On cooling colorless needle shaped compound was separated. Yield 70%. Elemental Anal. Found (Calcd.) (%): C, 62.94 (63.15); H, 5.39 (5.30); N, 14.46 (14.73).

H₂hmhb: Benzhydrazide (0.136 g, 1 mmol) dissolved in methanol was refluxed with 2-hydroxy-4-methoxybenzaldehyde (0.152 g, 1 mmol) in methanol in presence of a few drops of glacial acetic acid for 4 hours. The compound was

separated as pale yellow colored solid. Yield 74%. Elemental Anal. Found (Calcd.) (%) C, 66.08 (66.66); H, 5.47 (5.22); N, 10.26 (10.36).

H₂hmab: Benzhydrazide (0.136 g, 1 mmol) dissolved in methanol was refluxed with 2-hydroxy- 4-methoxyacetophenone (0.166 g, 1 mmol) in methanol in presence of a few drops of glacial acetic acid for 4 hours. On cooling colorless needle shaped compound was separated. Yield 68%. Elemental Anal. Found (Calcd.) (%): C, 67.25 (67.59); H, 5.61 (5.67); N, 9.68 (9.85).

2.3 Results and discussion

All the four acylhydrazones were synthesized in a very facile and essentially identical way. All of them act as tridentate ligands during the synthesis of their metal complexes.

2.3.1 Crystal structure of H₂hmbn·H₂O

Crystals suitable for single crystal diffraction studies were grown from a solution of the compound in ethanol. Compound H₂hmbn·H₂O crystallized into a triclinic space group *P* $\bar{1}$. Unit cell contains two molecules. The molecular structure of H₂hmbn·H₂O is shown in Fig. 2.1 and selected geometric parameters are listed in Table 2.1. The molecule is non-planar with a dihedral angle of 1.78(8)^o between the aromatic rings. The compound exists in an *anti* configuration with respect to the C9–N2 and C8–N1 bonds. This is confirmed by the torsion angles of 178.11(15)^o and -178.34(15)^o respectively for N(1)–N(2)–C(9)–C(10) and N(2)–N(1)–C(8)–C(5) moieties. The bond angles and bond lengths are summarized in Table 2.2. The N1–N2 and C9–O3 bond distances are in agreement with those in the related compounds p-methoxybenzaldehyde benzoylhydrazone monohydrate and isonicotinoylhydrazone monohydrate, indicate that these bonds correspond to single and double bonds [21,22]. The C1–O1 and

C2–O1 bond lengths in the hydroxyphenyl moiety are consistent with those [O(1)–C(1), 1.430(3) and O(1)–C(2), 1.360(2)] found in the related compounds [23-25].

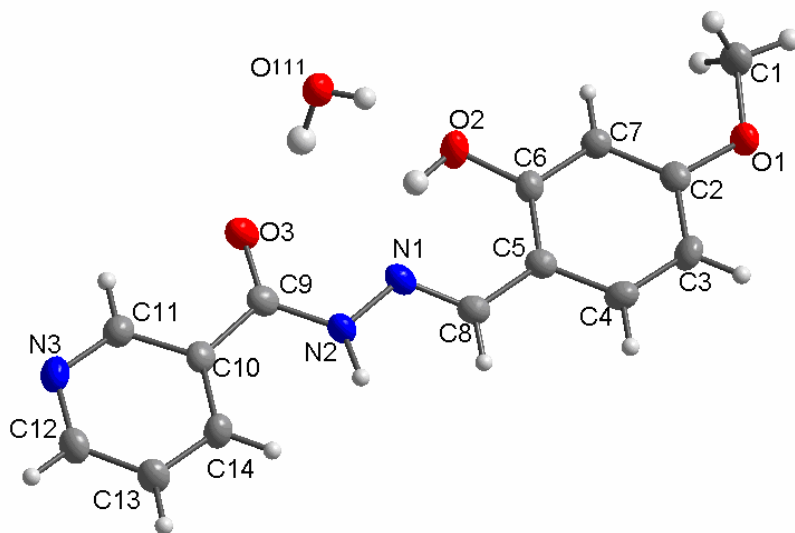


Fig. 2.1. Structure and labeling diagram for $H_2hmbn \cdot H_2O$.

In the crystal lattice, the molecules of the compound are arranged in two individual parallel layers with water and hydrazone group involved in O–H \cdots O and N–H \cdots O hydrogen bonds forming a one dimensional network along [010] axis (Fig. 2.2). The torsion angles C6–C5–C8–N1 of $-5.02(0.30)^\circ$ and C14–C10–C9–N2 of $4.82(0.28)^\circ$ indicate that the methoxyphenyl and phenyl substituents are in synperiplanar with respect to the central hydrazone plane. The methoxyphenyl ring makes a dihedral angle of $2.27(6)^\circ$ with the hydrazone bridge and the phenyl ring is twisted by an angle of $2.76(7)^\circ$ with respect to the plane of the central hydrazone linkage. The water molecules present in the lattice are involved in a three-center hydrogen bond. The novelty about this crystal lies in the packing; three molecules are involved in intermolecular hydrogen bonding interactions with one water molecule. H(111) from water is connected to O3 of

one molecule, H(112) of the same water is connected to N3 of second molecule and oxygen atom O(111) from water connected to N2–H(2N) of third molecule through intermolecular hydrogen bonding interactions. Fig. 2.3 displays the packing diagram with intra- and intermolecular hydrogen bonding.

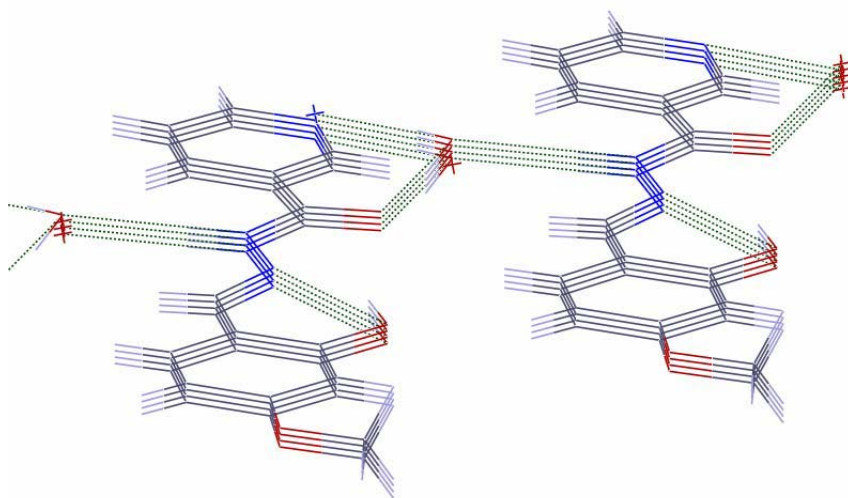


Fig. 2.2. One dimensional arrangement of $H_2hmbn \cdot H_2O$ along b axis.

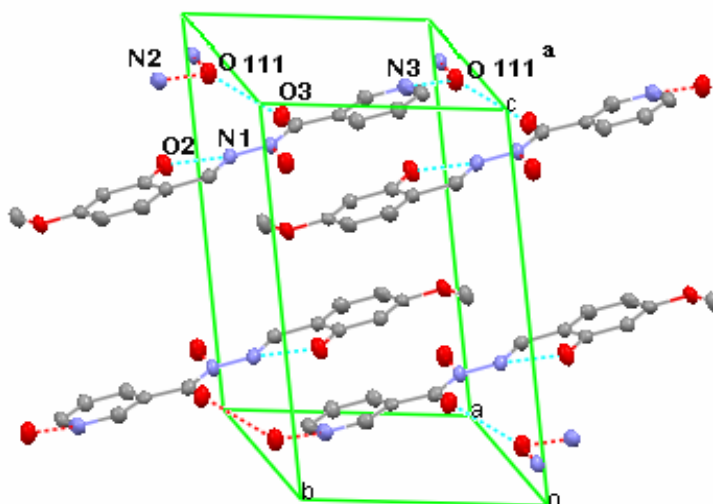


Fig. 2.3. Packing diagram of $H_2hmbn \cdot H_2O$ with intra- and intermolecular hydrogen bonding interactions viewed along a axis.

Table 2.1 Crystal data and structure refinement for H₂hmbn·H₂O

Empirical formula	C ₁₄ H ₁₅ N ₃ O ₄
Formula weight	289.29
Temperature	150(2) K
Wavelength	0.71073 Å
Crystal system, space group	Triclinic, <i>P</i> 1
Unit cell	a = 6.452(2) Å b = 7.884(3) Å c = 14.128(4) Å α = 80.11(3)° β = 77.24(3)° γ = 75.90(3)°
Volume	674.5(4) Å ³
Z, Calculated density	2, 1.424 Mg/ m ³
Absorption coefficient	0.107 mm ⁻¹
F(000)	304
Crystal size	0.33 x 0.26 x 0.21 mm ³
Theta range for data collection	2.90 to 25.00°.
Limiting indices	-7 ≤ h ≤ 7 -9 ≤ k ≤ 8 -16 ≤ l ≤ 16
Reflections collected	7088
Independent reflections	2370 [R(int) = 0.0221]
Absorption correction	Semi-empirical from equivalents
Max. and min. transmission	0.9780 and 0.9657
Refinement method	Full-matrix least-squares on F ²
Data / restraints / parameters	2370 / 0 / 207
Goodness-of-fit on F ²	1.064
Final R indices [I > 2σ(I)]	R ₁ = 0.0462, wR ₂ = 0.1294
R indices (all data)	R ₁ = 0.0651, wR ₂ = 0.1484
Largest diff. peak and hole	0.529 and -0.265 e. Å ⁻³

$$R_1 = \frac{\sum ||F_o| - |F_c||}{\sum |F_o|}$$

$$wR_2 = [\sum w(F_o^2 - F_c^2)^2 / \sum w(F_o^2)^2]^{1/2}$$

Table 2.2 Bond lengths [Å] and angles [°] for H₂hmbn·H₂O

Bond lengths		Bond angles	
O(1)–C(2)	1.360(2)	C(8)–N(1)–N(2)	116.23(16)
O(1)–C(1)	1.430(2)	C(9)–N(2)–N(1)	118.30(16)
O(2)–C(6)	1.353(2)	C(6)–C(5)–C(8)	122.80(17)
O(3)–C(9)	1.227(2)	N(1)–C(8)–C(5)	121.52(18)
N(1)–C(8)	1.283(2)	O(3)–C(9)–C(10)	120.84(17)
N(1)–N(2)	1.386(2)	N(2)–C(9)–C(10)	116.75(16)
N(2)–C(9)	1.352(2)	O(3)–C(9)–N(2)	122.41(17)
C(5)–C(8)	1.446(3)		
C(9)–C(10)	1.498(3)		

2.3.2 NMR spectral studies

Proton Nuclear Magnetic Resonance (¹H NMR) Spectroscopy is a powerful tool used for the determination of the structure of compounds. The ¹H NMR spectrum of an organic compound provides useful information about the number of different types of hydrogens present in the molecule and their electronic environment. Here the ¹H NMR spectra of all the four hydrazones were taken in DMSO.

H₂hmbn·H₂O: The ¹H NMR spectrum of the compound is shown in Fig. 2.4. The two sharp singlets in the very downfield region of the spectrum *ie.* at 12.15 ppm and 11.49 ppm each having a peak area corresponds to one are assigned to iminol OH and phenolic OH protons respectively. The high δ values of these are due to their attachment with highly electronegative elements. Upon deuterium exchange, the intensity of these peaks were considerably reduced confirmed the assignments. Methoxy protons give a sharp singlet at 3.78 ppm with an area integral of three. The azomethine singlet is observed at 9.08 ppm and aromatic protons give peaks in the region of 6.5-9.5 ppm.

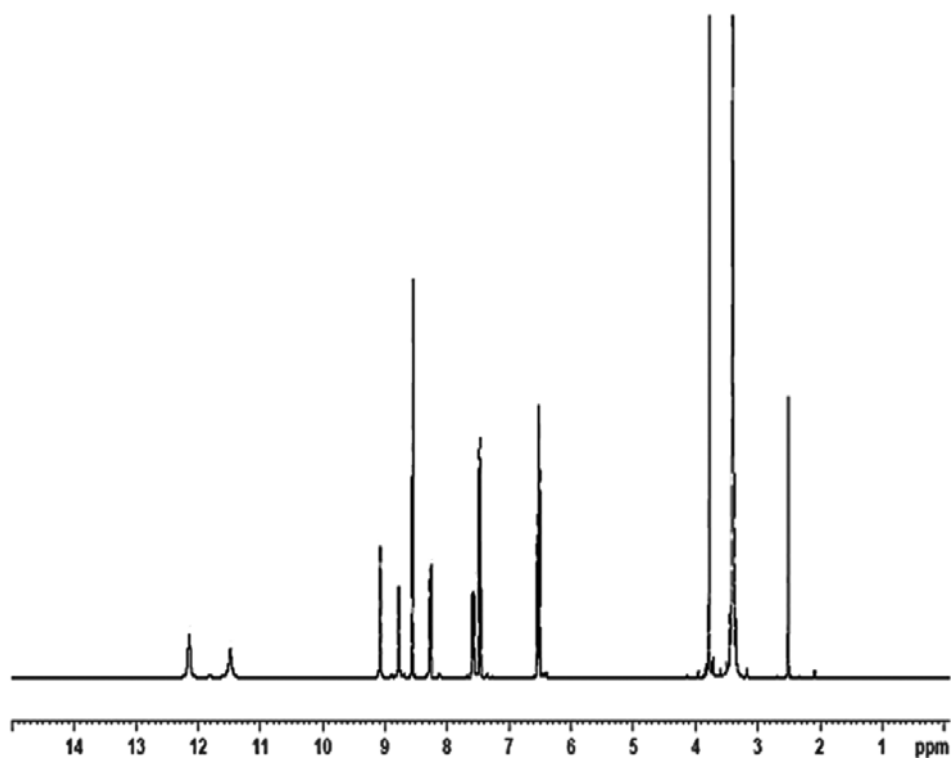


Fig. 2.4. ^1H NMR spectrum of $\text{H}_2\text{hmbn}\cdot\text{H}_2\text{O}$.

H₂hman: In the ^1H NMR spectrum of the compound, OH and iminol protons gave sharp singlets at 11.43 ppm and 13.56 ppm respectively with a peak area corresponds to one each. These assignments are confirmed by D_2O exchange studies. During D_2O exchange the intensity of these peaks are considerably reduced. Here the methoxy protons gave a singlet at 3.78 ppm and the methyl protons show a singlet at 2.45 ppm. Here also the aromatic protons show multiplets in the region of 6-9.5 ppm. Fig. 2.5 shows the ^1H NMR spectrum of the compound.

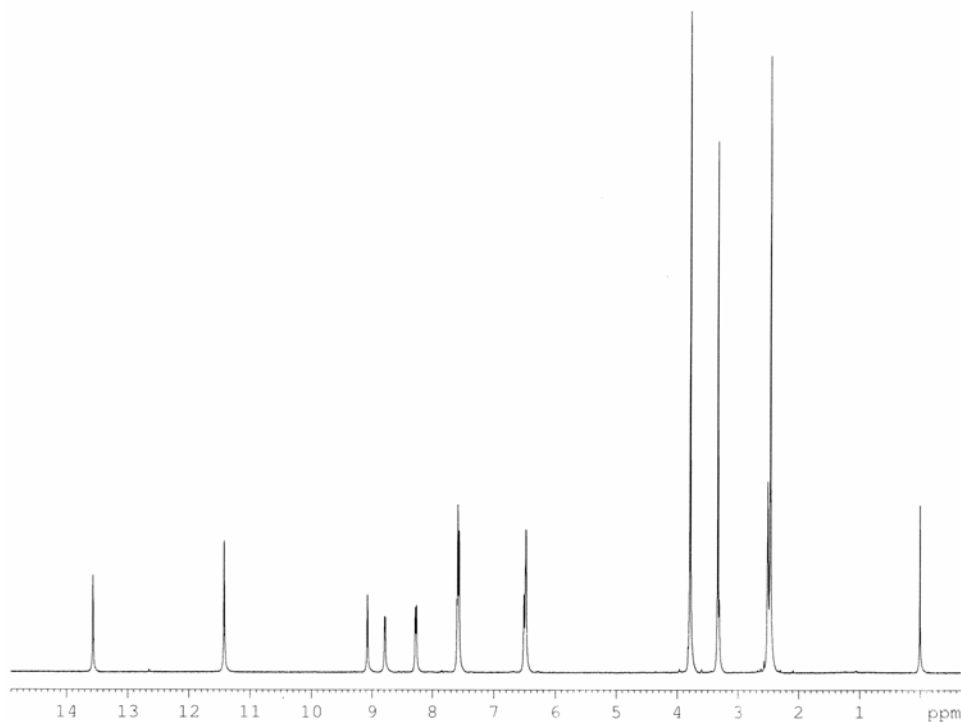


Fig. 2.5. ¹H NMR spectrum of H₂hman.

H₂hmbb: Here a singlet peak observed at 11.19 ppm is assigned to phenolic proton and another singlet observed at 13.63 ppm is assigned to proton attached to the iminol oxygen. Both of them have peak area corresponds to one. These assignments are confirmed by deuterium exchange studies. The methoxy protons gave a singlet peak at 3.81 ppm and azomethine proton singlet at 8.01 ppm. Aromatic proton multiplets were observed in between 6-9.5 ppm. Fig. 2.6 shows the ¹H NMR spectrum of H₂hmbb.

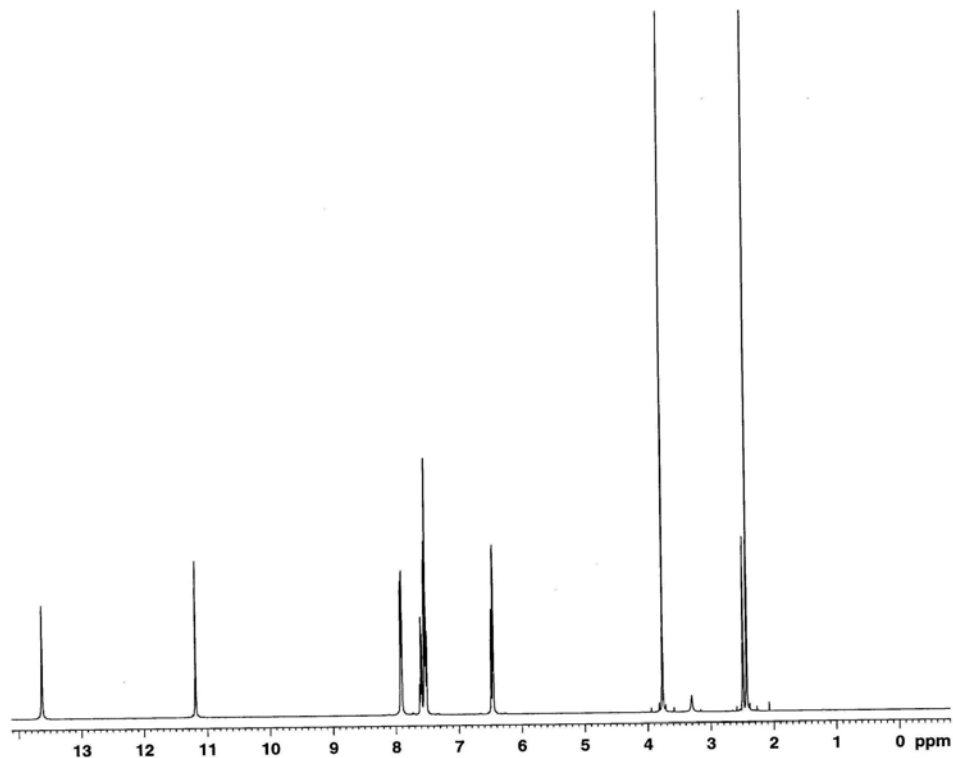


Fig. 2.6. ^1H NMR spectrum of H_2hmab .

H_2hmab : The ^1H NMR spectrum of the compound is shown in Fig. 2.7. The singlet observed at 13.65 ppm is assigned to proton attached to iminol oxygen and singlet peak observed at 11.22 ppm is assigned to phenolic proton. Both of them have peak area corresponds to one. These assignments are confirmed by deuterium exchange studies. Here the methoxy protons gave a singlet at 3.76 ppm and the methyl protons show a singlet at 2.43 ppm. Here also the aromatic protons show multiplets in the region of 6-8 ppm.

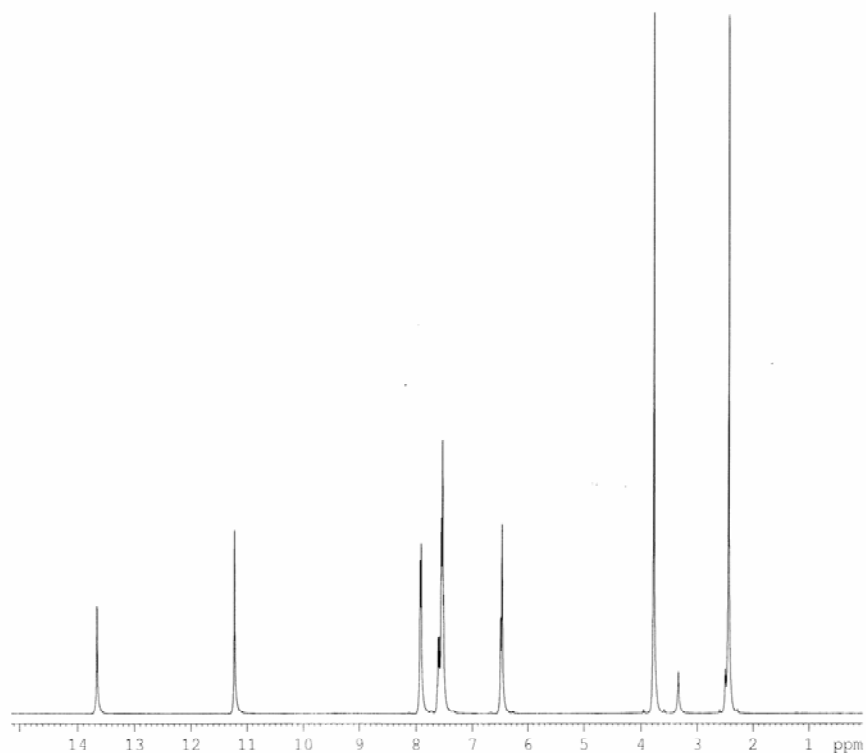


Fig. 2.7. ^1H NMR spectrum of H_2hmab .

2.3.3 Infrared spectral studies

The IR spectral analysis gave an insight to the structure of the compounds. The characteristic bands of different functional groups provide valuable information regarding the structure. Table 2.3 lists the main vibrational bands of the hydrazones. In $\text{H}_2\text{hmbn}\cdot\text{H}_2\text{O}$ a band is observed at 3382 cm^{-1} which is due to the presence of lattice water in the molecule. And this is confirmed by the single crystal X ray diffraction studies. In the remaining compounds there are no bands in this region indicating the absence of water molecules. In all the four hydrazones a band observed around 3200 cm^{-1} is assigned to phenolic O–H, and N–H groups gave bands around 3050 cm^{-1} . A strong band is observed in between

1630-1650 cm^{-1} which indicates the presence of carbonyl group in these compounds. The azomethine bands are observed around 1600 cm^{-1} [26]. The C–O stretching is observed around 1275 cm^{-1} . The N–N stretching vibrations are found in between 1110 and 1140 cm^{-1} . Figs. 2.8-2.11 depict the infrared spectra of the four hydrazones.

Table 2.3 Selected IR frequencies (cm^{-1}) of the hydrazones.

Compound	$\nu(\text{O-H})$	$\nu(\text{N-H})$	$\nu(\text{C=O})$	$\nu(\text{C=N})$	$\nu(\text{N-N})$	$\nu(\text{C-O})$
H ₂ hmbn·H ₂ O	3371,3208	3074	1643	1604	1110	1284
H ₂ hman	3219	3029	1638	1602	1135	1262
H ₂ hmbb	3224	3038	1630	1600	1130	1286
H ₂ hmab	3226	3025	1650	1601	1127	1265

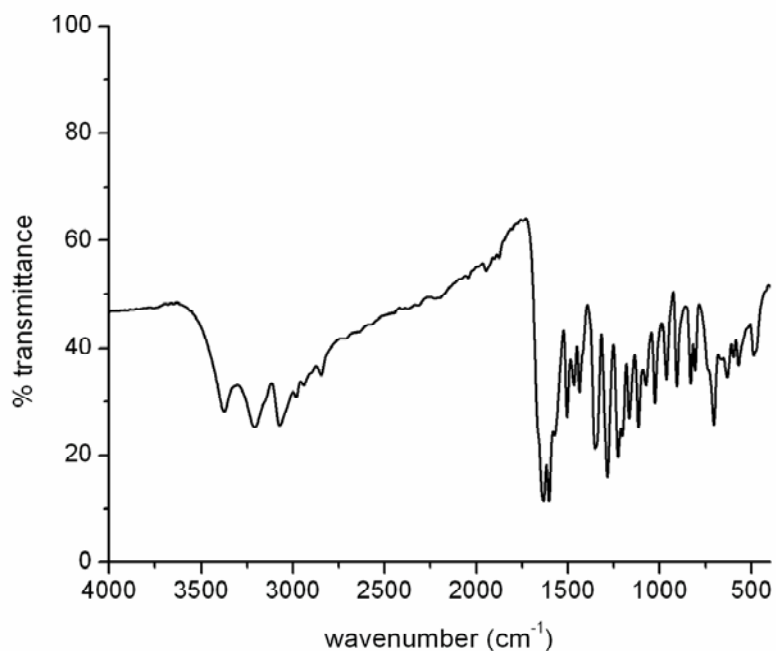


Fig. 2.8. IR spectrum of H₂hmbn·H₂O.

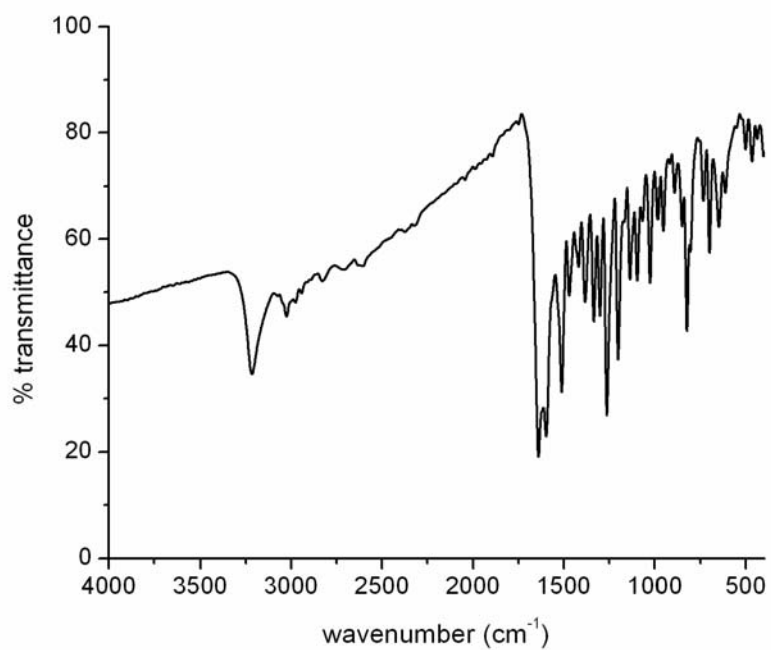


Fig. 2.9. IR spectrum of H₂hman.

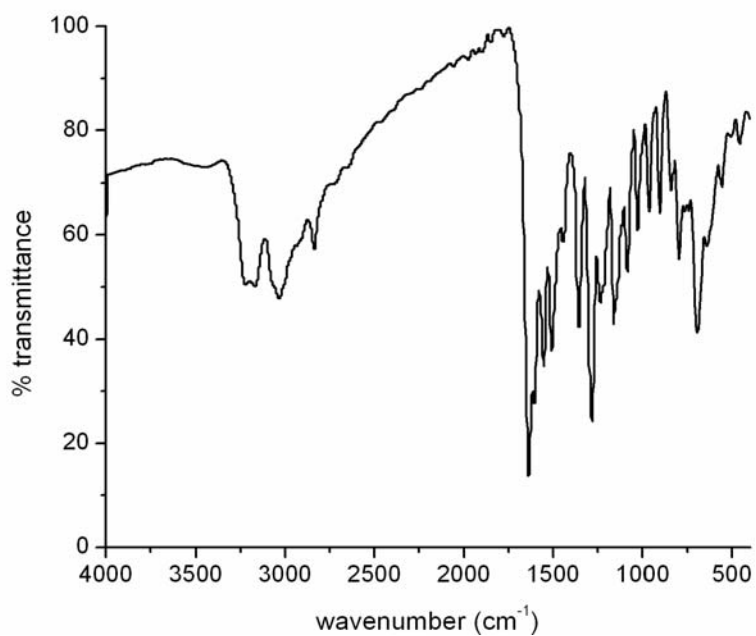


Fig. 2.10. IR spectrum of H₂hmbb.

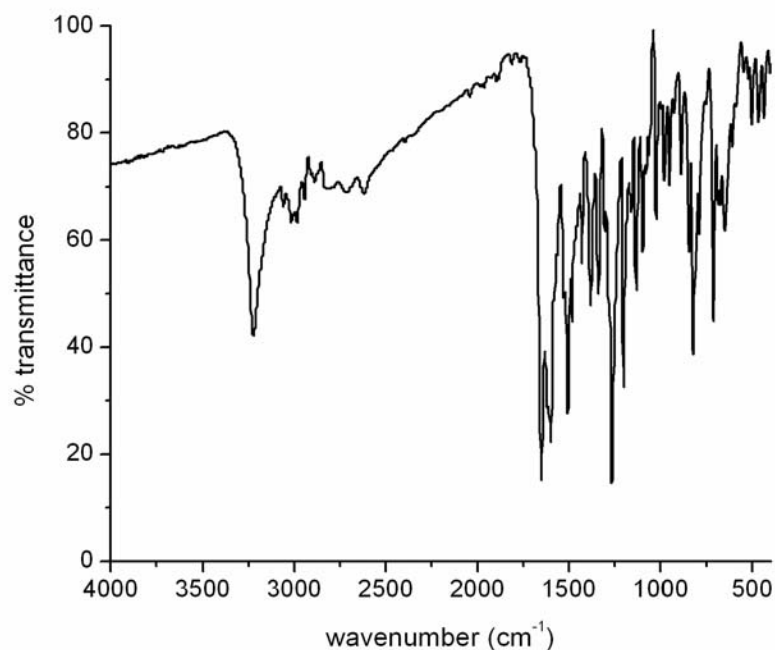


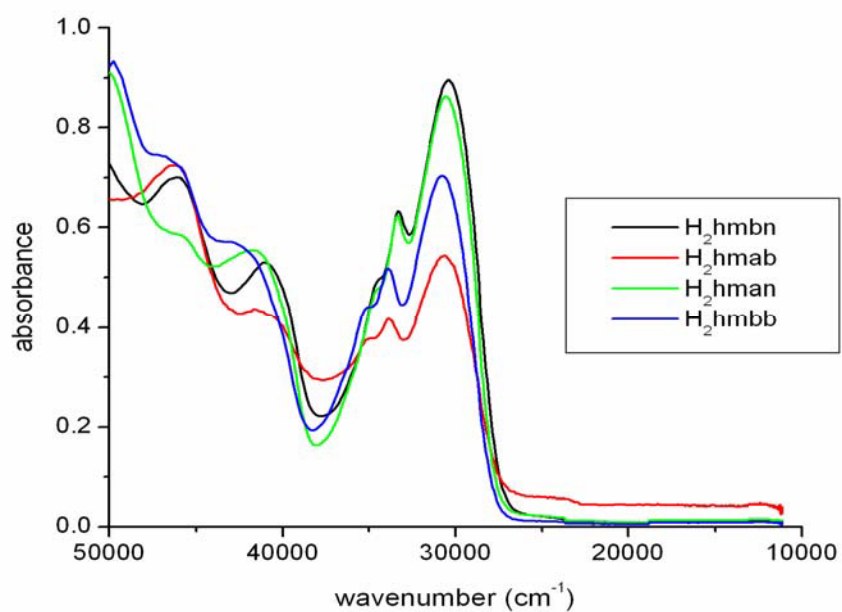
Fig. 2.11. IR spectrum of H₂hmab.

2.3.4 Electronic spectral studies

The electronic spectra of the prepared hydrazones were taken in acetonitrile. Important bands observed are listed in Table 2.4. The electronic spectra of all the four acylhydrazones show bands in the region 30400–46000 cm^{-1} due to π - π^* transitions. The conjugation of azomethine chromophore with olefinic or aryl groups change the spectrum significantly, since rather weak bands due to n - π^* transitions are submerged by strong absorptions associated with π - π^* transitions [27]. These bands are found to be slightly shifted during complexation. Fig. 2.12 represents the electronic spectra of the compounds.

Table 2.4 Important bands (cm^{-1}) of the electronic spectra of hydrazones

Compound	Absorption bands
$\text{H}_2\text{hmbn}\cdot\text{H}_2\text{O}$	30450, 33370, 40860, 45800
H_2hman	30710, 33810, 41660, 45720
H_2hmbb	30630, 33450, 41920, 45540
H_2hmab	30710, 33890, 42100, 45800

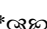
**Fig. 2.12. Electronic spectra of hydrazones.**

References

1. I. Sakyan, E. Logoglu, N. Sari, N. Akiyan, *Biometals* 17 (2004) 115- 120.
2. Z. Huang, J.L. Tian, X.H. Bu, *Inorg. Chem. Commun.* 8 (2005) 194-198.
3. B.Y. Li, Y.M. Yao, Y.R. Wang, Y. Zhang, Q. Shen, *Polyhedron* 27 (2008) 709-716.

4. R.N. Patel, V.L.N. Gundla, D.K. Patel, *Polyhedron* 27 (2008) 1054-1060.
5. M. Tumer, H. Koksall, M.K. Senser, S. Serin, *Trans. Met. Chem.* 24 (1999) 414-420.
6. D. Sriram, P. Yogeewari, D.R.K. Vyas, P. Senthilkumar, P. Bhat, M. Srividya, *Bioorg. Med. Chem. Lett.* 20 (2010) 4313-4316.
7. R.C. Maurya, S. Rajput, *J. Mol. Struct.* 833 (2007) 133-144.
8. G. Tamasi, L. Chiasserini, L. Savini, A. Segal, R. Cini, *J. Inorg. Biochem.* 99 (2005) 1347-1359.
9. A.A. El-Sherif, *Inorg. Chim. Acta* 362 (2009) 4991-5000.
10. Q.B. Song, Z.L. Lu, X.L. Wu, Y.X. Ma, *Trans. Met. Chem.* 19 (1994) 503-505.
11. J.R. Dilworth, *Coord. Chem. Rev.* 21 (1976) 29-40.
12. S. Rollas, Ş.G. Küçükgülzel, *Molecules* 12 (2007) 1910-1939.
13. M.R. Ganjali, M. Rezapour, S. Rasoolipour, P. Norouzi, M. Adib, *J. Braz. Chem. Soc.* 18 (2007) 352-358.
14. S.A. Berger, *Microchim. Acta* 84 (1984) 275-282.
15. F. Cariati, U. Caruso, R. Centore, W. Marcolli, A. De Maria, B. Panunzi, A. Roviello, A. Tuzi, *Inorg. Chem.* 41 (2002) 6597-6603.
16. K. Naseema, K.V. Sujith, K.B. Manjunatha, B. Kalluraya, G. Umesh, V. Rao, *Optic. Laser Tech.* 42 (2010) 741-748.
17. P.V. Bernhardt, J. Mattsson, D.R. Richardson, *Inorg. Chem.* 45 (2006) 752-760.
18. D.S. Kalinowski, P.C. Sharpe, P.V. Bernhardt, D.R. Richardson, *J. Med. Chem.* 51 (2008) 331-344.
19. P.V. Bernhardt, *Dalton Trans.* (2007) 3214-3220.

20. P.V. Bernhardt, P. Chin, P.C. Sharpe, D.R. Richardson, Dalton Trans. (2007) 3232-3244.
21. S.S.S. Raj, H.-K. Fun, Z.-L. Lu, W. Xiao, Y.-X. Tong, B.-S. Kang, Acta Cryst. C 55 (1999) 942-944.
22. S.S.S. Raj, H.-K. Fun, Z.-L. Lu, W. Xiao, X.-Y Gong, C.-M. Gen, Acta Cryst. C 56 (2000) 1013-1014.
23. H.-K. Fun, Z.-L. Lu, C.-Y. Duan, Y.-P. Tian, X.-Z. You, X.-Y Gong , Y.-M. Guo, Acta Cryst. C53 (1997) 1454-1455.
24. H.-K. Fun, K. Chinnakali, I.A. Razak, Z.-L. Lu, B.-S. Kang, Acta Cryst. C55 (1999) 574-576.
25. S.S.S. Raj, S. Renganayaki, E. Subramanian, H.-K. Fun, Acta Cryst. C55 (1999) 2182-2184.
26. M. Kuriakose, M.R.P. Kurup, E. Suresh, Spectrochim. Acta Part A 66 (2007) 353-358.
27. S. Patai, The Chemistry of Carbon-Nitrogen Double Bond, Interscience publishers, John Wiley & Sons, London (1970).

**********

SYNTHESES, SPECTRAL AND STRUCTURAL STUDIES OF OXOVANADIUM(IV/V) COMPLEXES DERIVED FROM TRIDENTATE ACYLHYDRAZONES

- 3.1 Introduction
- 3.2 Experimental
- 3.3 Results and discussion
- References

3.1 Introduction

Vanadium displays a rich and fascinating chemistry depending on the electronic and steric nature of coordinating ligands. It is a trace element known to be essential for a number of species that is widely distributed on earth. This is the only metal named after a goddess, Vanadis, the Norse goddess of beauty and fertility [1-3]. The interaction of simple vanadium species (VO^{2+} and VO^{3+}) with hydrazones having pharmacological activity is of growing interest. The use of oxovanadium complexes in oxidation and oxotransfer catalysis have been noted [4,5]. Medicinal applications of vanadium compounds have focused on their *in vitro* and *in vivo* activity in the treatment of type I and type II diabetes [6-8]. Different types of vanadium compounds have potent anticarcinogenic activity. The anticarcinogenic activity of vanadocenedichloride [Cp_2VCl_2], which is active against animal tumors such as the Ehrlich ascites tumor and certain types of leukaemia, is comparable to cisplatin. Among inorganic vanadium compounds, vanadylsulfate VOSO_4 as a diet constituent found to be an effective non-toxic agent for the chemoprevention of breast cancer in rats [9]. Vanadium complexes

with hydrazone-based ligands have antiamebic activity and are thus potential drugs against amoebiasis [10].

The VO^{2+} complexes of ONO donor α -amino acid Schiff bases and NN donor phenanthroline bases as DNA binder cum photosensitizer display efficient DNA binding propensity [11]. Synthesis and structural studies of an interesting series of heterocyclic adducts of oxovanadium(IV) complexes of some aroylhydrazones have been reported [12]. In the case of oxovanadium complexes, monomeric and five coordinated oxovanadium(IV) complexes are formed with several bidentate Schiff bases, but dimeric and five or six coordinated are formed with tridentate Schiff bases [13].

The coordination chemistry of vanadium is dominated by its variable oxidation numbers. The most common oxidation states of vanadium are +2, +3, +4, and +5, although oxidation states of +1, 0 and -1 are known. Among these different oxidation states, +3, +4 and +5 are biologically important. Vanadium easily switches between the higher oxidation states +4 and +5. As the oxidation state increases the oxophilicity of vanadium also increased [14]. The common geometry adopted in the case of pentacoordinated complexes is square pyramidal, while in the case of hexacoordinated complexes octahedral geometry predominates.

3.2 Experimental

3.2.1 Materials

2-Hydroxy-4-methoxyacetophenone (Aldrich), 2-hydroxy-4-methoxybenzaldehyde (Aldrich), nicotinic acid hydrazide (Aldrich), benzhydrazide (Aldrich), vanadyl sulphate monohydrate (Aldrich), 2,2'-bipyridine (Qualigens), 1,10-phenanthroline (Ranchem) were used as received. Solvents used were water and methanol.

3.2.2 Syntheses of the acylhydrazones

The acylhydrazones, 2-hydroxy-4-methoxybenzaldehyde nicotinoylhydrazone monohydrate ($\text{H}_2\text{hmbn}\cdot\text{H}_2\text{O}$), 2-hydroxy-4-methoxyacetophenone nicotinoylhydrazone (H_2hman), 2-hydroxy-4-methoxybenzaldehyde benzoylhydrazone (H_2hmbb) and 2-hydroxy-4-methoxyacetophenone benzoylhydrazone (H_2hmab) were synthesized as described in Chapter 2.

3.2.3 Syntheses of vanadium complexes

[VO(hmbn)]₂·H₂O (1): This complex was prepared by refluxing equimolar mixture of $\text{VOSO}_4\cdot\text{H}_2\text{O}$ (0.163 g, 1 mmol) in water and $\text{H}_2\text{hmbn}\cdot\text{H}_2\text{O}$ (0.289 g, 1 mmol) in methanol for 4 hours under argon atmosphere. The brown colored product obtained was filtered, washed with methanol, followed by ether and dried over P_4O_{10} *in vacuo*. Elemental Anal. Found (Calcd.) (%): C, 48.60 (48.71); H, 3.51 (3.50); N, 14.08 (14.22).

[VO(hmbn)(bipy)] (2): To prepare this complex, methanolic solutions of 2,2'-bipyridine (0.156 g, 1 mmol) and $\text{H}_2\text{hmbn}\cdot\text{H}_2\text{O}$ (0.289 g, 1 mmol) were added to aqueous solution of $\text{VOSO}_4\cdot\text{H}_2\text{O}$ (0.163 g, 1 mmol). The resulting dark brown solution is refluxed for 4 hours under inert atmosphere. The product formed was brown in color and was filtered, washed with methanol, followed by ether and dried over P_4O_{10} *in vacuo*. Elemental Anal. Found (Calcd.) (%): C, 58.26 (58.54); H, 3.95 (3.89); N, 13.35 (12.89).

[VO(hmbn)(phen)]·1¹/₂H₂O (3): This complex was prepared by refluxing a mixture of $\text{VOSO}_4\cdot\text{H}_2\text{O}$ (0.163 g, 1 mmol) in water, 1,10-phenanthroline (0.198 g, 1 mmol) and $\text{H}_2\text{hmbn}\cdot\text{H}_2\text{O}$ (0.289 g, 1 mmol) in methanol for about 4 hours under inert atmosphere. Dark brown product obtained was filtered, washed with

methanol followed by ether and dried over P_4O_{10} *in vacuo*. Elemental Anal. Found (Calcd.) (%): C, 57.50 (57.46); H, 4.04 (4.08); N, 12.96 (12.89).

[VO(hman)]₂·H₂O (4): This complex was prepared by refluxing a mixture of $VOSO_4 \cdot H_2O$ (0.163 g, 1 mmol) in water and H_2hman (0.285 g, 1 mmol) in methanol for 4 hours under argon atmosphere. The product separated was greenish yellow in color and was filtered, washed with methanol, followed by ether and dried over P_4O_{10} *in vacuo*. Elemental Anal. Found (Calcd.) (%): C, 50.20 (50.15); H, 3.70 (3.93); N, 11.70 (11.70).

[VO(hman)(OCH₃)₂] (5): Methanolic solutions of H_2hman (0.285 g, 1 mmol) and 2,2'-bipyridine (0.156 g, 1 mmol) was added to aqueous solution of $VOSO_4 \cdot H_2O$ (0.163 g, 1 mmol) and the resulting solution was refluxed for about 4 hours under argon atmosphere. The resulting dark brown solution is kept for three days. Brown colored single crystals of the compound isolated was filtered, washed with methanol, followed by ether and dried over P_4O_{10} *in vacuo*. But in this complex, the base added was not incorporated, instead a dimeric product formed. Elemental Anal. Found (Calcd.) (%): C, 50.52 (50.40); H, 4.38 (4.23); N, 11.01 (11.02).

[VO(hman)(phen)]·2H₂O (6): Methanolic solutions of H_2hman (0.285 g, 1 mmol) and 1,10-phenanthroline (0.198 g, 1 mmol) was added to an aqueous solution of $VOSO_4 \cdot H_2O$ (0.163 g, 1 mmol) and refluxed for about 4 hours in inert atmosphere. The dark brown crystalline product obtained was filtered, washed with methanol followed by ether and dried over P_4O_{10} *in vacuo*. Elemental Anal. Found (Calcd.) (%): C, 57.30 (57.25); H, 4.60 (4.45); N, 11.80 (12.36).

[VO(hmhb)]₂·H₂O (7): This complex was prepared by refluxing a mixture of $VOSO_4 \cdot H_2O$ (0.163 g, 1 mmol) in aqueous medium and H_2hmhb (0.270 g, 1 mmol) in methanol for 4 hrs under inert atmosphere. The brown product obtained

was filtered, washed with methanol followed by ether and dried over P_4O_{10} *in vacuo*. Elemental Anal. Found (Calcd.) (%): C, 52.36 (52.34); H, 4.24 (3.81); N, 7.72 (8.14).

[VO(hmbb)(bipy)] (8): This complex was obtained by refluxing a mixture of methanolic solutions of H_2hmbb (0.270 g, 1 mmol), 2,2'-bipyridine (0.156 g, 1 mmol) and aqueous solution of $VOSO_4 \cdot H_2O$ (0.163 g, 1 mmol) for 4 hours under argon atmosphere. The crystalline brown product separated was washed with methanol followed by ether and dried over P_4O_{10} *in vacuo*. Elemental Anal. Found (Calcd.) (%): C, 61.00 (61.11); H, 3.81 (4.10); N, 11.40 (11.40).

[VO(hmbb)(phen)]·H₂O (9): Methanolic solutions of H_2hmbb (0.270 g, 1 mmol) and 1,10-phenanthroline (0.198 g, 1 mmol) and aqueous solution of $VOSO_4 \cdot H_2O$ (0.163 g, 1 mmol) were mixed and refluxed for about 4 hours under argon atmosphere. The dark brown product separated was filtered washed with methanol followed by ether and dried over P_4O_{10} *in vacuo*. Elemental Anal. Found (Calcd.) (%): C, 60.36 (60.56); H, 4.17 (4.52); N, 10.42 (10.46).

[VO(hmab)]₂ (10): The complex $[VO(hmab)]_2$ was prepared by refluxing a mixture of $VOSO_4 \cdot H_2O$ (0.163 g, 1 mmol) in aqueous solution and ligand, H_2hmab (0.284 g, 1 mmol) in methanol for 4 hours under inert atmosphere. Brown colored product obtained was filtered, washed with methanol followed by ether and dried over P_4O_{10} *in vacuo*. Elemental Anal. Found (Calcd.) (%): C, 54.59 (55.03); H, 4.06 (4.04); N, 7.76 (8.02).

[VO(hmab)(bipy)]·H₂O (11): Compound **11** was prepared by the same procedure as that of compound **8**. Color of the compound was dark brown. Elemental Anal. Found (Calcd.) (%): C, 59.84 (59.66); H, 4.34 (4.62); N, 10.41 (10.70).

[VO(hmab)(phen)]·2H₂O (12): Compound **12** was prepared by the same procedure as that of compound **9**. The compound was brown colored and has crystalline nature. Elemental Anal. Found (Calcd.) (%): C, 59.63 (59.47); H, 4.44 (4.63); N, 9.65 (9.91).

3.3 Results and discussion

Twelve vanadium complexes were prepared and are found to be stable. In all the complexes, hydrazones coordinated to the metal centre in enolic form and hence act as dideprotonated tridentate ligands. The complexes are soluble in organic solvents like acetonitrile and DMF. The elemental analyses values showed that the found and calculated values are in close agreement with the general formula of the complexes. Magnetic susceptibility measurements revealed that all complexes except **5** are found to be paramagnetic. Complexes **1**, **4**, **7** and **10** exhibit subnormal magnetic moments ($\mu_{\text{eff}} = 1.2\text{--}1.4$ B.M. at room temperature) due to the strong antiferromagnetic exchange, suggesting dimeric nature to these complexes [15]. Magnetic susceptibility values for other complexes showed slight deviations from the spin only value for a d^1 system. The molar conductivity values for all the complexes in 10^{-3} M DMF solution are found to be less than $15 \text{ ohm}^{-1} \text{ cm}^2 \text{ mol}^{-1}$ which is much less than the value of $65\text{--}90 \text{ ohm}^{-1} \text{ cm}^2 \text{ mol}^{-1}$ reported for a 1:1 electrolyte in the same solvent confirmed the non-electrolytic nature of the complexes [16]. The magnetic susceptibility and molar conductivity values of the complexes are listed in Table 3.1. X-ray quality single crystals of one of the compounds, $[\text{VO}(\text{hman})(\text{OCH}_3)]_2$ (**5**) were obtained from reaction mixture.

Table 3.1 Molar conductivities and magnetic susceptibilities of vanadium complexes

Compound	$\lambda_m^{\#}$	μ_{eff} (B.M.)
[VO(hmbn)] ₂ ·H ₂ O (1)	7	1.33
[VO(hmbn)(bipy)] (2)	11	1.78
[VO(hmbn)(phen)]·1½H ₂ O (3)	9	1.82
[VO(hman)] ₂ ·H ₂ O (4)	10	1.23
[VO(hman)(OCH ₃) ₂] (5)	8	diamagnetic
[VO(hman)(phen)]·2H ₂ O (6)	6	1.79
[VO(hmbb)] ₂ ·H ₂ O (7)	11	1.28
[VO(hmbb)(bipy)] (8)	8	1.77
[VO(hmbb)(phen)]·H ₂ O (9)	6	1.81
[VO(hmab)] ₂ (10)	4	1.40
[VO(hmab)(bipy)]·H ₂ O (11)	8	1.76
[VO(hmab)(phen)]·2H ₂ O (12)	6	1.80

[#]molar conductivity (in mho cm² mol⁻¹) taken in 10⁻³ M DMF solution.

3.3.1 Crystal structure of the compound [VO(hman)(OCH₃)₂] (5)

The molecular structure of the compound **5** along with atom numbering scheme is given in Fig. 3.1. A summary of the key crystallographic information is given in Table 3.2. Compound **5** crystallized into triclinic space group *P* $\bar{1}$. This is a centrosymmetric bis(μ -methoxy) bridged vanadium(V) dimer consisting of one vanadium atom (V1), one terminal oxo group (O4), one methoxy oxygen (O5), tridentate hydrazone ligand binding to the metal center *via* phenoxy oxygen (O2), azomethine nitrogen (N1), enolic oxygen (O3) atoms. The vanadium(V) ions in the dimer exhibited distorted octahedral geometry with O3, N1, O2 and O5 atoms defining the equatorial plane, and O4 and O5a atoms at the apical positions. The metal atom is displaced towards the axial oxo atom (O4) by 0.3548 Å from the equatorial plane. The selected bond lengths and bond angles of the molecule are summarized in Table 3.3.

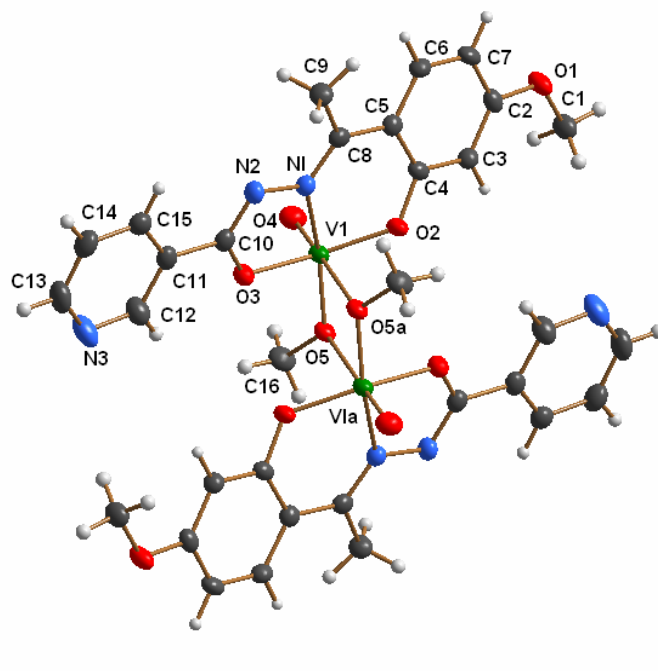


Fig. 3.1. Structure and labeling scheme for $[\text{VO}(\text{hman})(\text{OCH}_3)_2]$.

The terminal V1–O4 (oxo) distance is 1.5896 Å, V1–O5a (bridging) is 2.3655 Å, V1–O2 (phenoxo) is 1.8215 Å and V1–O3 (enolic) is 1.9258 Å, these agree well with the corresponding values reported for related systems [17]. Upon dimerization, the main difference of one half of the molecule with the other half is V1–O5 and V1a–O5a. The trans influence of the oxo (O4) ligand in one apical position of the vanadium octahedron manifests itself by elongation of the bond distance for the apically bonded bridging methoxy oxygen atom [V1–O5a = 2.3655 Å] when compared to the distance for the methoxy oxygen atom [V1–O5 = 1.8208 Å]. The intramolecular V1⋯V1a distance is found to be 3.338 Å and falls within the range of known V⋯V distances in double bridged vanadium polynuclear systems. The centrosymmetric dimer is formed *via* the bridging oxygens connecting two vanadium atoms. Hence the vanadium atom adopts a distorted octahedral geometry [18,19].

The mean plane deviation calculations shows that the atoms in the basal plane O3, N1, O2 and O5 is nearly planar with a maximum mean plane deviation of 0.007 Å and V1 is slightly deviated from planarity with a distance of 0.3548 Å. Ring puckering analyses and least-square plane calculations shows that the ring Cg(3) comprising of atoms V1, O2, C4, C5, C8 and N1 confirms the ‘screw boat’ conformation (‘S’ configuration) [20].

Fig. 3.2 shows the contents of the unit cell packing. The assemblage of molecules in the respective manner in the unit cell is resulted by the π - π and C-H \cdots π interactions as depicted in Table 3.4. The centroid Cg(2) is involved in π - π interaction with Cg(1) of the neighboring unit at a distance of 2.6355 Å and C-H \cdots π interactions C(1)-H(1C) \cdots Cg(5) at a distance of 2.80 Å contribute stability to the unit cell packing. A weak intramolecular hydrogen bonding interaction is observed between C12-H12 and O3 with an angle of 102°. No classic hydrogen bonds were found in this compound.

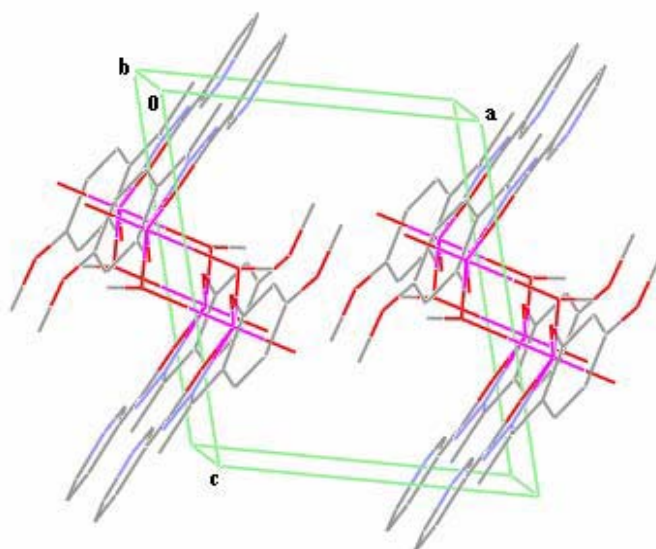


Fig. 3.2. Unit cell packing diagram of the compound [VO(hman)(OCH₃)₂]₂ viewed along the *b* axis.

Table 3.2 Crystal data and structure refinement parameters for [VO(hman)(OCH₃)₂] (5)

CCDC No.	669785
Empirical formula	C ₃₂ H ₃₂ N ₆ O ₁₀ V ₂
Formula weight	762.52
Temperature	150(2) K
Wavelength	0.71073 Å
Crystal system	Triclinic
Space group	<i>P</i> $\bar{1}$
Unit cell dimensions	a = 7.8134(8) Å b = 10.7745(11) Å c = 11.329(4) Å α = 61.36(2)° β = 79.627(16)° γ = 70.835(9)°
Volume	790.3(3) Å ³
Z	1
Density (calculated)	1.602 Mg/ m ³
Absorption coefficient	0.662 mm ⁻¹
F(000)	392
Crystal size	0.33 x 0.18 x 0.16 mm ³
θ range for data collection	2.99 to 25.00°
Index ranges	-9 ≤ h ≤ 9, -12 ≤ k ≤ 12, -13 ≤ l ≤ 13
Reflections collected	7950
Independent reflections	2760 [R(int) = 0.0152]
Refinement method	Full-matrix least-squares on F ²
Data / restraints / parameters	2760 / 0 / 229
Goodness-of-fit on F ²	1.083
Final R indices [I > 2σ(I)]	R ₁ = 0.0235, wR ₂ = 0.0655
R indices (all data)	R ₁ = 0.0257, wR ₂ = 0.0666
Largest diff. peak and hole	0.269 and -0.305 e.Å ⁻³

$$R_1 = \frac{\sum ||F_o| - |F_c||}{\sum |F_o|}$$

$$wR_2 = [\sum w(F_o^2 - F_c^2)^2 / \sum w(F_o^2)^2]^{1/2}$$

Table 3.3 Selected bond lengths (Å) and bond angles (°) for the compound (5)

<i>Bond lengths</i>		<i>Bond angles</i>		<i>Bond angles</i>	
V(1)–O(4)	1.5895(12)	O(4)–V(1)–O(5)	104.33(6)	O(2)–V(1)–O(5a)	79.74(5)
V(1)–O(5)	1.8207(13)	O(4)–V(1)–O(2)	100.96(6)	O(3)–V(1)–O(5a)	80.04(4)
V(1)–O(2)	1.8215(11)	O(5)–V(1)–O(2)	104.11(5)	N(1)–V(1)–O(5a)	83.64(5)
V(1)–O(3)	1.9258(11)	O(4)–V(1)–O(3)	99.47(6)	C(4)–O(2)–V(1)	129.08(10)
V(1)–N(1)	2.1062(15)	O(5)–V(1)–O(3)	88.97(5)	C(10)–O(3)–V(1)	118.21(10)
V(1)–O(5a)	2.3656(11)	O(2)–V(1)–O(3)	152.07(5)	C(16)–O(5)–V(1)	123.43(10)
O(2)–C(4)	1.3381(19)	O(4)–V(1)–N(1)	96.92(6)	C(16)–O(5)–V(1a)	120.55(9)
O(5)–C(16)	1.4283(19)	O(5)–V(1)–N(1)	155.34(5)	V(1)–O(5)–V(1a)	105.01(5)
O(5)–V(1a)	2.3656(11)	O(2)–V(1)–N(1)	83.62(5)	C(8)–N(1)–N(2)	116.57(13)
N(1)–C(8)	1.310(2)	O(3)–V(1)–N(1)	75.16(5)	C(8)–N(1)–V(1)	127.99(11)
N(1)–N(2)	1.3999(18)	O(4)–V(1)–O(5a)	179.14(5)	N(2)–N(1)–V(1)	115.44(9)
N(2)–C(10)	1.305(2)	O(5)–V(1)–O(5a)	74.99(5)	C(10)–N(2)–N(1)	108.11(13)
V(1)··V(1a)	3.338				

Table 3.4 Interaction parameters of the compound (5)

π-π interactions			
Cg(I)···Cg(J)	Cg···Cg (Å)	α (°)	β (°)
Cg(2)···Cg(1) ^a	2.6355	79.49	55.81

Equivalent position codes : ^a = 2-x, 1-y, -z

Cg(2) = V(1), O(3), C(10), N(2), N(1); Cg(1) = V(1), O(5), V(1A), O(5a)

α (°) = Dihedral angle between planes I and J;

β (°) = Angle between Cg(I)–Cg(J) vector and normal to plane I.

C–H···π interactions			
C–H(I)···Cg(J)	H···Cg (Å)	C–H···Cg (°)	C···Cg (Å)
C(1)–H(1C)···Cg(5) ^b	2.80	145	3.6214

Equivalent position codes : ^b = 1-x, 1-y, 1-z

Cg(5) = C(2), C(3), C(4), C(5), C(6), C(7)

H bonding				
D–H···A	D–H	H···A	D···A	D–H···A
C(12)–H(12)···O(3)	0.93	2.39	2.748(3)	102

(D=Donor, A=acceptor, Cg=Centroid)

3.3.2 EPR spectra

EPR spectroscopy can offer a great deal of information regarding the bonding in vanadyl complexes. In vanadyl complexes vanadium is in +4 oxidation state with d^1 configuration, and since the orbital angular momentum is quenched by the crystalline fields, the paramagnetism of the vanadyl ion arises from the single unpaired electron.

In V(IV) complexes value of g is below the value for free electron. The spin of ^{51}V nucleus is $I = 7/2$. In mononuclear V(IV) complexes the EPR signals are split into eight and in binuclear complexes fifteen hyperfine lines. Under the influence of magnetic field, the electronic ground state ($S = 1/2$) is split into two ($m_s = +1/2$ and $-1/2$) and additional splitting occurs through the different magnetic orientations of the nuclear spin (m_I).

VO^{2+} is one of the most stable diatomic cation and its paramagnetism is almost due to spin angular momentum, and EPR absorptions are obtained over a wide range of temperature including room temperature [21].

EPR spectra of all the oxovanadium(IV) complexes were recorded in polycrystalline state at 298 K and in DMF solution at 77 K and the spectral parameters are summarized in Table 3.5. Compound **5** is diamagnetic and hence EPR silent. Some of the EPR spectra are simulated and the experimental (green) and simulated (purple) best fits are included [22].

The spectrum of compound **1** in polycrystalline state at 298 K (Fig. 3.3) is axial with $g_{\parallel} = 1.985$ and $g_{\perp} = 1.990$ and $A_{\parallel} = 152 \times 10^{-4} \text{ cm}^{-1}$.

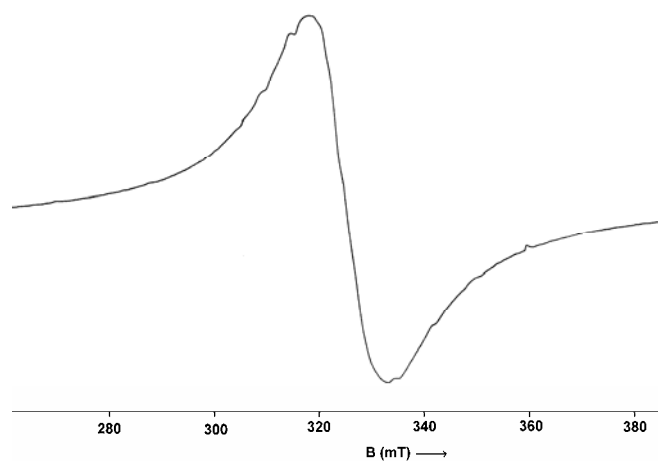


Fig. 3.3. EPR spectrum of compound **1** in polycrystalline state at 298 K.

In frozen DMF at 77 K, tumbling motions of the molecules are restricted which results in anisotropic spectrum. Here compound **1** displays well resolved axial anisotropy with two sets of eight line pattern with $g_{\parallel} = 1.950$, $g_{\perp} = 1.984$, $A_{\parallel} = 148 \times 10^{-4} \text{ cm}^{-1}$ and $A_{\perp} = 49 \times 10^{-4} \text{ cm}^{-1}$. In a tetragonal complex $g_{\parallel} < g_{\perp}$ and $A_{\parallel} > A_{\perp}$, this relationship is characteristic of an axially compressed d_{xy}^1 configuration. The experimental and simulated best fits of compound **1** are shown in Fig. 3.4.

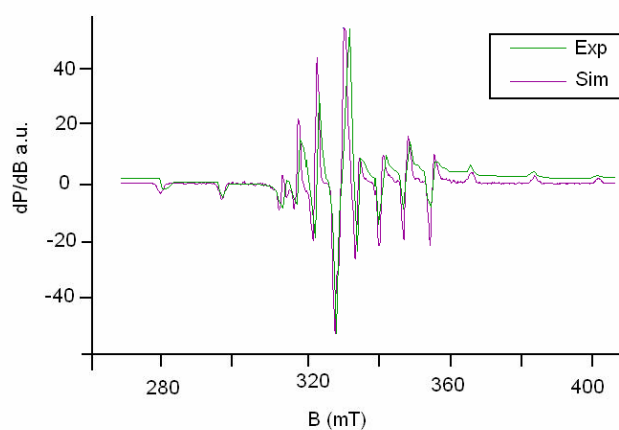


Fig. 3.4. EPR spectrum of compound **1** in DMF at 77 K.

Compound **2** in polycrystalline state at 298 K (Fig. 3.5) displayed an isotropic spectrum with $g_{\text{iso}} = 1.989$.

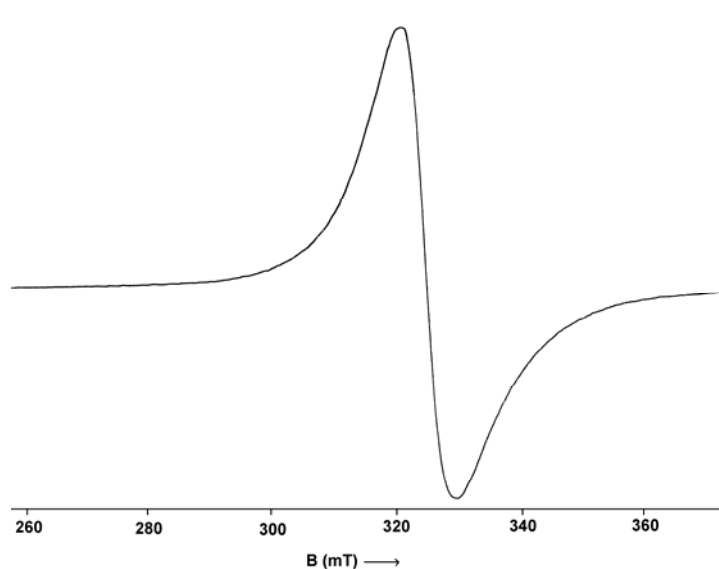


Fig. 3.5. EPR spectrum of compound **2** in polycrystalline state at 298 K.

EPR spectrum of compound **2** in frozen DMF is shown in Fig. 3.6. In the case of oxovanadium complexes, primary axis (z axis) is defined by V=O unit and which is in the direction of magnetic field B. So the resulting axial spectra with two sets of eight line pattern with different g and A values provides valuable information regarding the electronic environment of the metal and orientation of ligand set. Compound **2** with $g_{\parallel} = 1.953$, $g_{\perp} = 1.978$, $A_{\parallel} = 146 \times 10^{-4} \text{ cm}^{-1}$ and $A_{\perp} = 48 \times 10^{-4} \text{ cm}^{-1}$, follow the relationship, $g_{\parallel} < g_{\perp}$ and $A_{\parallel} > A_{\perp}$ suggesting d_{xy}^1 ground state configuration. The anisotropic parameters are related with isotropic parameters by the equations, $A_{\text{iso}} = \frac{1}{3}(A_{\parallel} + 2A_{\perp})$ and $g_{\text{iso}} = \frac{1}{3}(g_{\parallel} + 2g_{\perp})$ [1]. In this compound the value obtained for $g_{\text{iso}} = 1.970$ which is near to the value obtained from the polycrystalline spectrum suggests that the molecules retaining their structural identity in solution.

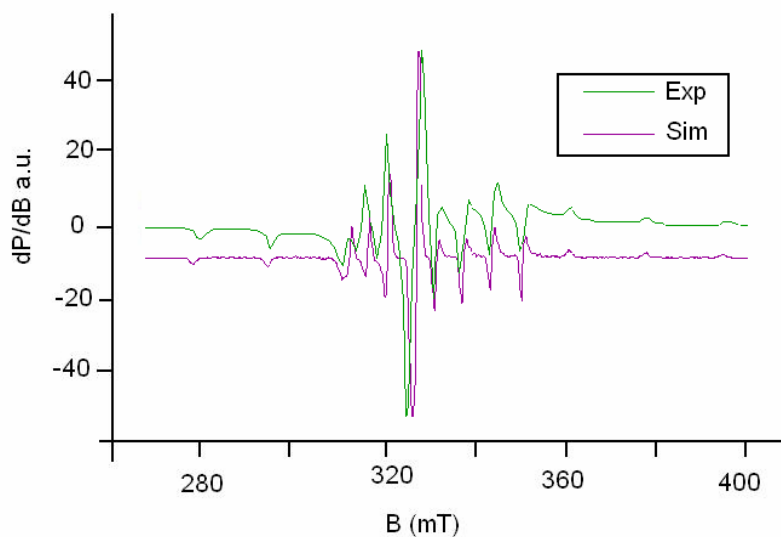


Fig. 3.6. EPR spectrum of compound 2 in DMF at 77 K.

The X-band EPR spectrum of compound 3 in polycrystalline state at 298 K (Fig. 3.7) exhibits an isotropic spectrum, which is not so resolved at room temperature to eight-hyperfine lines. The g_{iso} value obtained for the compound is 1.984.

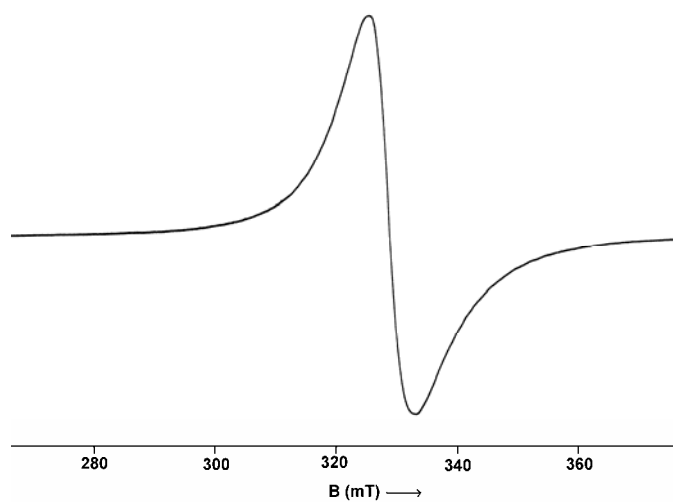


Fig. 3.7. EPR spectrum of compound 3 in polycrystalline state at 298 K.

The frozen solution EPR spectrum of **3** in DMF (Fig. 3.8) at 77 K is exhibits well-resolved axial anisotropy with two sets of eight line pattern with $g_{\parallel} < g_{\perp}$ and $A_{\parallel} > A_{\perp}$. Here also g_{iso} calculated is in agreement with that obtained from polycrystalline state spectrum retaining of structural identity of the compound. Ligand nitrogen or hydrogen superhyperfine splittings are not observed on the vanadium line. This indicates that the unpaired electron to be in b_{2g} (d_{xy} , 2B_2 ground state) orbital localized on metal, thus excluding the possibility of its direct interaction with the ligand [23,24].

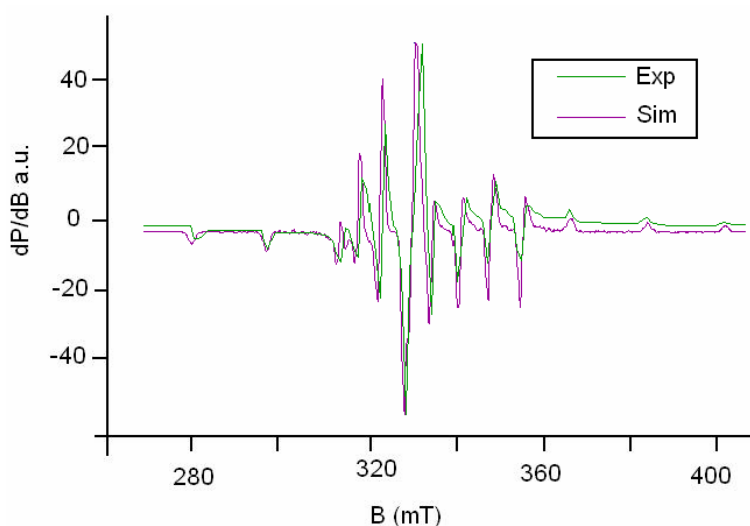


Fig. 3.8. EPR spectrum of compound 3 in DMF at 77 K.

Compound **4** in polycrystalline state at 298 K (Fig. 3.9) displayed an isotropic spectrum with $g_{\text{iso}} = 1.991$. The solution EPR spectrum of the compound **4** in DMF at 77 K (Fig. 3.10) shows similar eight line pattern to that of mononuclear complexes. In case of dinuclear complexes a half field signal is expected due to forbidden $\Delta M_s = \pm 2$ transition. But in this compound half field signal is absent, indicating that the spin-spin interaction of this compound is not so significant such that each unpaired electron virtually interact with only one vanadium center [25].

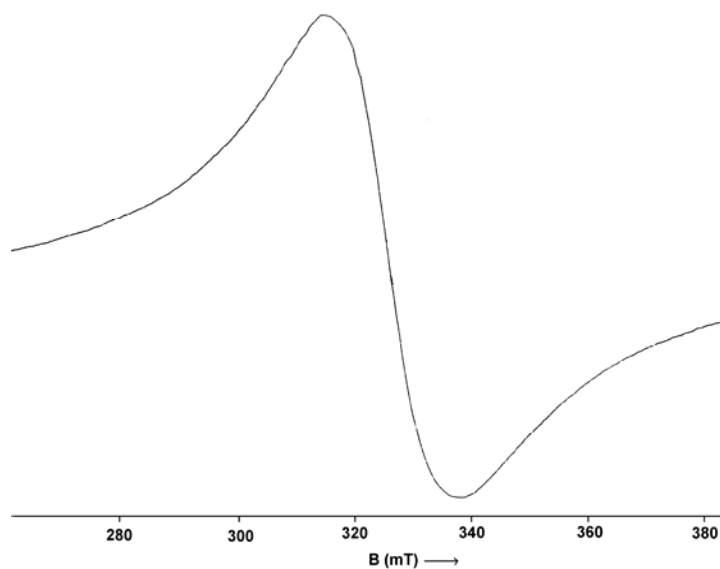


Fig. 3.9. EPR spectrum of compound 4 in polycrystalline state at 298 K.

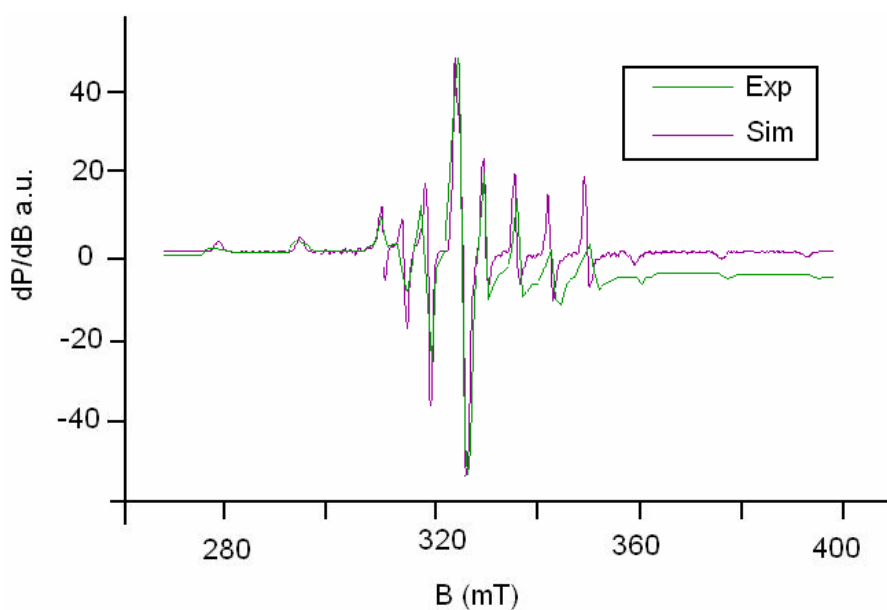


Fig. 3.10. EPR spectrum of compound 4 in DMF at 77 K.

In polycrystalline state at 298 K compound **6** displayed an isotropic spectrum (Fig. 3.11) and in DMF at 77 K (Fig. 3.12) an axial spectrum with two sets of g and A values.

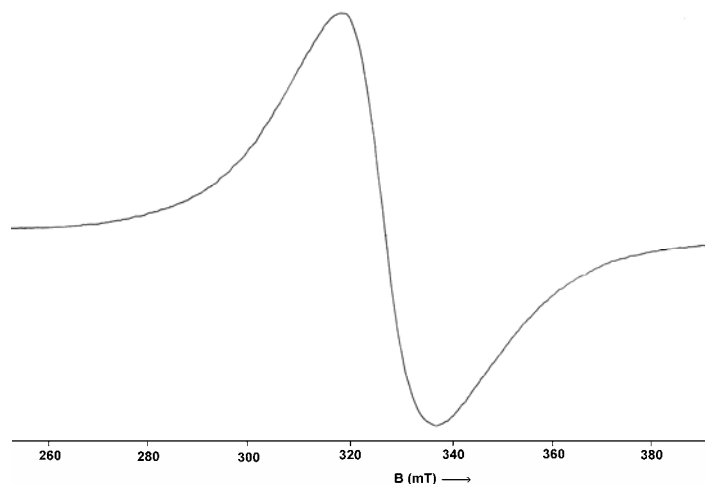


Fig. 3.11. EPR spectrum of compound **6** in polycrystalline state at 298 K.

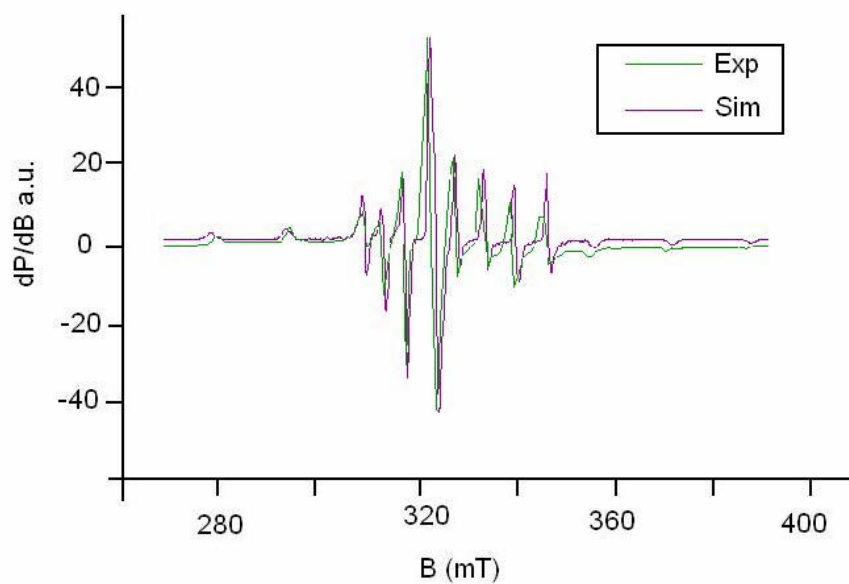


Fig. 3.12. EPR spectrum of compound **6** in DMF at 77 K.

The spectrum of compound **7** in polycrystalline state at 298 K (Fig. 3.13) is axial with $g_{\parallel} = 1.969$ and $g_{\perp} = 1.984$ and $A_{\parallel} = 105 \times 10^{-4} \text{ cm}^{-1}$.

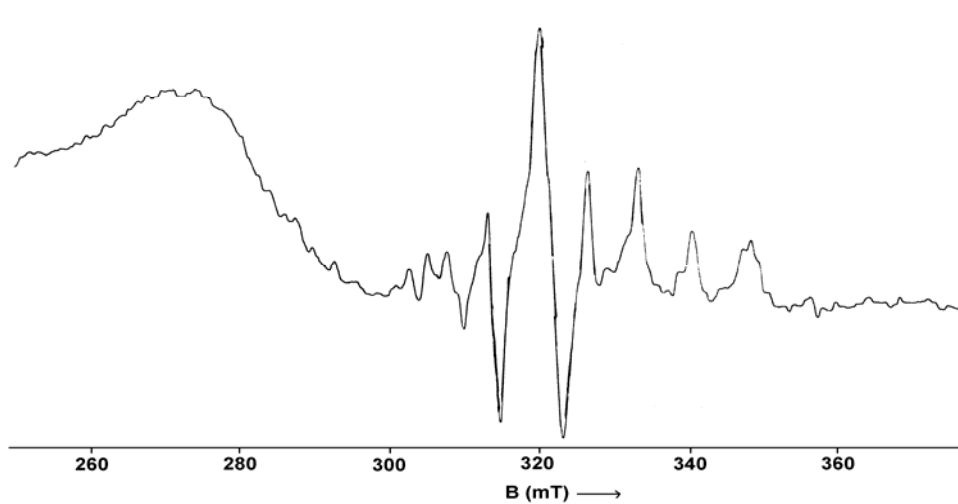


Fig. 3.13. EPR spectrum of compound **7** in polycrystalline state at 298 K.

In DMF at 77 K compound **7** gave an axial spectrum (Fig. 3.14) with $g_{\parallel} = 1.968$ and $g_{\perp} = 1.998$ and $A_{\parallel} = 150 \times 10^{-4} \text{ cm}^{-1}$.

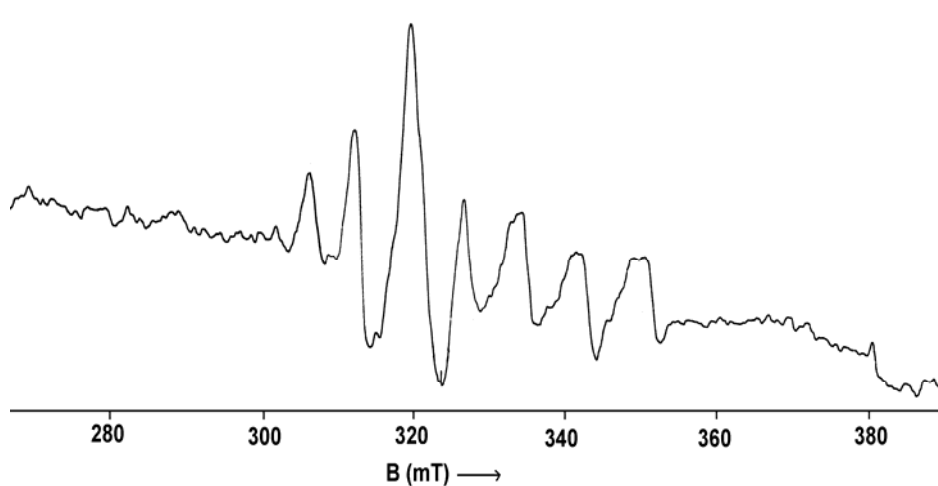


Fig. 3.14. EPR spectrum of compound **7** in DMF at 77 K.

Compound **8** shows an isotropic spectrum in polycrystalline state at 298 K (Fig. 3.15) with $g_{\text{iso}} = 1.984$.

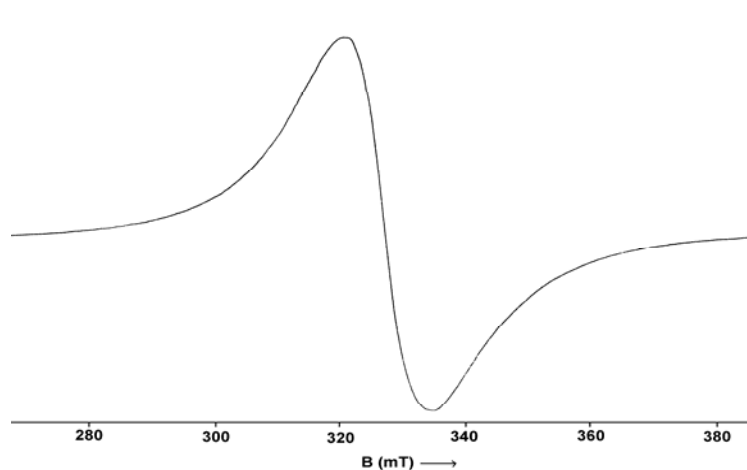


Fig. 3.15. EPR spectrum of compound **8** in polycrystalline state at 298 K.

Anisotropic EPR spectrum obtained for compound **8** in frozen DMF is depicted in Fig. 3.16. The $g_{\parallel} < g_{\perp}$ and $A_{\parallel} > A_{\perp}$ relationships is consistent with an axially compressed octahedral geometry around the vanadium(IV) centre with the unpaired electron in the d_{xy} orbital.

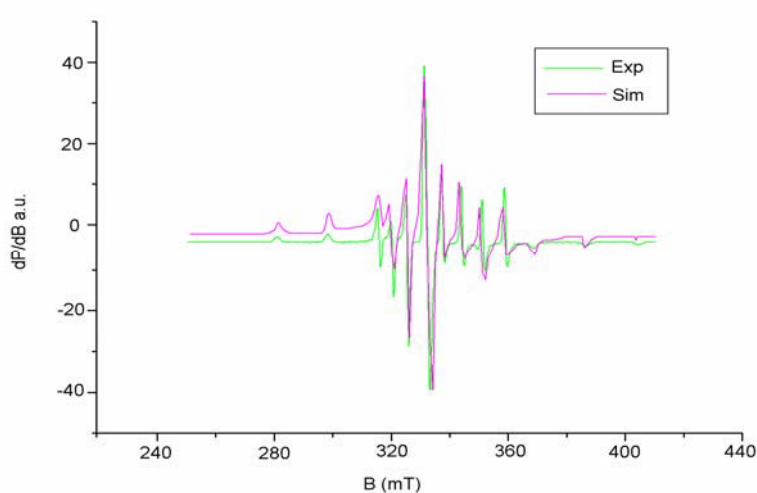


Fig. 3.16. EPR spectrum of compound **8** in DMF at 77 K.

In polycrystalline state at 298 K compound **9** (Fig. 3.17) displayed an isotropic spectrum with $g_{\text{iso}} = 1.981$.

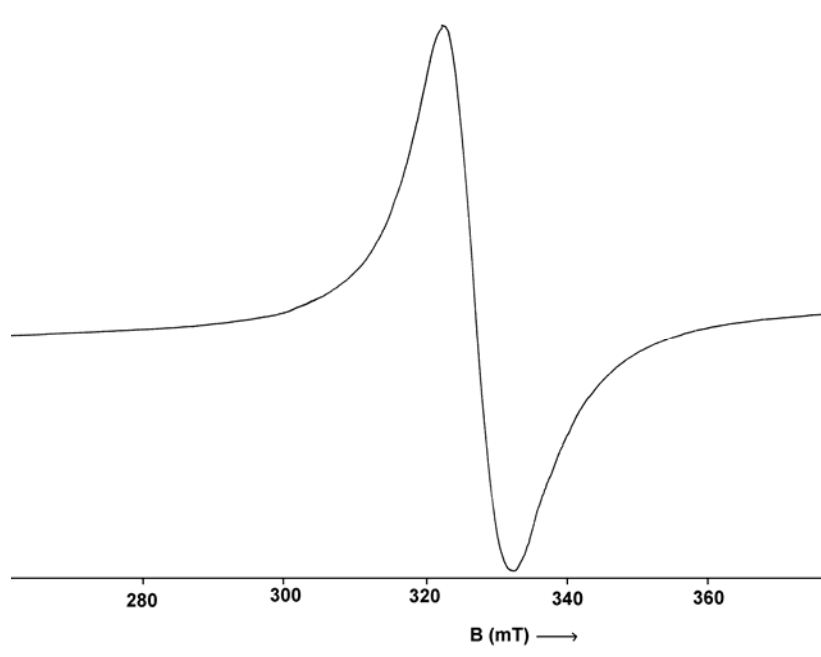


Fig. 3.17. EPR spectrum of compound **9** in polycrystalline state at 298 K.

The frozen-solution spectrum of compound **9** (Fig. 3.18) is attributable to a VO^{2+} ion in a nearly axially distorted octahedral ligand field and displays both parallel and perpendicular features of the hyperfine structure. Superhyperfine splittings due to ligand nitrogens are absent because the unpaired electron has only a weak interaction with ligand nitrogen, so that the size of the coupling is less than EPR bandwidth and it is an indication of the presence of electron in b_{2g} (d_{xy} , 2B_2 ground state) orbital.

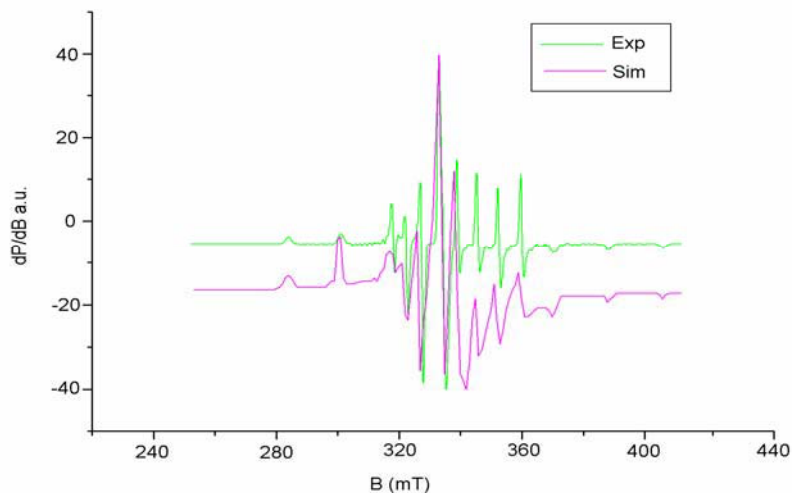


Fig. 3.18. EPR spectrum of compound 9 in DMF at 77 K.

The spectrum of compound **10** in polycrystalline state at 298 K (Fig. 3.19) is axial with $g_{\parallel} = 1.943$ and $g_{\perp} = 1.981$ and $A_{\parallel} = 68 \times 10^{-4} \text{ cm}^{-1}$.

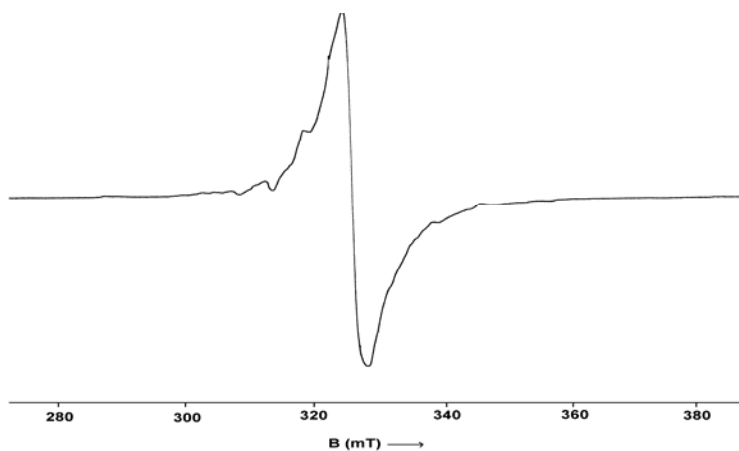


Fig. 3.19. EPR spectrum of compound 10 in polycrystalline state at 298 K.

In frozen DMF at 77 K compound **10** (Fig. 3.20) displayed an axial spectrum with two sets of eight line pattern. Here also the expected half field signal due to forbidden $\Delta M_s = \pm 2$ transitions is absent indicates that the spin-spin interaction of this compound is not so significant.

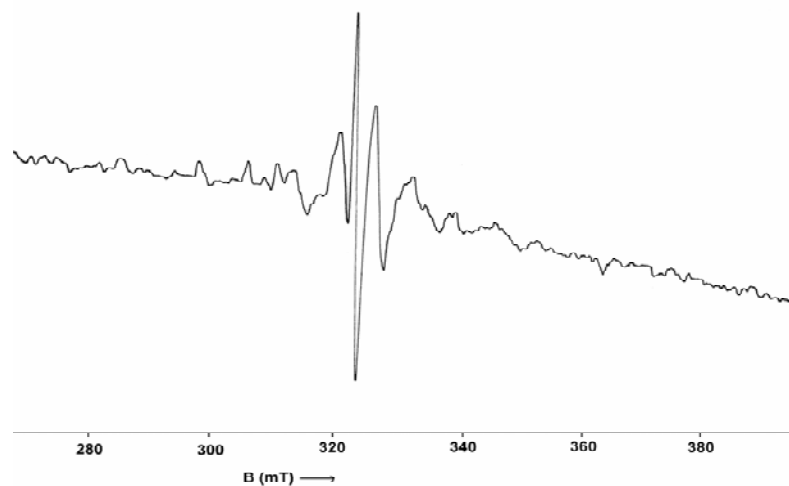


Fig. 3.20. EPR spectrum of compound 10 in DMF at 77 K.

The polycrystalline state spectrum of compound **11** at 298 K (Fig. 3.21) is isotropic with $g_{\text{iso}} = 1.978$.

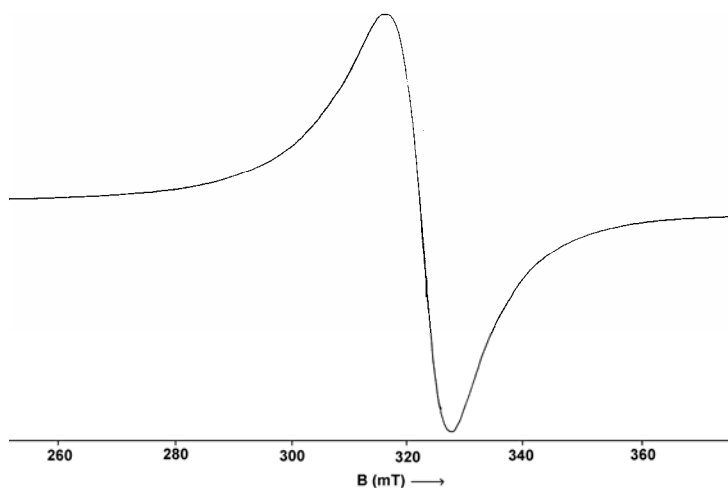


Fig. 3.21. EPR spectrum of compound 11 in polycrystalline state at 298 K.

The frozen DMF spectrum of compound **11** (Fig. 3.22) exhibits a well resolved axial anisotropy with 16-line hyperfine structure, characteristic of an interaction of vanadium nuclear spin (^{51}V , $I = 7/2$). Superhyperfine splittings due

to azomethine nitrogen and nitrogens from 2,2' bipyridine are absent suggesting that the unpaired electron is in inner d_{xy} orbital.

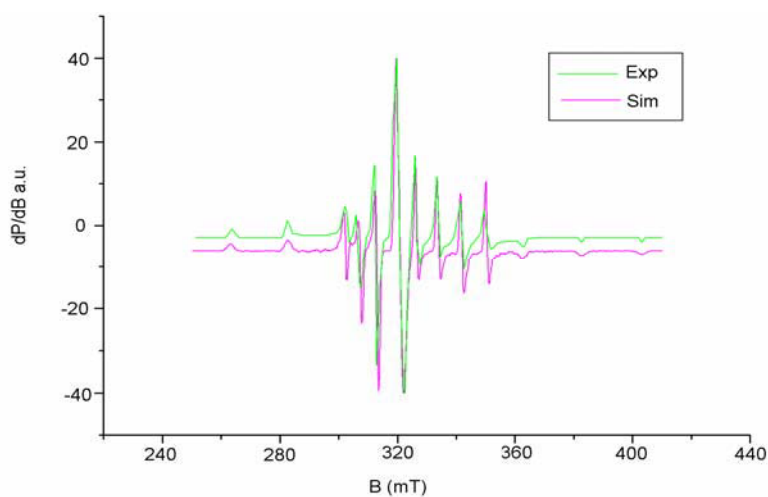


Fig. 3.22. EPR spectrum of compound 11 in DMF at 77 K.

The spectrum of compound **12** in polycrystalline state at 298 K (Fig. 3.23) is axial with $g_{\parallel} = 1.937$ and $g_{\perp} = 1.993$ and $A_{\parallel} = 103 \times 10^{-4} \text{ cm}^{-1}$.

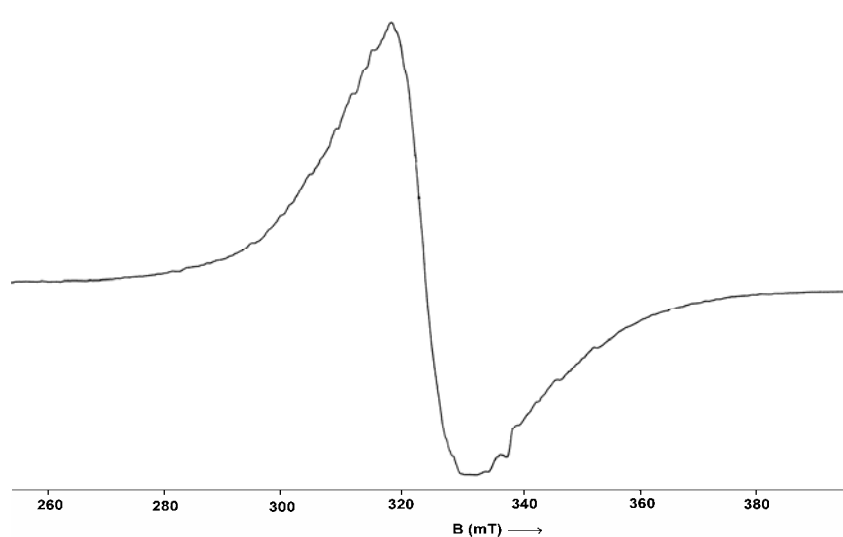


Fig. 3.23. EPR spectrum of compound 12 in polycrystalline state at 298 K.

In DMF at 77 K compound **12** (Fig. 3.24) gave an axial spectrum two sets of eight line pattern with $g_{\parallel} < g_{\perp}$ and $A_{\parallel} > A_{\perp}$.

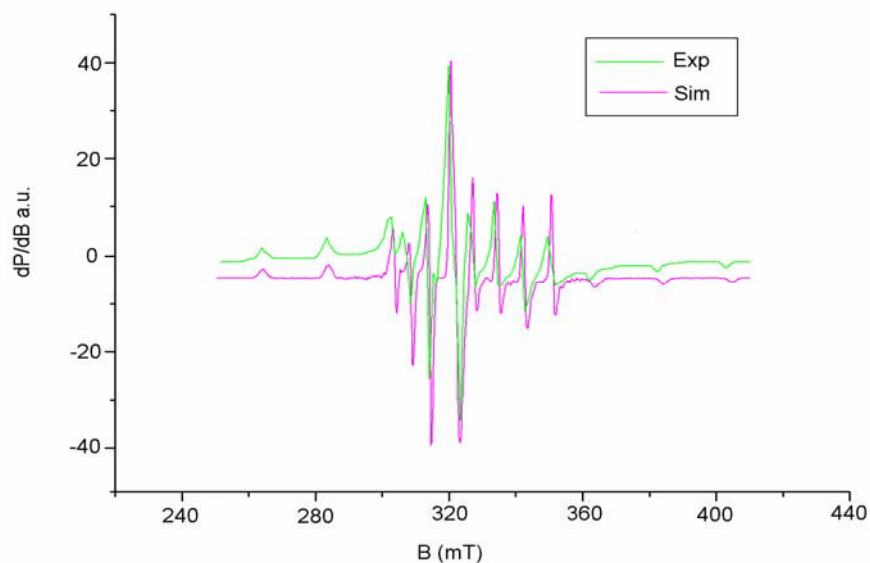


Fig. 3.24. EPR spectrum of compound 12 in DMF at 77 K.

The EPR parameters g_{\parallel} , g_{\perp} , A_{\parallel} and A_{\perp} and energies of $d-d$ transitions were used to evaluate the molecular orbital coefficients α^2 and β^2 for the complexes by using the following equations:

$$\alpha^2 = \frac{(2.00277 - g_{\parallel})E_{d-d}}{8\lambda\beta^2}$$

$$\beta^2 = \frac{7}{6} \left[\left(\frac{-A_{\parallel}}{P} \right) + \left(\frac{A_{\perp}}{P} \right) + \left(g_{\parallel} - \frac{5}{14}g_{\perp} \right) - \frac{9}{14}g_e \right]$$

where $P = 128 \times 10^{-4} \text{ cm}^{-1}$, $\lambda = 135 \text{ cm}^{-1}$ and E_{d-d} is the energy of $d-d$ transition.

Table 3.5 EPR spectral assignments of oxovanadium(IV) complexes in polycrystalline state at 298 K and DMF solution at 77 K

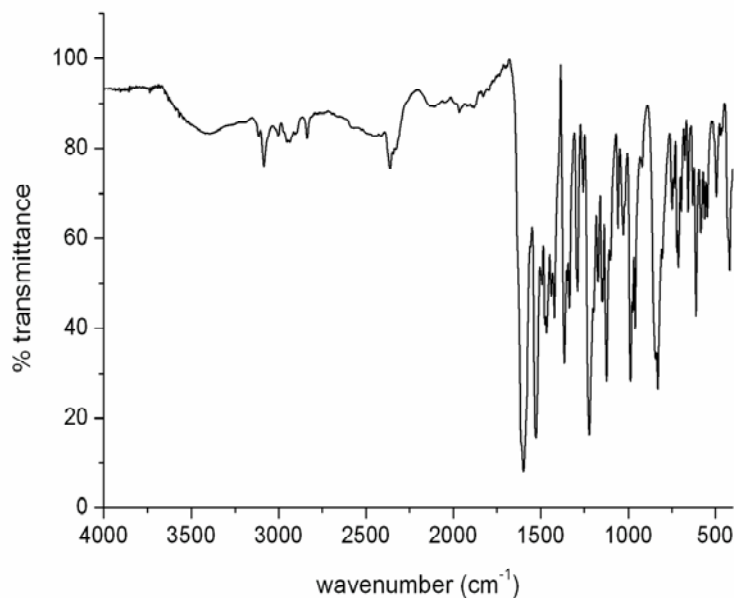
Compound	Polycrystalline state (298 K)	DMF solution (77 K)							α^2	β^2
		g_{\parallel}	g_{\perp}	$g_{iso}g_{av}$	A_{\parallel}^a	A_{\perp}^a	A_{iso}/A_{av}^a			
[VO(hmbn)] ₂ ·H ₂ O (1)	1.985/1.990 (g_{\parallel}, g_{\perp})	1.950	1.984	1.973	148	49	82	0.862	0.951	
[VO(hmbn)(bipy)] (2)	1.989 (g_{iso})	1.953	1.978	1.970	146	48	81	0.875	0.937	
[VO(hmbn)(phen)]·1/2H ₂ O (3)	1.984 (g_{iso})	1.949	1.983	1.972	146	51	83	-----	0.919	
[VO(hman)] ₂ ·H ₂ O (4)	1.991 (g_{iso})	1.951	1.981	1.971	145	51	83	0.895	0.909	
[VO(hman)(phen)]·2H ₂ O (6)	1.990 (g_{iso})	1.948	1.977	1.967	148	55	86	0.908	0.895	
[VO(hmbb)] ₂ ·H ₂ O (7)	1.969/1.984 (g_{\parallel}, g_{\perp})	1.968	1.998	1.988	150	56	88	-----	0.896	
[VO(hmbb)(bipy)] (8)	1.984 (g_{iso})	1.953	1.980	1.971	146	52	84	-----	0.906	
[VO(hmbb)(phen)]·H ₂ O (9)	1.981 (g_{iso})	1.950	1.981	1.971	144	51	82	-----	0.908	
[VO(hmab)] ₂ (10)	1.943/1.981 (g_{\parallel}, g_{\perp})	1.945	1.978	1.967	156	62	93	-----	0.875	
[VO(hmab)(bipy)]·H ₂ O (11)	1.978 (g_{iso})	1.952	1.983	1.973	145	51	82	-----	0.909	
[VO(hmab)(phen)]·2H ₂ O (12)	1.937/1.993	1.946	1.978	1.967	145	50	81	-----	0.922	

3.3.3 Infrared spectra

Selected vibrational bands of the free ligands and their vanadium complexes, which are useful for determining the mode of coordination of the ligands, are given in Table 3.6. Free ligands exhibit bands in the regions 1630-1650, 3025-3075, 3219-33371 cm^{-1} due to C=O, N-H and O-H stretches, respectively. These bands disappear on complexation, indicating the transformation of carbonyl moiety to enolic moiety and consequent replacement of the phenolic and enolic hydrogens by the metal ion [11]. Presence of a band in the region 1515-1550 cm^{-1} , assigned to newly formed C=N due to enolization of the ligands during complexation. Bands appearing in the 1220-1258 cm^{-1} region in the metal complexes was assigned to the $\nu(\text{C-O})$ (enolato) mode [26]. The shifting of $\nu(\text{C=N})$ (azomethine) of the ligands (1600-1604 cm^{-1}) to lower wavenumbers in the metal complexes (1587-1600 cm^{-1}) indicates the coordination of azomethine nitrogen to the metal. A ligand characteristic band at *ca.* 1125 cm^{-1} due to $\nu(\text{N-N})$ stretch undergoes a shift to a higher wavenumbers upon complexation due to diminished repulsion between the lone pairs of adjacent nitrogen atoms [27]. Furthermore, the bands in the regions 548-562 and 422-428 cm^{-1} can be assigned to the stretching modes of the metal to ligand bonds, $\nu(\text{V-O})$ and $\nu(\text{V-N})$, respectively [2]. In addition, the compounds exhibit a strong band in the 940-977 cm^{-1} range due to the terminal V=O stretching, and this is close to the usual range ($960 \pm 50 \text{ cm}^{-1}$) observed for the majority of oxovanadium(IV) complexes [28]. A characteristic feature in the form of a prominent band in the region 833-845 cm^{-1} are also observed for the binuclear complexes **1**, **4**, **7** and **10** due to V-O-V bridge vibrations [29,30]. Fig.3.25 and 3.26 depict the infrared spectra of two of the complexes.

Table 3.6 Selected IR bands (cm^{-1}) with tentative assignments of oxovanadium(IV) complexes

Compound	$\nu(\text{C}=\text{N})$	$\nu(\text{C}=\text{N})^a$	$\nu(\text{V}=\text{O})$	$\nu(\text{C}-\text{O})$	$\nu(\text{V}-\text{O})$	$\nu(\text{V}-\text{N})$
$[\text{VO}(\text{hmbn})_2 \cdot \text{H}_2\text{O}]$ (1)	1600	1531	961	1227	548	427
$[\text{VO}(\text{hmbn})(\text{bipy})]$ (2)	1601	1530	953	1232	560	427
$[\text{VO}(\text{hmbn})(\text{phen})] \cdot 1\frac{1}{2}\text{H}_2\text{O}$ (3)	1596	1524	956	1239	555	424
$[\text{VO}(\text{hman})_2 \cdot \text{H}_2\text{O}]$ (4)	1587	1539	977	1246	562	422
$[\text{VO}(\text{hman})(\text{OCH}_3)_2]$ (5)	1593	1513	950	1233	553	411
$[\text{VO}(\text{hman})(\text{phen})] \cdot 2\text{H}_2\text{O}$ (6)	1597	1524	940	1246	561	428
$[\text{VO}(\text{hmbb})_2 \cdot \text{H}_2\text{O}]$ (7)	1594	1535	951	1221	541	447
$[\text{VO}(\text{hmbb})(\text{bipy})]$ (8)	1597	1520	959	1220	562	419
$[\text{VO}(\text{hmbb})(\text{phen})] \cdot \text{H}_2\text{O}$ (9)	1594	1517	950	1227	560	412
$[\text{VO}(\text{hmab})_2]$ (10)	1593	1549	988	1250	587	459
$[\text{VO}(\text{hmab})(\text{bipy})] \cdot \text{H}_2\text{O}$ (11)	1594	1529	964	1257	567	452
$[\text{VO}(\text{hmab})(\text{phen})] \cdot 2\text{H}_2\text{O}$ (12)	1596	1516	930	1258	559	425

^a newly formed**Fig. 3.25. IR spectrum of compound 1.**

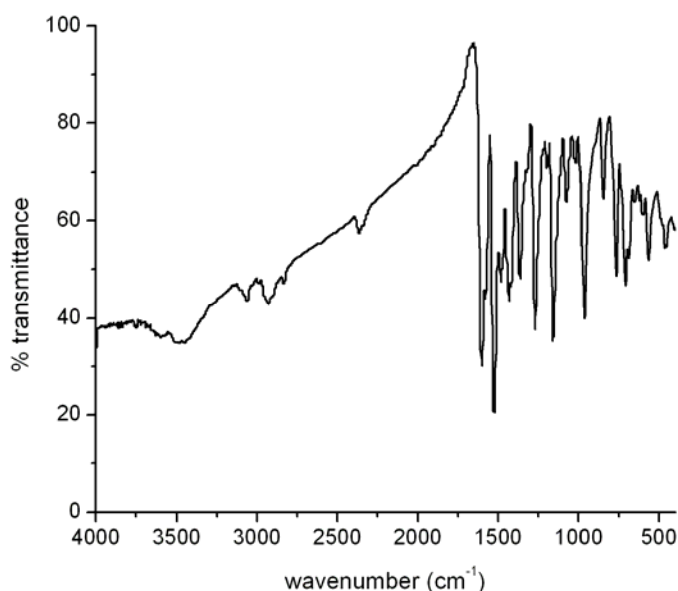


Fig. 3.26. IR spectrum of compound 11.

3.3.4 Electronic spectra

The electronic spectral assignments of the complexes in acetonitrile solution are presented in the Table 3.7. In VO^{2+} complexes vanadium is in +4 oxidation state with the electronic structure $[\text{Ar}] 3d^1$. The expected coordination numbers in oxovanadium complexes are five and six. Most of the oxovanadium complexes show three prominent bands in the electronic spectral region and Selbin has classified these as band I (11,000-16,000 cm^{-1}), band II (15,000-18,000 cm^{-1}) and band III (24,000 – 29,000 cm^{-1}) [31]. According to Ballhausen and Grey, band I is assigned as, ${}^2E \leftarrow {}^2B_2 (d_{xy} \rightarrow d_{xz}, d_{yz})$, band II as ${}^2B_1 \leftarrow {}^2B_2 (d_{xy} \rightarrow d_{x^2-y^2})$ and band III as ${}^2A_1 \leftarrow {}^2B_2 (d_{xy} \rightarrow d_{z^2})$. But the 2E and 2B_1 levels may be very close in energy and may cross results a weak broad band. The third band is not always observed and being buried beneath a high intensity charge transfer band [31,32].

The intraligand transitions are found to be slightly shifted in complexes and they are observed in between 30,130 – 44,490 cm^{-1} . In all the complexes an intense band at *ca.* 24900 cm^{-1} is assignable to the phenolic oxygen $\rightarrow V_{(dn)}$ ligand to metal charge transfer (LMCT) band [33,34]. In complexes **1**, **2**, **4**, **6**, **7** and **12**, weak *d-d* bands are observed in between 15180-18520 cm^{-1} . In other complexes, expected *d-d* bands are not found and are probably obscured by the tail of the LMCT absorption. Electronic spectra of some complexes are presented in Figs. 3.27- 3.30.

Table 3.7 Electronic spectral assignments of oxovanadium(IV/V) complexes

Compound	Intraligand transitions	LMCT	<i>d-d</i>
[VO(hmbn)] ₂ ·H ₂ O (1)	30130, 37430, 44490	24540	17030
[VO(hmbn)(bipy)] (2)	30260, 33590, 43200	24320	17650
[VO(hmbn)(phen)]·1½H ₂ O (3)	30360, 37270, 44140	24420	-----
[VO(hman)] ₂ ·H ₂ O (4)	30200, 37180, 44100	24660	17630
[VO(hman)(OCH ₃) ₂] (5)	30550(sh), 34630, 42380	25400	
[VO(hman)(phen)]·2H ₂ O (6)	30650, 37080, 43800	25110	17650
[VO(hmhb)] ₂ ·H ₂ O (7)	30600, 36590, 41590	25250	15180
[VO(hmhb)(bipy)] (8)	30450, 34130(sh), 36780, 43310	24370	-----
[VO(hmhb)(phen)]·H ₂ O (9)	30500(sh), 33250, 41590	24420	-----
[VO(hmab)] ₂ (10)	30400, 33750, 44410	25790	-----
[VO(hmab)(bipy)]·H ₂ O (11)	30600, 34520, 42230	25450	-----
[VO(hmab)(phen)]·2H ₂ O (12)	30650, 33730(sh), 36980, 43511	25050	18520

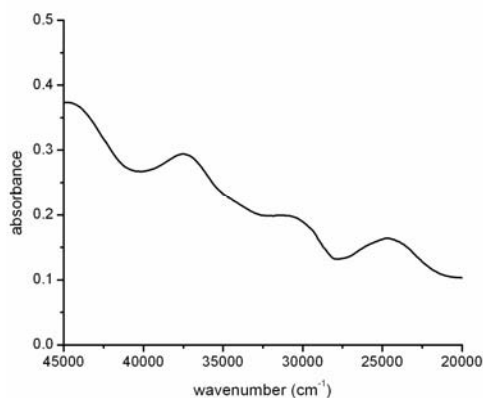


Fig. 3.27. Electronic spectrum of compound 1.

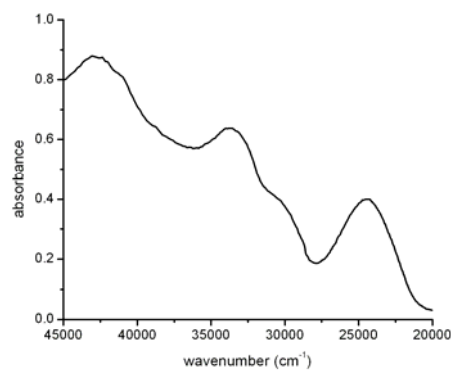


Fig. 3.28. Electronic spectrum of compound 2.

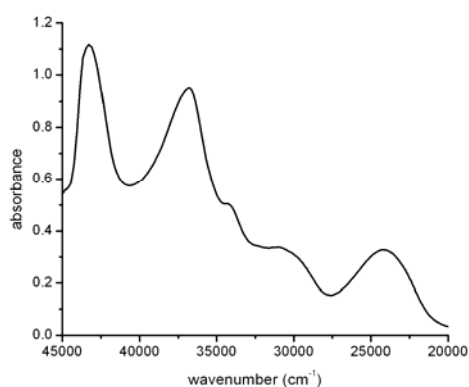


Fig. 3.29. Electronic spectrum of compound 11.

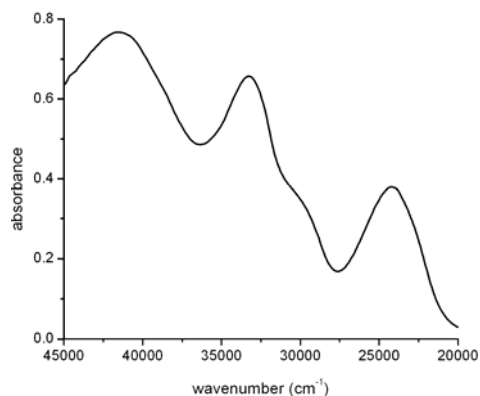


Fig. 3.30. Electronic spectrum of compound 12.

3.3.5 Thermal analyses

Thermal behaviors of the complexes were investigated by TG-DTA measurements under N_2 atmosphere in the temperature range of 50-800 °C. The nature of water in hydrated complexes can be explained with the help of thermal analyses. In complexes **1**, **3**, **4**, **6**, **7**, **9**, **11** and **12** weight loss is observed in between 50-120 °C suggest the presence of water molecules outside the

coordination sphere [35,36]. Weight losses due to the decomposition of ligands were found over 250 °C. The decomposition was not seen to be completed even after 800 °C. TG-DTG curves of complexes **1** and **2** are shown in Figs. 3.31 and 3.32 respectively.

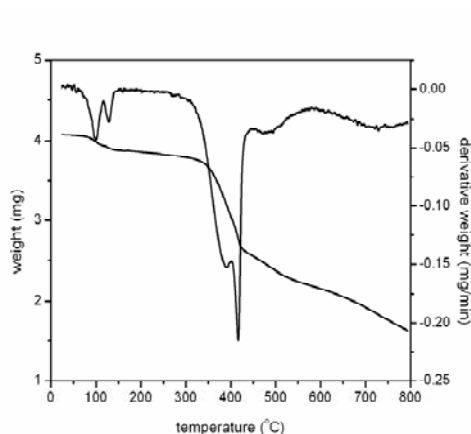


Fig. 3.31. TG-DTG plots of compound 1.

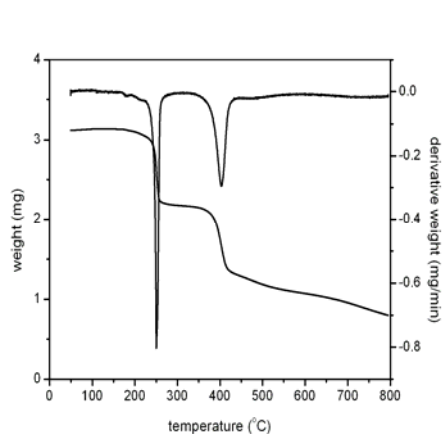


Fig. 3.32. TG-DTG plots of compound 2.

References

1. D. Rehder, *Bioinorganic Vanadium Chemistry*, Wiley, Chichester, 2008.
2. E.J. Baran, *J. Coord. Chem.* 54 (2001) 215-238.
3. A.S. Tracey, G.R. Willsky, E.S. Takeuchy, *Vanadium chemistry biochemistry pharmacology and practical applications*, CRC/Taylor & Francis, 2007.
4. T. Hirao, M. Mori, Y. Oshiro, *J. Org. Chem.* 55 (1990) 358-360.
5. P. Adão, M.R. Maurya, U. Kumar, F. Avecilla, R.T. Henriques, M.L. Kusnetsov, J.C. Pessoa, I. Correia, *Pure Appl. Chem.* 81 (2009) 1279–1296.
6. D. Rehder, *Coord. Chem. Rev.* 182 (1999) 297-322.

7. D. Rehder, J.C. Pessoa, C.F.G.C. Geraldés, M.M.C.A. Castro, T. Kabanos, T. Kiss, B. Meier, G. Micera, L. Pettersson, M. Rangel, A. Salifoglou, I. Turel, D. Wang, *J. Biol. Inorg. Chem.* 7 (2002) 384–396.
8. V. Badmaev, S. Prakash, M. Majeed, *J. Altern. Complem. Med.* 5 (1999) 273-291.
9. D. Rehder, *Inorg. Chem. Commun.* 6 (2003) 604–617.
10. M.R. Maurya, S. Agarwal, M. Abid, A. Azam, C. Bader, M. Ebel, D. Rehder, *Dalton Trans.* (2006) 937-947.
11. P.K. Samal, A.K. Patra, M. Nethaji, A.R. Chakravarthy, *Inorg. Chem.* 46 (2007) 11112-11121.
12. P.B. Sreeja, M.R.P. Kurup, *Spectrochim. Acta A* 61 (2005) 331-336.
13. S.N. Rao, D.D. Mishra, R.C. Maurya, N.N. Rao, *Polyhedron* 16 (1997) 1825-1829.
14. D. Nicholls, *Coord. Chem. Rev.* 1 (1966) 379-414.
15. S.N. Chol, Y.I. Kim, Y.B. Shim, H.S. Choo, Y.J. Kim, *Bull. Korean Chem. Soc.* 10 (1989) 138-142.
16. W.J. Geary, *Coord. Chem. Rev.* 7 (1971) 81-122.
17. C. Tsiamis, B. Voulgaropoulos, D. Charistos, G.P. Voutsas, C.A. Kavounis, *Polyhedron* 19 (2000) 2003-2010.
18. S. Mondal, M. Mukherjee, K. Dhara, S. Ghosh, J. Ratha, P. Banerjee, A.K. Mukherjee, *Cryst. Growth Des.* 7 (2007) 1716-1721.
19. A Sreekanth, S. Sivakumar, M.R.P. Kurup, *J. Mol. Struct.* 655 (2003) 47-58.
20. D. Cremer, J.A. Pople, *J. Am. Chem. Soc.* 97 (1975) 1354-1358.

21. D. Mustafi, M.W. Makinen, *Inorg. Chem.* 44 (2005) 5580-5590.
22. G. Swarnabala, M.V. Rajasekharan, *Inorg. Chem.* 28 (1989) 662-666.
23. T. Ghosh, S. Bhattacharya, A. Das, G. Mukherjee, M.G.B. Drew, *Inorg. Chim. Acta* 358 (2005) 989-996.
24. N. Raman, J.D. Raja, A. Sakthivel, *J. Chem. Sci.* 119 (2007) 303-310.
25. S.K. Dutta, E.R.T. Tiekink, M. Chaudhury, *Polyhedron* 16 (1997) 1863-1871.
26. T. Ghosh, *Trans. Met. Chem.* 31 (2006) 560-565.
27. P.B. Sreeja, M.R.P. Kurup, A. Kishore, C. Jasmin, *Polyhedron* 23 (2004) 575-581.
28. A. Syamal, K. S. Kale, *Inorg. Chem.* 18 (1979) 992 - 995.
29. S.K. Dutta, S.B. Kumar, S. Bhattacharyya, E.R.T. Tiekink, M. Chaudhury, *Inorg. Chem.* 36 (1997) 4954-4960.
30. N.A. Mangalam, S. Sivakumar, S.R. Sheeja, M.R.P. Kurup, E.R.T. Tiekink, *Inorg. Chim. Acta* 362 (2009) 4191- 4197.
31. J. Selbin, *Chem. Rev.* 65 (1965) 153-175.
32. C.J. Ballhausen, H.B. Grey, *Inorg. Chem.* 1 (1962) 111-122.
33. F.A. Walker, R.L. Carlin, P.H. Rieger, *J. Chem. Phys.* 45 (1966) 4181-4189.
34. M. Kuriakose, M.R.P. Kurup, E. Suresh, *Polyhedron* 26 (2007) 2713-2718.
35. X.F. Chen, P. Cheng, X. Liu, B. Zhao, D.Z. Liao, P.P. Yan, Z.H. Jiang, *Inorg. Chem.* 40 (2001) 2652-2659.
36. H.J. Choi, M.P. Suh, *Inorg. Chem.* 38 (1999) 6309-6312.

SYNTHESES AND CHARACTERIZATION OF Mn(II) AND Fe(III) COMPLEXES OF ONO DONOR ACYLHYDRAZONES

- 4.1 Introduction
- 4.2 Experimental
- 4.3 Results and discussion
- References

4.1 Introduction

Manganese is an essential and one of the least toxic trace elements. Its deficiency leads to diseases like skeletal abnormalities and depressed reproductive functions. It is an activator of a number of metalloenzymes like arginase in the liver, glutamine synthase in the brain, pyruvate carboxylase etc. Due to its action as an activator of superoxide dismutase (SOD), it is necessary for normal antioxidant defenses [1-3]. The production of oxygen by photosynthetic plants is a striking symbol of life on earth. The oxygen evolving complex (OEC) with four manganese centers of photosystem II catalyses the oxidation of water in photosynthesizing organisms [4,5]. Manganese complexes play an important role in industrial catalysis. Complexes of manganese with non-heme ligands are found to be effective catalysts in olefin epoxidation and alkane hydroxylation [6-8].

The coordination chemistry of manganese with N and/or O containing ligands has been getting a great deal of interest, due to the structural diversity of manganese complexes and the importance of manganese enzyme models, the possibility of magnetic coupling interactions, and the application of manganese

compounds in industrial catalysis [9-13]. The fascinating chemistry of manganese is due to its ability to exhibit variety of oxidation states ranging from +2 to +7. Among these different oxidation states, +2 is the most stable and dominant oxidation state. Most of the Mn(II) complexes are high spin complexes with d^5 configuration because of the extra stability of half filled d electron configuration. Six coordinate manganese(II) complexes are most common, while complexes with lower coordination numbers are somewhat rare.

Iron is one of the most important elements in body and it is essential for almost all types of cells. The physiological functions of two major iron heme proteins, myoglobin and hemoglobin are oxygen storage and transport respectively. Cytochromes, a group of iron heme proteins play significant role in biological electron transfer reactions [14]. Iron is an essential element for brain cells, and the shortage or excess of iron have been associated with different brain disorders like restless legs syndrome, Alzheimer disease, Parkinson disease etc. [15]. Importance of studies on iron hydrazone complexes is based on the iron chelating efficiency of hydrazones and their application in the treatment of iron overload diseases [16,17]. The catalytic applications of metallic iron and its oxides are best described by the synthesis of ammonia by Haber process and hydrocarbons by Fischer-Tropsch synthesis.

The most common oxidation states of iron are +2 has a d^6 outer electronic configuration and +3 has d^5 outer electronic configuration referred to as ferrous and ferric iron respectively. The most common geometry associated with both the oxidation states is octahedral, although there are reports on four, five, seven and even eight coordination.

4.2 Experimental

4.2.1 Materials

2-Hydroxy-4-methoxyacetophenone (Aldrich), 2-hydroxy-4-methoxybenzaldehyde (Aldrich), nicotinic acid hydrazide (Aldrich), benzhydrazide (Aldrich), manganese(II) acetate tetrahydrate (Merck), ferric chloride (Himedia), ferric nitrate nonahydrate (S.D fine) were used as received. Solvents used were methanol and ethanol.

4.2.2 Syntheses of the acylhydrazones

The syntheses of acylhydrazones were done as described in Chapter 2.

4.2.3 Syntheses of manganese(II) complexes

[Mn(Hhmbn)₂·H₂O (13): Methanolic solutions of H₂hmbn·H₂O (0.289 g, 1 mmol) and Mn(CH₃COO)₂·4H₂O (0.245 g, 1 mmol) were mixed and refluxed for 6 hrs. The dark brown colored product obtained was filtered, washed with methanol, followed by ether and dried over P₄O₁₀ *in vacuo*. Elemental Anal. Found (Calcd.) (%): C, 55.40 (55.00); H, 3.68 (3.96); N, 13.75 (13.74).

[Mn(Hhmbb)₂·H₂O (14): To a methanolic solution Mn(CH₃COO)₂·4H₂O (0.245 g, 1 mmol), H₂hmbb (0.270 g, 1 mmol) in methanol was added and the resulting brown colored solution is refluxed for 6 hrs. The dark brown colored product obtained was filtered, washed with methanol, followed by ether and dried over P₄O₁₀ *in vacuo*. Elemental Anal. Found (Calcd.) (%): C, 58.74 (59.12); H, 4.50 (4.30); N, 9.01 (9.19).

4.2.4 Syntheses of iron(III) complexes

[Fe(Hhmbn)Cl₂] (15): To an ethanolic solution of FeCl₃ (0.162 g, 1 mmol), H₂hmbn·H₂O (0.289 g, 1 mmol) in methanol was added and refluxed for 5 hrs. Black colored product obtained was filtered, washed with methanol, followed by ether and dried over P₄O₁₀ *in vacuo*. Elemental Anal. Found (Calcd.) (%): C, 42.25 (42.25); H, 3.80 (3.29); N, 10.77 (10.56).

[Fe(Hhmbn)₂NO₃]·2H₂O (16): This complex was prepared by refluxing a mixture of Fe(NO₃)₃·9H₂O (0.404 g, 1 mmol) in ethanol and H₂hmbn·H₂O (0.289 g, 1 mmol) in methanol for 5 hrs. The product separated was black colored solid and it was filtered, washed with methanol, followed by ether and dried over P₄O₁₀ *in vacuo*. Elemental Anal. Found (Calcd.) (%): C, 48.58 (48.43); H, 4.18 (4.06); N, 14.27 (14.12).

[Fe(Hhman)Cl₂] (17): This complex was prepared by the same procedure as that of compound **15**. Color of the compound is dark brown. Elemental Anal. Found (Calcd.) (%): C, 43.85 (43.83); H, 2.99 (3.43); N, 10.49 (10.22).

Fe(Hhman)₂NO₃]·H₂O (18): This complex was prepared by the same procedure as that of compound **16**. Color of the compound is black. Elemental Anal. Found (Calcd.) (%): C, 54.28 (54.71); H, 4.21 (4.59); N, 9.34 (9.97).

[Fe(Hhmab)Cl₂(C₂H₅OH)] (19): This complex was prepared by refluxing a mixture of FeCl₃ (0.162 g, 1 mmol) in ethanol and H₂hmab (0.284 g, 1 mmol) in methanol for 5 hrs. Few single crystals of the compound were isolated after two days from the resulting dark brown solution and its structure was determined by single crystal X-ray diffraction. As the quantity of the product was small, we could not undertake other studies.

4.3 Results and discussion

Two manganese(II) complexes and five iron complexes were prepared using different acylhydrazones. The analytical data indicate that the observed C, H, N values of the complexes were in close agreement with that of the formula suggested. Magnetic susceptibility measurements of the compounds suggest the paramagnetic nature to the complexes with a d^5 high spin configuration. The non-electrolytic nature of the compounds was proved by molar conductivity measurements in 10^{-3} M DMF solution [18]. Table 4.1 summarizes the molar conductivities and magnetic susceptibilities of the complexes. Single crystals of one of the iron(III) compounds $[\text{Fe}(\text{Hhman})\text{Cl}_2(\text{C}_2\text{H}_5\text{OH})]$, were isolated from the reaction mixture and its structure was determined

Table 4.1 Molar conductivities and magnetic susceptibilities of Mn(II) and Fe(III) complexes

Compound	$\lambda_m^{\#}$	μ_{eff} (B.M.)
$[\text{Mn}(\text{Hhmbn})_2] \cdot \text{H}_2\text{O}$ (13)	12	5.93
$[\text{Mn}(\text{Hhmbb})_2] \cdot \text{H}_2\text{O}$ (14)	14	5.86
$[\text{Fe}(\text{Hhmbn})\text{Cl}_2]$ (15)	21	5.79
$[\text{Fe}(\text{Hhmbn})_2\text{NO}_3] \cdot 2\text{H}_2\text{O}$ (16)	18	5.74
$[\text{Fe}(\text{Hhman})\text{Cl}_2]$ (17)	16	5.87
$[\text{Fe}(\text{Hhman})_2\text{NO}_3] \cdot \text{H}_2\text{O}$ (18)	19	5.85

[#]molar conductivity (in $\text{mho cm}^2 \text{mol}^{-1}$) taken in 10^{-3} M DMF solution.

4.3.1 Spectral characterization of Mn(II) complexes

4.3.1a EPR spectral studies

Electron paramagnetic resonance (EPR) spectroscopy is one of the few techniques that can selectively sense and be used to characterize Mn(II) ions. The Mn(II) state possesses Kramers doublets and exhibits characteristic transitions in the normal X-band regime. The spin Hamiltonian for Mn(II) [19] may be defined by the equation

$$\hat{H} = g\beta BS + D[S_z^2 - S(S+1)/3] + E(S_x^2 - S_y^2)$$

where B - magnetic field vector, g - spectroscopic splitting factor, β - Bohr magneton, D - axial zero field splitting parameter, E - rhombic zero field splitting parameter and S - electron spin vector.

In the case of weak field ligands, Mn(II) ions give a single transition with $g \approx 2$, which is split into six hyperfine lines by ^{55}Mn (nuclear spin $I=5/2$). But this is the case only when the ligand environment is a cubic one, *ie.* the zero field splitting parameter D is negligible resulting degenerate $\Delta M_s = \pm 1$ transitions. If D is small and finite degeneracy is removed the spectrum displays five fold fine structure. However, in the case when D is comparable to $h\nu$ the Mn^{2+} system exhibits tetragonal spectrum with two g values, *ie.* $g_{\parallel} \approx 2$ and $g_{\perp} \approx 6$ [20,21].

EPR spectra of both the complexes were taken in polycrystalline state at 298 K and DMF at 77 K. But in polycrystalline state spectra of both the compounds were very broad.

EPR spectrum of compound **13** in DMF at 77 K is shown in Fig. 4.1. In this spectrum only a single sextet is observed due to electron spin-nuclear spin coupling. In addition to this a pair of low intensity lines is observed in-between

two major hyperfine splitting. These forbidden lines corresponds to $\Delta M_I = \pm 1$ transitions, due to the mixing of the nuclear hyperfine levels by the zero field splitting parameter D of the Hamiltonian [22]. In this case the observed g value is 1.998, and it is very close to the free electron g value. And the hyperfine coupling constant A is found to be $95 \times 10^{-4} \text{ cm}^{-1}$ consistent with an octahedral environment.

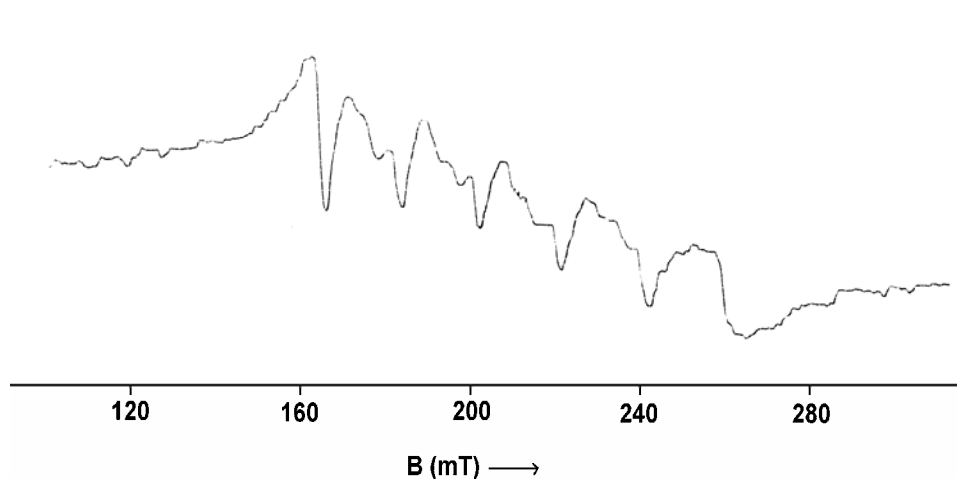


Fig. 4.1. EPR spectrum of compound 13 in DMF at 77 K.

Compound **14** exhibits a spectrum (Fig. 4.2) similar to that of compound **13**, in DMF at 77 K. Here the hyperfine splitting constant is found to be $97 \times 10^{-4} \text{ cm}^{-1}$ and it is lower than that of pure ionic compounds reflect the covalent nature of metal-ligand bonds [23,24]. The g value of the compound is 2.199, close to free electron g value indicating the absence of spin-orbit coupling.

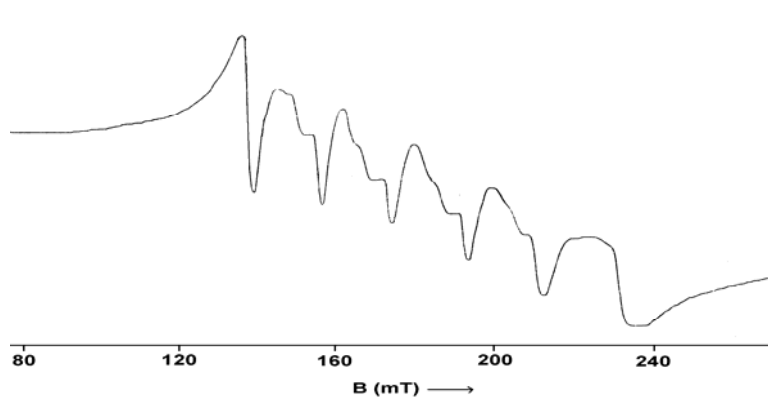


Fig. 4.2. EPR spectrum of compound 14 in DMF at 77 K.

4.3.1b Infrared spectra

Infrared spectral assignments of the compounds are listed in Table 4.2. Bands in the range 1630-1645 cm^{-1} assigned to carbonyl group in free hydrazones are shifted to lower energy with the formation of the complexes suggest that the coordination of amido oxygen to the metal centre [25,26]. Bands correspond to NH group in free hydrazones are shifted to lower wavenumbers suggest that, in complexes ligands are in amido form. Lower shift in azomethine stretching frequency indicates the coordination of azomethine nitrogen to the metal centre [27]. Presence of water molecules in complexes **13** and **14** are evident from presence of broad bands at 3440 and 3410 cm^{-1} respectively. In both the complexes, metal-nitrogen and metal-oxygen bands are centered on 575 and 506 cm^{-1} respectively [28]. IR spectra of compounds **13** and **14** are shown in Figs 4.3 and 4.4.

Table 4.2 Infrared spectral assignments (cm^{-1}) of Mn(II) complexes.

Compound	$\nu(\text{C}=\text{O})$	$\nu(\text{C}=\text{N})$	$\nu(\text{N}-\text{H})$	$\nu(\text{Mn}-\text{N})$	$\nu(\text{Mn}-\text{O})$
H ₂ hmbn·H ₂ O	1643	1604	3074	----	----
[Mn(Hhmbn) ₂]·H ₂ O (13)	1630	1590	3014	575	505
H ₂ hmbb	1630	1600	3038	----	----
[Mn(Hhmbb) ₂]·H ₂ O (14)	1623	1580	3014	576	507

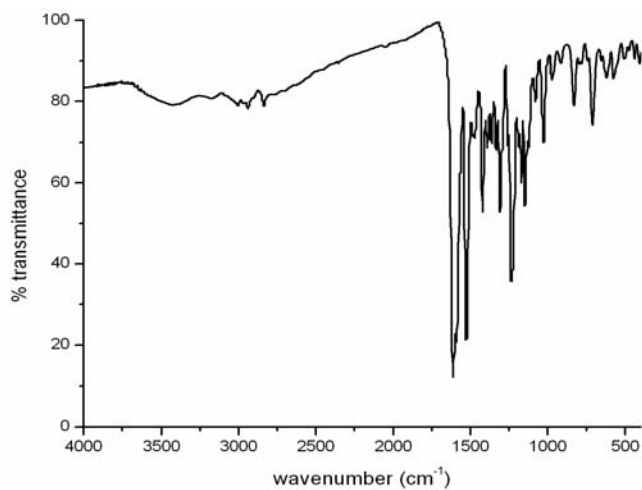


Fig. 4.3. IR spectrum of compound 13.

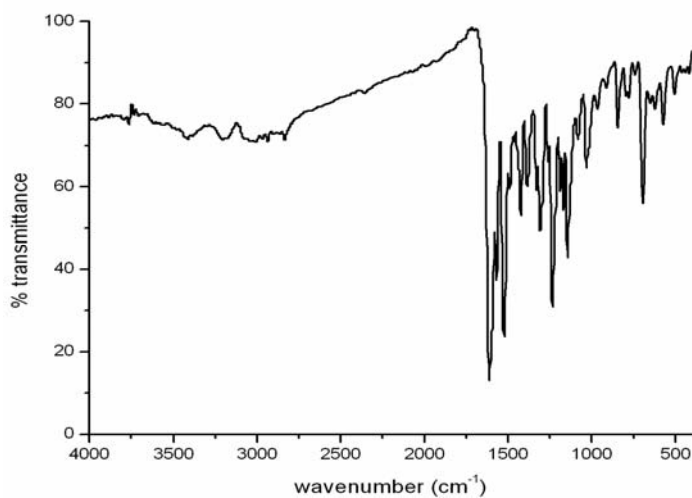


Fig. 4.4. IR spectrum of compound 14.

4.3.1c Electronic spectra

In d^5 high spin Mn(II) complexes, the ground state term is ${}^6A_{1g}$. Because of the absence of excited states of same spin multiplicity, electronic transitions associated with Mn(II) complexes are spin forbidden. Thus for octahedral manganese(II) complexes $d-d$ transitions are doubly forbidden (spin as well as

parity). Absorptions associated with doubly forbidden transitions are very weak. However some forbidden transitions can occur to the quartet excited states and they are ${}^4A_{1g}(G), {}^4E_g(G) \leftarrow {}^6A_{1g}, {}^4E_g(D) \leftarrow {}^6A_{1g}, {}^4T_{1g}(G) \leftarrow {}^6A_{1g}$ and ${}^4T_{2g}(G) \leftarrow {}^6A_{1g}$ [29]. Electronic spectra of both the complexes were taken in acetonitrile solution ($50000\text{-}20000\text{ cm}^{-1}$) as well as in DMF solution ($20000\text{-}10000\text{ cm}^{-1}$) and the spectral data is listed in Table 4.3. For the complexes **13** and **14**, weak *d-d* bands are observed at 16350 and 16300 cm^{-1} respectively. Electronic spectra of the complexes are shown in Fig. 4.5.

Table 4.3 Electronic spectral assignments (cm^{-1}) of Mn(II) complexes

Compound	Intraligand transitions	LMCT	<i>d-d</i>
[Mn(Hhmbn) ₂] \cdot H ₂ O (13)	30630, 38510, 43160	24180	16350
[Mn(Hhmbb) ₂] \cdot H ₂ O (14)	31120, 38820, 43280	23570	16300

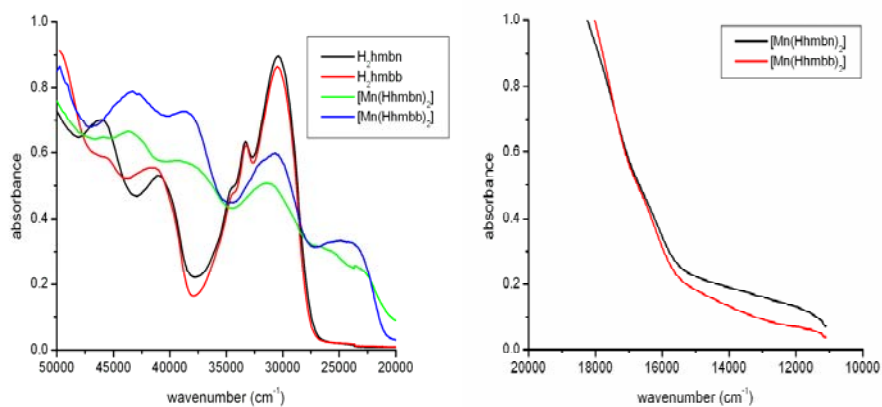


Fig. 4.5. Comparative electronic spectra of the complexes **13 and **14** with ligands in acetonitrile solution in the region $50000\text{-}20000\text{ cm}^{-1}$ (left), *d-d* spectra of complexes **13** and **14** in DMF solution in the region $20000\text{-}10000\text{ cm}^{-1}$ (right).**

4.3.2 Thermal analyses

Thermogravimetric techniques are based on the change in weight of the substances with respect to temperature or time. Thermogravimetric analyses are used to (i) get information regarding thermal stability of these new complexes, (ii) decide whether the water molecules (if present) are inside or outside the inner coordination sphere of the central metal ion and (iii) suggest a general scheme for thermal decomposition of the ligands. The thermogram of both the complexes has a weight loss in between 50-130 °C suggests that the water molecules are outside the coordination sphere [30]. Both the complexes were found to be thermally stable and decomposition starts from 250 °C. TG-DTG curves of compound **14** are shown in Fig. 4.6.

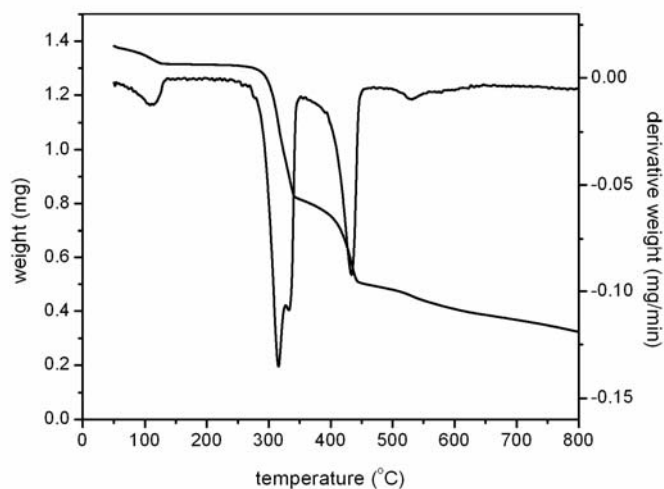


Fig. 4.6. TG-DTG plots of compound 14.

4.3.3 Crystal structure of the compound [Fe(Hhmab)Cl₂(C₂H₅OH)] (19)

A perspective view of the molecular structure of the compound with atom numbering scheme is illustrated in Fig. 4.7, and the key crystallographic

informations are summarized in Table 4.4. Compound **19** crystallized in to triclinic space group $P\bar{1}$ with $Z = 2$. The complex exhibits distorted octahedral geometry around Fe(III) centre. Equatorial plane of the octahedron is defined by the atoms O1, N1 and O3 from the ligand and one of the chlorine atoms Cl1. The apical positions are occupied by O4 from ethanol and Cl2. In this compound ligand is tricoordinated and in monodeprotonated amido form, which is evident from the C9–O3 bond length (1.247 Å) corresponds to double bond length, and C7–N1 bond length (1.299 Å) comparable to that of similar compounds containing azomethine linkage [31]. The Fe–O_{phenolate} bond length in this compound is 1.8601 Å, shorter than the average octahedral Fe^{III}–O_{phenolate} bond length of ~ 1.98 Å, suggests strong iron-oxygen overlap [32-34]. Relevant bond lengths and angles are given in Table 4.5. The substantial deviation from the ideal geometry of the compound is reflected in the trans angles values, O(1)–Fe(1)–O(3) 157.14(8)°, N(1)–Fe(1)–Cl(1) 168.09(6)° and O(4)–Fe(1)–Cl(2) 171.25(6)°.

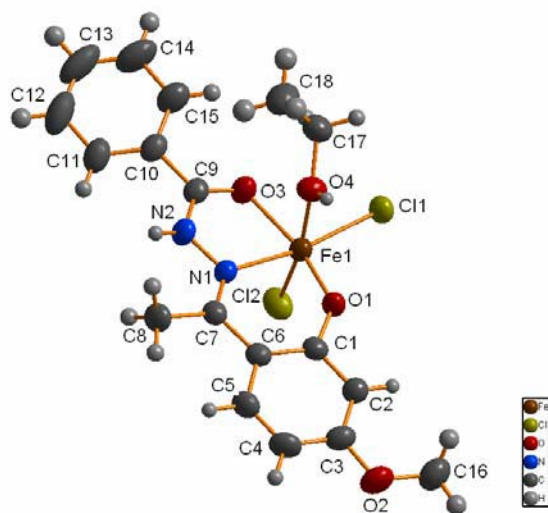


Fig. 4.7. Structure and labeling scheme for [Fe(Hhmab)Cl₂(C₂H₅OH)] (**19**).

**Table 4.4 Crystal data and structure refinement parameters for
[Fe(Hhmab)Cl₂(C₂H₅OH)] (19)**

Empirical formula	C ₁₈ H ₂₁ Cl ₂ FeN ₂ O ₄
Formula weight	456.12
Temperature	298(2) K
Wavelength	0.71073 Å
Crystal system	Triclinic
Space group	<i>P</i> ₁
Unit cell dimensions	a = 7.4497(15) Å b = 11.611(2) Å c = 12.058(2) Å α = 87.62(3)° β = 79.41(3)° γ = 74.79(3)°
Volume	989.4(3) Å ³
Z	2
Density (calculated)	1.531 Mg/m ³
Absorption coefficient	1.058 mm ⁻¹
F(000)	470
Crystal size	0.30 x 0.21 x 0.13 mm ³
θ range for data collection Index ranges	1.72 to 25.9° -9 ≤ h ≤ 9, -14 ≤ k ≤ 14, -14 ≤ l ≤ 14
Reflections collected	8901
Independent reflections	3839 [R(int) = 0.0230]
Refinement method	Full-matrix least-squares on F ²
Data / restraints / parameters	3766 / 0 / 256
Goodness-of-fit on F ²	1.021
Final R indices [I > 2σ(I)]	R ₁ = 0.0385, wR ₂ = 0.0946
R indices (all data)	R ₁ = 0.0503, wR ₂ = 0.1008
Largest diff. peak and hole	0.377 and -0.213 e.Å ⁻³

$$R_1 = \frac{\sum ||F_o| - |F_c||}{\sum |F_o|}$$

$$wR_2 = [\frac{\sum w(F_o^2 - F_c^2)^2}{\sum w(F_o^2)^2}]^{1/2}$$

Table 4.5 Selected bond lengths (Å) and bond angles (°) for the compound 19

<i>Bond lengths</i>		<i>Bond angles</i>		<i>Bond angles</i>	
Fe(1)–O(1)	1.8601(17)	O(1)–Fe(1)–O(3)	157.14(8)	N(1)–Fe(1)–Cl(2)	94.39(6)
Fe(1)–O(3)	2.0302(17)	O(1)–Fe(1)–N(1)	83.20(8)	O(4)–Fe(1)–Cl(2)	171.25(6)
Fe(1)–N(1)	2.1550(19)	O(3)–Fe(1)–N(1)	75.97(7)	Cl(1)–Fe(1)–Cl(2)	96.59(4)
Fe(1)–O(4)	2.2140(2)	O(1)–Fe(1)–O(4)	87.41(9)	C(1)–O(1)–Fe(1)	135.06(15)
Fe(1)–Cl(1)	2.3118(10)	O(3)–Fe(1)–O(4)	80.66(8)	C(3)–O(2)–C(16)	117.8(2)
Fe(1)–Cl(2)	2.2920(10)	N(1)–Fe(1)–O(4)	82.37(8)	C(9)–O(3)–Fe(1)	117.97(15)
O(3)–C(9)	1.247(3)	O(1)–Fe(1)–Cl(1)	99.32(6)	C(17)–O(4)–Fe(1)	124.68(18)
O(1)–C(1)	1.316(3)	O(3)–Fe(1)–Cl(1)	99.25(6)	C(7)–N(1)–Fe(1)	131.71(16)
O(4)–C(17)	1.449(3)	N(1)–Fe(1)–Cl(1)	168.09(6)	N(2)–N(1)–Fe(1)	109.93(14)
N(1)–C(7)	1.299(3)	O(4)–Fe(1)–Cl(1)	86.10(6)	C(9)–N(2)–N(1)	116.3(2)
N(1)–N(2)	1.385(3)	O(1)–Fe(1)–Cl(2)	100.32(7)	O(1)–C(1)–C(6)	123.2(2)
N(2)–C(9)	1.341(3)	O(3)–Fe(1)–Cl(2)	90.68(6)	C(1)–C(6)–C(7)	123.4(2)
				N(2)–C(9)–O(3)	119.7(2)

Table 4.6 Interaction parameters of the compound 19

C–H...π interactions			
C–H(I)...Cg(J)	H...Cg (Å)	C–H...Cg (°)	C...Cg (Å)
C(8)–H(8C)...Cg(3) ^a	2.84	146	3.675(3)

Equivalent position codes : ^a = -x, 1-y, 1-z
 Cg(3) = C(1), C(2), C(3), C(4), C(5), C(6)

H bonding				
D–H...A	D–H	H...A	D...A	D–H...A
O(4)–H(4)...Cl(1)	0.71	2.62(3)	3.267(2)	152(2)
C(5)–H(5)...Cl(2)	0.93	2.81	3.702(3)	161
C(17)–H(17b)...O(1)	0.97	2.38	3.346(3)	175
C(17)–H(17a)...O(3)	0.97	2.55	3.077(3)	114

(D=Donor, A=acceptor, Cg=Centroid)

The mean plane deviation calculation shows that the atoms in the basal plane O3, N1, O1 and C11 are nearly planar and Fe1 is slightly deviated from planarity with a distance of 0.2065(3) Å. The mode of molecular association of compound **19** along *a* axis is illustrated in Fig. 4.8. A beautiful arrangement of molecules in the crystal system in a quadruple cell along *a* axis is shown in Fig. 4.9. In the crystal, molecules are connected *via* O–H···Cl, C–H···Cl and C–H···O interactions (Fig. 4.10) and the interaction parameters are summarized in Table 4.6. The C–H···Cl and C–H···O distances and bond angles are in good agreement with relevant reports [35-37], and play a significant role in crystal packing. Packing of the compound is also stabilized by C–H··· π interactions.

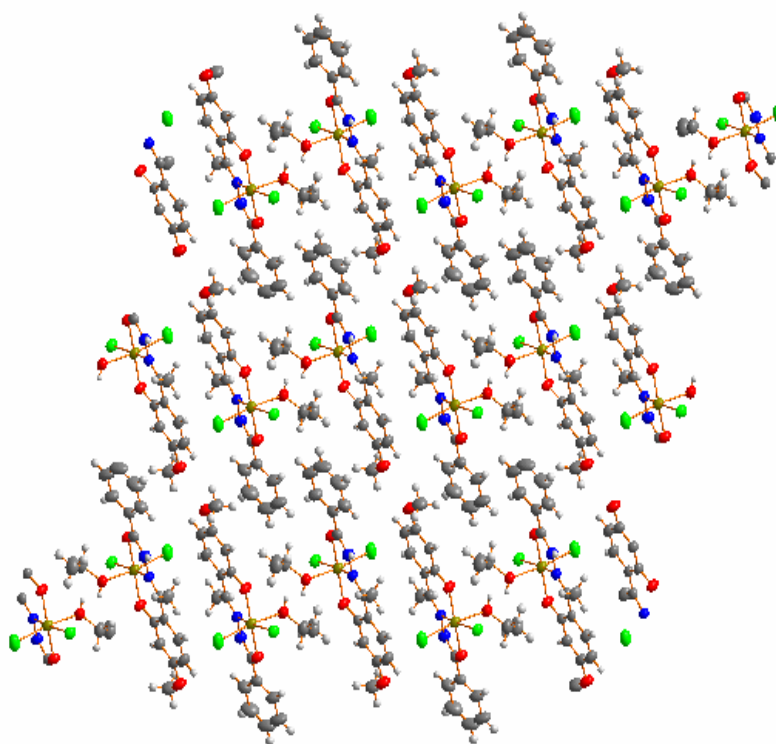


Fig. 4.8. Packing diagram of [Fe(Hhmab)Cl₂(C₂H₅OH)] (**19**) along *a* axis.

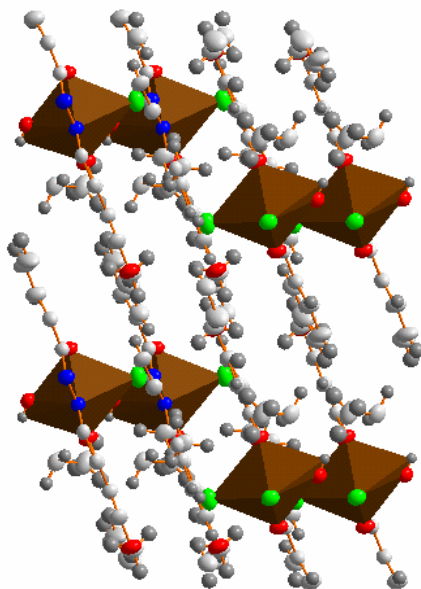


Fig. 4.9. Quadruple cell packing of the compound
 $[\text{Fe}(\text{Hhmab})\text{Cl}_2(\text{C}_2\text{H}_5\text{OH})]$ (19) viewed along a axis.

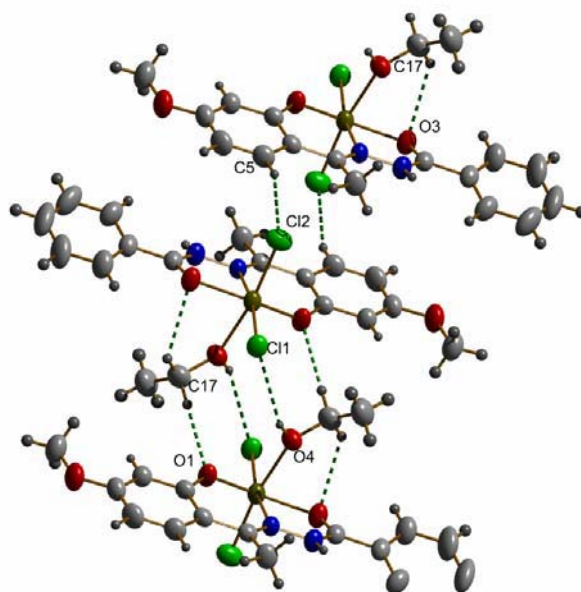


Fig. 4.10. Hydrogen bonding interactions of the compound
 $[\text{Fe}(\text{Hhmab})\text{Cl}_2(\text{C}_2\text{H}_5\text{OH})]$ (19).

4.3.4 Spectral characterization of Fe(III) complexes

4.3.4a EPR spectral studies

The spin Hamiltonian for d^5 high spin Fe(III) is same as that of spin Hamiltonian of Mn(II)

$$\text{i.e. } \hat{H} = g\beta BS + D[S_z^2 - S(S+1)/3] + E(S_x^2 - S_y^2)$$

where B - magnetic field vector, g - spectroscopic splitting factor, β - Bohr magneton, D - axial zero field splitting parameter, E - rhombic zero field splitting parameter and S - electron spin vector. If D and E are zero then an isotropic absorption line with a g value slightly greater than 2 is observed. If D and E are finite but small ($0.001\text{-}0.05\text{ cm}^{-1}$) five EPR transitions centered on $g \approx 2$ are observed and these are $|5/2, -5/2\rangle \rightarrow |5/2, -3/2\rangle$; $|5/2, -3/2\rangle \rightarrow |5/2, -1/2\rangle$; $|5/2, -1/2\rangle \rightarrow |5/2, +1/2\rangle$; $|5/2, +1/2\rangle \rightarrow |5/2, +3/2\rangle$ and $|5/2, +3/2\rangle \rightarrow |5/2, +5/2\rangle$. If D or E is large compared to $g\beta B$, for the two limiting cases $D \neq 0, E = 0$ and $D = 0, E \neq 0$, the eigen values and eigen vectors of the Hamiltonian in zero magnetic field are easily found to be three Kramer's doublets. In the first case the lowest doublet has the effective g values $g_{\parallel} \approx 2, g_{\perp} \approx 6$ and represents strong axially symmetric electric fields. If both D and E are large compared to $g\beta B$ another signal arises with $g \approx 4.29$ and the λ value (E/D) is $1/3$. Because of its isotropic nature and statistical effects this signal is more intense than others and usually dominates the spectrum [38].

EPR spectra of the complexes were taken both in polycrystalline state at 298 K and in DMF at 77 K. But in polycrystalline state all the complexes are EPR silent.

EPR spectrum of compound **15** in DMF at 77 K is given in Fig. 4.11. At first glance the spectrum is dominated by an intense signal at $g = 4.214$ may be assigned to a rhombic high-spin Fe(III) with $\lambda = E/D = 1/3$, while the small feature in the low field with $g = 8.112$ could be associated with an intermediate λ suggesting the presence of two different iron species. But, a recent, detailed EPR study by Nilges and Wilker on high-spin Fe(III) catecholate complexes shows that only one high spin Fe(III) component with $\lambda < 1/3$ reproduce all of the same spectral features seen for compound **15** [39,40].

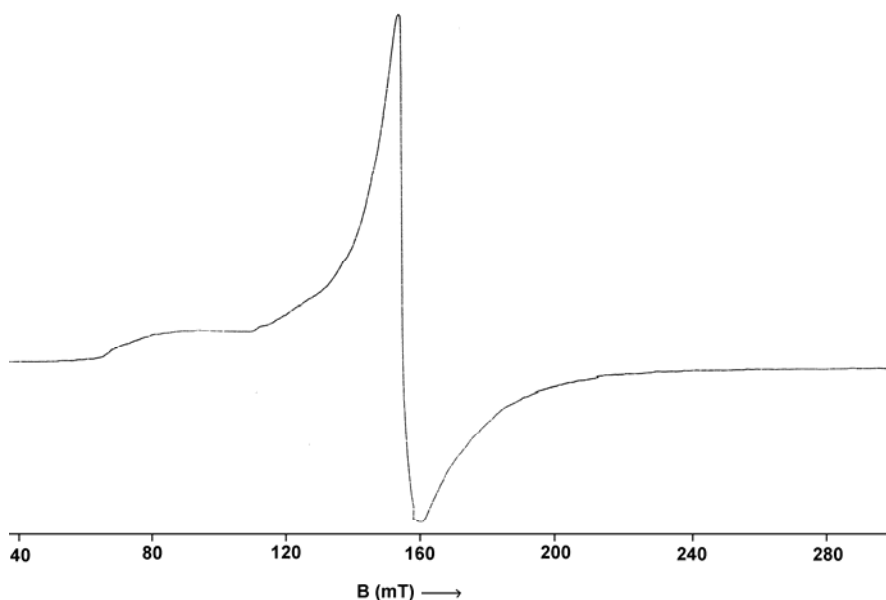


Fig. 4.11. EPR spectrum of compound **15** in DMF at 77 K.

Compound **16** exhibits (Fig. 4.12) a spectrum similar to that of compound **15** in DMF solution at 77 K with two g values *ie.* $g_1 = 8.319$ and $g_2 = 4.172$. Here also the signal with $g = 4.172$ dominates the spectrum and is a characteristic signal for rhombic systems, but a similar resonance occurs in axial systems if the D value is large (on the order of 1 cm^{-1}) [41].

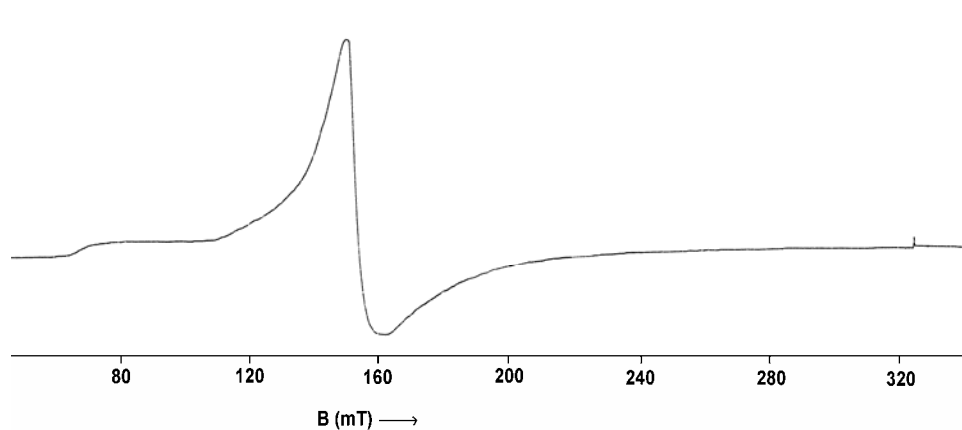


Fig. 4.12. EPR spectrum of compound 16 in DMF at 77 K.

EPR spectrum of compound 17 in DMF solution at 77 K (Fig. 4.13) is dominated by a signal at $g = 4.093$. Small broad peak is observed in the downfield region with $g = 6.662$ and a weak signal with $g = 2.024$ is observed at 300 mT. And the values are consistent with d^5 high spin Fe(III) systems [40].

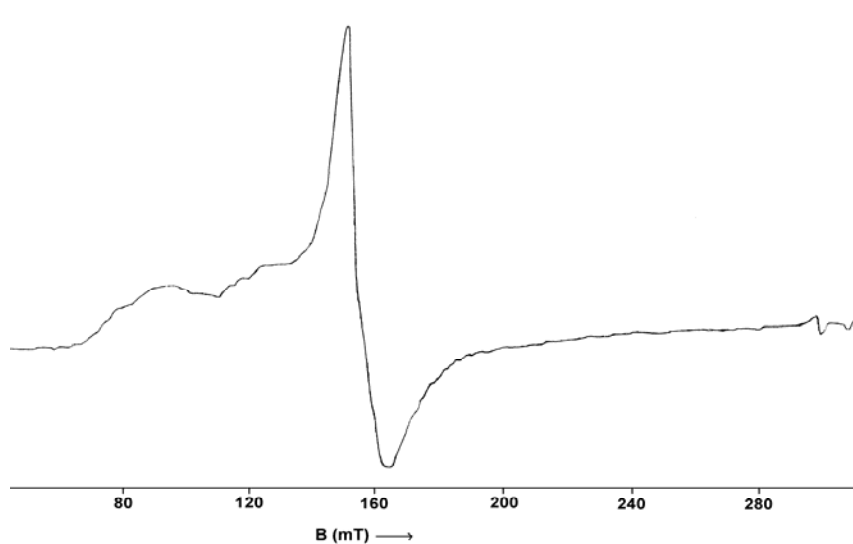


Fig. 4.13. EPR spectrum of compound 17 in DMF at 77 K.

EPR spectrum of compound **18** is similar to that of compound **15**. Here two signals are observed, one broad signal with $g = 7.913$ and an intense signal with $g = 4.241$ represent d^5 high spin Fe(III) species.

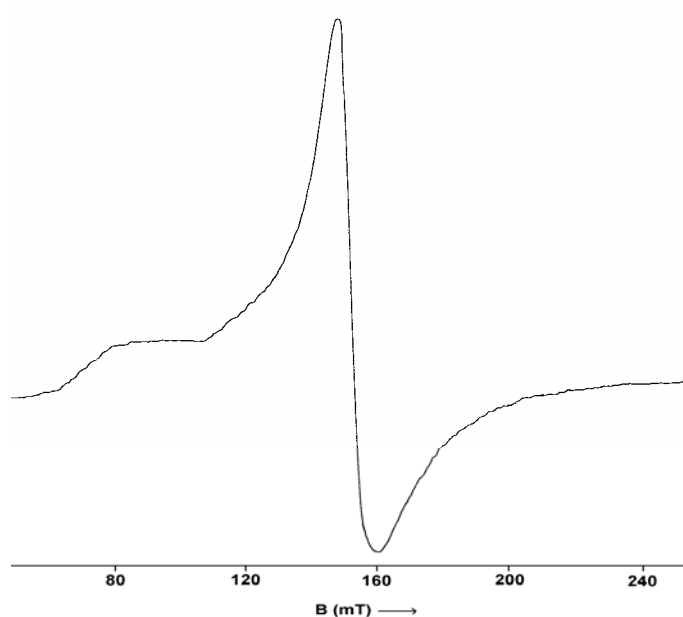


Fig. 4.14. EPR spectrum of compound **18** in DMF at 77 K.

4.3.4b IR spectral studies

In all the complexes ligands can act as tridentate one coordinating *via* amido oxygen, azomethine nitrogen and phenolic oxygen. This is confirmed by infrared spectroscopy. In complexes, binding of azomethine nitrogen to Fe(III) centre has been identified from lowering of azomethine stretching frequencies. The coordination of ligands in amido form is evident from lowering of carbonyl stretching in complexes [42]. Complexes **16** and **18** show broad bands in the region at $\sim 3440\text{ cm}^{-1}$, confirming the presence of lattice water. Nitrate complexes exhibit three NO stretching bands and if the separation between the two highest

bands is less than 130 cm^{-1} for unidentate complexes and 186 cm^{-1} for bidentate complexes. Here in compound **16**, three bands are observed at 1420 , 1300 and 1020 cm^{-1} due to nitrate group indicating the presence of unidentate nitrate group. In compound **18** stretching bands are observed at 1404 , 1282 and 1028 cm^{-1} confirming the presence of unidentate nitrate group [43,44]. IR spectra of compounds **16** and **18** are showed in Figs. 4.15 and 4.16 and the assignments are summarized in Table 4.7.

Table 4.7 Infrared spectral assignments (cm^{-1}) of Fe(III) complexes

Compound	$\nu(\text{C}=\text{O})$	$\nu(\text{C}=\text{N})$	$\nu(\text{N}-\text{H})$	$\nu(\text{O}-\text{H})$
$\text{H}_2\text{hmbn}\cdot\text{H}_2\text{O}$	1643	1604	3074	3417, 3208
$[\text{Fe}(\text{Hhmbn})\text{Cl}_2]$ (15)	1628	1590	3064	----
$[\text{Fe}(\text{Hhmbn})_2\text{NO}_3]\cdot 2\text{H}_2\text{O}$ (16)	1633	1586	3056	3440
H_2hman	1638	1602	3029	----
$[\text{Fe}(\text{Hhman})\text{Cl}_2]$ (17)	1626	1586	3010	----
$[\text{Fe}(\text{Hhman})_2\text{NO}_3]\cdot\text{H}_2\text{O}$ (18)	1621	1588	3015	3437

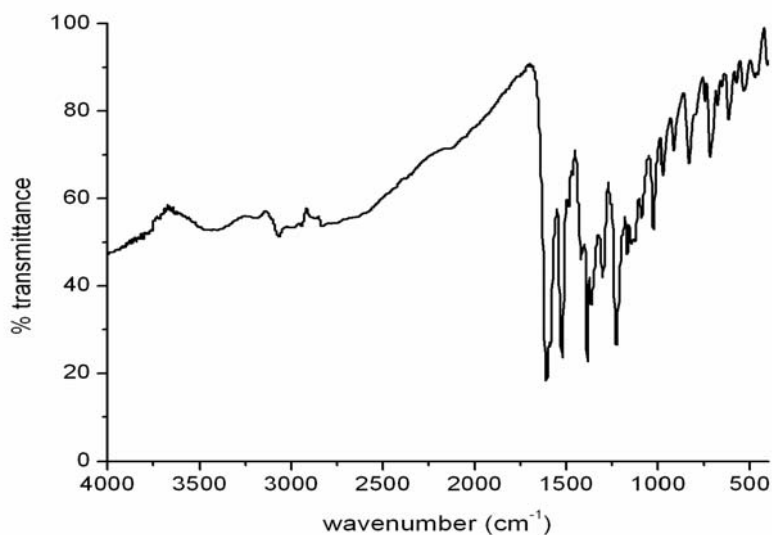


Fig. 4.15. IR spectrum of compound 16.

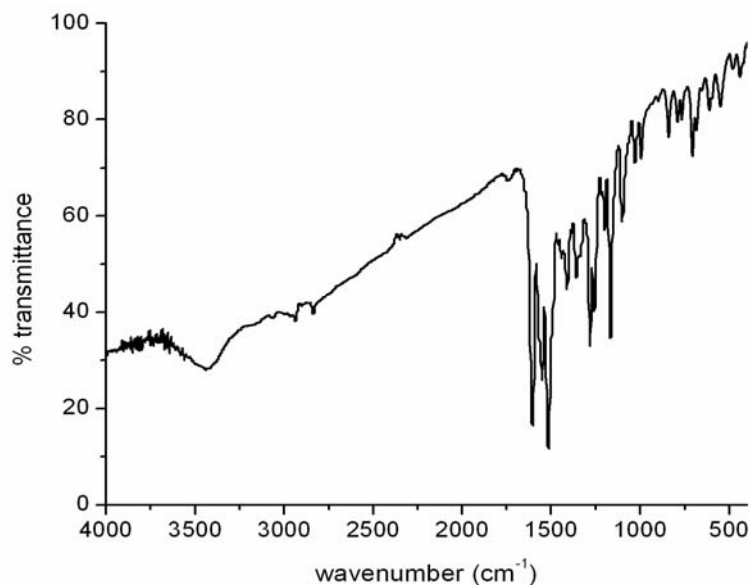


Fig. 4.16. IR spectrum of compound 18.

4.3.4c Electronic spectral studies

Electronic spectra of all the complexes were taken in acetonitrile (50000-20000 cm^{-1}) as well as in DMF solutions (20000-10000 cm^{-1}) and the spectral data is summarized in Table 4.8. Because of the greater oxidizing power of Fe(III) relative to Mn(II), LMCT bands often mask the low intensity *d-d* absorption. But in general where observed, *d-d* band intensities are somewhat larger than that of Mn(II) especially in acentric systems, may be this is because of increased metal-ligand bond covalency [29]. In all the compounds intra-ligand transitions are found in between 33000-45600 cm^{-1} . Charge transfer transitions are observed in the 27530-28640 cm^{-1} region and weak *d-d* bands are observed in between 16170-16970 cm^{-1} . Fig. 4.17 illustrates the electronic spectra of the complexes in acetonitrile as well as DMF solutions.

Table 4.8 Electronic spectral assignments (cm⁻¹) of Fe(III) complexes

Compound	Intraligand transitions	LMCT	<i>d-d</i>
[Fe(Hhmbn)Cl ₂] (15)	33350, 40170, 45080	27530	16170
[Fe(Hhmbn) ₂ NO ₃]·2H ₂ O (16)	33150, 39560, 45180	27900	16600
[Fe(Hhman)Cl ₂] (17)	34280, 38820(sh), 45500	28020	17840
Fe(Hhman) ₂ NO ₃ ·H ₂ O (18)	34100, 40360(sh), 45570	28640	16970

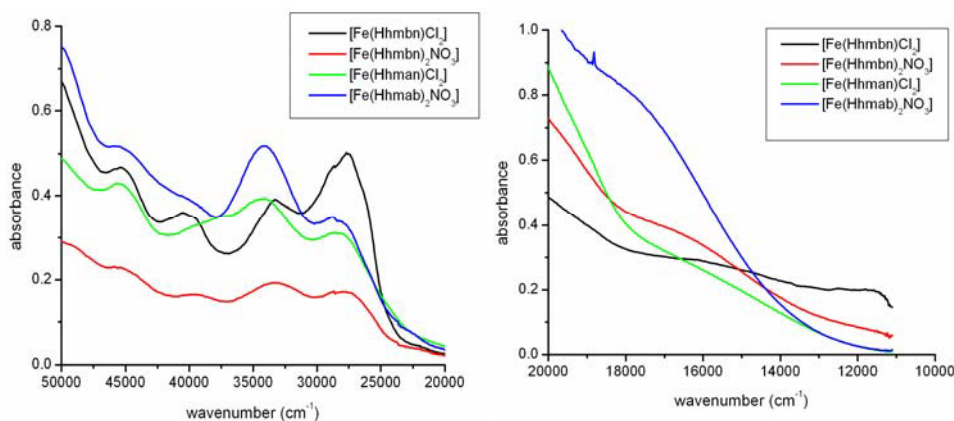


Fig. 4.17. Electronic spectra of the complexes 15, 16, 17 and 18 in acetonitrile solution in the region 50000-20000 cm⁻¹ (left) and *d-d* spectra in DMF solution in the region 20000-10000 cm⁻¹ (right).

4.3.5 Thermal analyses

Thermogravimetric analyses of the complexes were done in the temperature range of 50-800 °C in nitrogen atmosphere at a heating rate of 10 °C/min. The loss of lattice water molecules occurs in complexes **16** and **18** below 130 °C. Multistage decomposition of ligands were taken place after 200 °C. The decomposition was not seen to be completed even after 800 °C. TG-DTG curves of compound **18** are shown in Fig. 4.18.

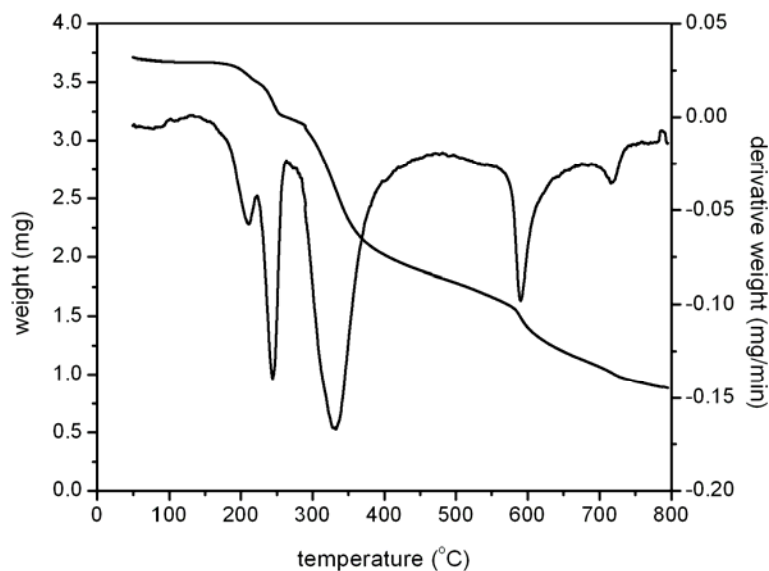


Fig. 4.18. TG-DTG plots of compound 18.

References

1. John N. Hathcock, Vitamin and mineral safety, 2nd Edition, CRN, 2004.
2. G.E.O. Borgstahl, H.E. Parge, M.J. Hickey, M.J. Johnson, M. Boissinot, R.A. Hallewell, J.R. Lepock, D.E. Cabelli, J.A. Tainer, *Biochemistry* 35 (2006) 4287-4297.
3. C.L. Keen, S. Zidenberg-Cherr, *Manganese in Health and Disease* (D. Klimis-Tavantzis, ed.), CRC Press, Boca Raton, FL (1994) 193-205.
4. P. Kurtz, *Dalton Trans.* (2009) 6103-6108.
5. K.N. Ferreira, T.M. Iverson, K. Maghlaoui, J. Barber, S. Iwata, *Science* 303 (2004) 1831-1838.
6. K. Nehru, S.J. Kim, I.Y. Kim, M.S. Seo, Y. Kim, Sung-Jin Kim, J. Kim, W. Nam, *Chem. Commun.* (2007) 4623-4625.

7. K.F. Sibbons, K. Shastri, M. Watkinson, Dalton Trans. (2006) 645-661.
8. G.J.P. Britovsek, J. England, A.J.P. White, Dalton Trans. (2006) 1399-1408.
9. G.A. van Albada, A. Mohamadou, W.L. Driessen, R. Gelder, S. Tanase, J. Reedijk, Polyhedron 23 (2004) 2387–2391.
10. A.J. Wu, J.E. Penner-Hahn, V.L. Pecoraro, Chem. Rev. 104 (2004) 903-938.
11. P.S. Mukherjee, S. Konar, E. Zangrando, T. Mallah, J. Ribas, N.R. Chaudhuri, Inorg. Chem. 42 (2003) 2695-2703.
12. W. Zhang, J.L. Loebach, S.R. Wilson, E.N. Jacobsen, J. Am. Chem. Soc. 112 (1990) 2801–2803.
13. P.G. Cozzi, Chem. Soc. Rev. 33 (2004) 410-421.
14. Encyclopedia of Inorganic Chemistry, 2nd Edition, R. Bruce King, Wiley (2005).
15. S.M.H. Sadrzadeh, Y. Saffari, Am. J. Clin. Pathol. 121 (Suppl. 1) (2004) S64-S70.
16. P.V. Bernhardt, Dalton Trans. (2007) 3214–3220.
17. P.V. Bernhardt, P. Chin, P.C. Sharpe, D.R. Richardson, Dalton Trans. (2007) 3232-3244.
18. W.J. Geary, Coord. Chem. Rev. 7 (1971) 81-122.
19. R.D. Dowsing, J.B. Gibbson, J. Chem. Phys. 50 (1969) 294-303.
20. M.T. Caudle, C.K. Mobley, L.M. Bafaro, R. LoBrutto, G.T. Yee, T.L. Groy, Inorg. Chem. 43 (2004) 506-514.

21. C. Mantel, C. Baffert, I. Romero, A. Deronzier, J. Pe'caut, M.N. Collomb, C. Duboc, *Inorg. Chem.* 43 (2004) 6455-6463.
22. B. Bleany, R.S. Rubins, *Proc. Phys. Soc. London* 77 (1961) 103-112.
23. A. Sreekanth, M. Joseph, H.-K. Fun, M.R.P. Kurup, *Polyhedron* 25 (2006) 1408–1414.
24. P.F. Rapheal, E. Manoj, M.R.P. Kurup, *Polyhedron* 26 (2007) 5088–5094.
25. O. Pouralimardan, A.C. Chamayou, C. Janiak, H. Hosseini-Monfared, *Inorg. Chim. Acta* 360 (2007) 1599–1608.
26. K. Mohanan, B. Murukan, *Synth. React. Inorg. Met.-Org. Nano-Met. Chem.* 35 (2005) 837-844.
27. V.K. Sharma, S. Srivastava, *Synth. React. Inorg. Met.-Org. Nano-Met. Chem.* 35 (2005) 311-318.
28. M.S. Abdel-Moez, S.L. Stefan, M.M. El-Beairy, B.A. El-Shetary, *Can. J. Chem.* 68 (1990) 774-781.
29. A.B.P. Lever, *Inorganic Electronic Spectroscopy*, 2nd Edition, Elsevier, Amsterdam 1984.
30. H. Cesur, T.K. Yazicilar, B. Bati, V.T. Yilmaz, *Synth. React. Inorg. Met.-Org. Chem.* 31 (2001) 1271–1283.
31. Z.K. Jacimovic, V.M. Leovac, G. Giester, Z.D. Tomic, K.M. Szécsényi, J. *Therm. Anal. Cal.* 90 (2007) 549-555.
32. R. Mayilmurugan, K. Visvaganesan, E. Suresh, M. Palaniandavar, *Inorg. Chem.* 48 (2009) 8771–8783.
33. M. Velusamy, M. Palaniandavar, *Inorg. Chem.* 42 (2003) 8283-8293.
34. M. Velusamy, R. Mayilmurugan, M. Palaniandavar, *Inorg. Chem.* 43 (2004) 6284-6293.

35. R. Taylor O. Kennard, *J. Am. Chem. Soc.* 104 (1982) 5063-5070.
36. G.R. Desiraju, *Acc. Chem. Res.* 24 (1991) 290-296.
37. T. Steiner, *Chem. Commun.* (1997) 727-734.
38. S.A. Cotton, *Coord. Chem. Rev.* 8 (1972) 185-218.
39. F. Namuswe, T. Hayashi, Y. Jiang, G.D. Kasper, A.A.N. Sarjeant, P.M. Loccoz, D.P. Goldberg, *J. Am. Chem. Soc.* 132 (2010) 157-167.
40. J.T. Weisser, M.J. Nilges, M.J. Sever, J.J. Wilker, *Inorg. Chem.* 45 (2006) 7736-7747.
41. D. Collison, A.K. Powell, *Inorg. Chem.* 29 (1990) 4735-4746.
42. H.M. El-Tabl, F.A. El-Said, M.I. Ayad, *Synth. React. Inorg. Met.-Org. Chem.* 32 (2002) 1245-1262.
43. Nakamoto, *Infrared and Raman Spectra of Inorganic and Coordination Compounds*, 5th ed., Wiley, New York, 1997.
44. D.N. Sathyanarayana, *Vibrational Spectroscopy Theory and Applications*, New age international publishers, 2000.

*****❧*****

SYNTHESES AND CHARACTERIZATION OF Cu(II) COMPLEXES OF TRIDENTATE ACYLHYDRAZONES

5.1	Introduction
5.2	Experimental
5.3	Results and discussion
	References

5.1 Introduction

Among the different transition metals, copper has gained a special position because of its presence in biological systems, which are essential to many biological processes. A number of proteins and enzymes have copper in their active sites, which are associated with a variety of biological functions like oxygen transport and activation, electron transfer etc. [1-4]. Nowadays researchers using copper complexes to look into the fine detail of the structure and folding pattern of nucleic acids [5,6]. Copper complexes of bis(thiosemicarbazones) are found to be hypoxia selective agents that can be used for imaging lack of oxygen in biological tissues [7]. Recently Chen *et al* have shown that the copper complexes of plumbagin (an extract from the plant *Plumbago zeylanica* and used as traditional Chinese medicine) have higher anticancer properties and are less toxic to healthy cells than commonly used platinum-based drugs, such as cisplatin [8]. The biomimetic catalytic activity of copper complexes towards the catechol oxidation and aerobic oxidation of ascorbic acid are reported [9,10].

The interest in the study of chemistry of copper complexes of hydrazones has been deepened by the findings of Johnson *et al.* that the copper(II) complex of the most potent of the chelators, salicylaldehyde benzoylhydrazone exhibits appreciably greater inhibitory activity than salicylaldehyde benzoylhydrazone itself [11]. There are so many reports on the studies of Cu(II) complexes with ligands containing O, N and S containing ligands [12-14].

Copper has +1 and +2 oxidation states in its complexes, and out of these most stable +2 oxidation state predominates over less stable +1 oxidation state. A wide variety of coordination compounds are formed by the combination of different types of ligands with Cu(II) cation. Normally the copper complexes are having square planar, tetrahedral and octahedral stereochemistries. In Cu(II) complexes, the $3d^9$ outer electronic configuration lacks cubic symmetry and hence there are distortions from basic stereochemistries and Jahn-Teller effect plays a major role in deciding the distortion effect of stereochemistries of Cu(II) complexes.

This chapter deals with the syntheses and characterization of Cu(II) complexes with different ONO donor hydrazones as ligands and some heterocyclic compounds as coligands.

5.2 Experimental

5.2.1 Materials

2-Hydroxy-4-methoxyacetophenone (Aldrich), 2-hydroxy-4-methoxybenzaldehyde (Aldrich), nicotinic acid hydrazide (Aldrich), benzhydrazide (Aldrich), copper(II) acetate monohydrate (Qualigens), 2,2'-bipyridine (Qualigens), 1,10-phenanthroline (Ranchem) were used without further purification. Solvent used was methanol.

5.2.2 Syntheses of the acylhydrazones

The acylhydrazones 2-hydroxy-4-methoxybenzaldehyde nicotinoylhydrazone monohydrate ($H_2hmbn \cdot H_2O$), 2-hydroxy-4-methoxyacetophenone nicotinoylhydrazone (H_2hman), 2-hydroxy-4-methoxybenzaldehyde benzoylhydrazone (H_2hmhb) and 2-hydroxy-4-methoxyacetophenone benzoylhydrazone (H_2hmab) were synthesized as described in Chapter 2.

5.2.3 Syntheses of copper(II) complexes

[Cu(hmbn)]₂·2H₂O (20): To a methanolic solution of $H_2hmbn \cdot H_2O$ (0.289 g, 1 mmol), $Cu(OAc)_2 \cdot H_2O$ (0.199 g, 1 mmol) dissolved in hot methanol was added. The resulting green colored solution was refluxed for 4 hours. The product separated was green colored and it was filtered, washed with methanol, followed by ether and dried over P_4O_{10} *in vacuo*. Elemental Anal. Found (Calcd.) (%): C, 48.33 (47.93); H, 4.19 (3.74); N, 11.98 (11.98).

[Cu(hman)]₂ (21): This complex was prepared by refluxing 1:1 ratio of $Cu(OAc)_2 \cdot H_2O$ (0.199 g, 1 mmol) and H_2hman (0.285 g, 1 mmol) in methanolic medium for 4 hours. The product separated was green colored solid and it was filtered, washed with methanol, followed by ether and dried over P_4O_{10} *in vacuo*. Elemental Anal. Found (Calcd.) (%): C, 52.50 (51.95); H, 3.68 (3.78); N, 12.16 (12.12).

[Cu(hmhb)]₂·2H₂O (22): Methanolic solutions of H_2hmhb (0.270 g, 1 mmol) and $Cu(OAc)_2 \cdot H_2O$ (0.199 g, 1 mmol) were mixed and refluxed for about 4 hours. The green product separated was filtered, washed with methanol followed by ether and dried over P_4O_{10} *in vacuo*. Elemental Anal. Found (Calcd.) (%): C, 51.87 (51.50); H, 4.30 (4.03); N, 8.45 (8.01).

[Cu(hmbb)phen]·1¹/₂H₂O (23): This complex was prepared by refluxing 1:1:1 ratio of Cu(OAc)₂·H₂O (0.199 g, 1 mmol), 1,10-phenanthroline (0.198 g, 1 mmol) and H₂hmbb (0.270 g, 1 mmol) in methanolic medium for about 4 hours. Dark green product obtained was filtered, washed with methanol followed by ether and dried over P₄O₁₀ *in vacuo*. Elemental Anal. Found (Calcd.) (%): C, 60.20 (60.16); H, 3.78 (4.30); N, 10.82 (10.39).

[Cu(hmbb)(bipy)H₂O] (24): Methanolic solutions of the ligand, H₂hmbb (0.270 g, 1 mmol), Cu(OAc)₂·H₂O (0.199 g, 1 mmol) and 2,2'-bipyridine (0.156 g, 1 mmol) were mixed and refluxed for about 4 hours. The dark green product obtained was filtered, washed with methanol followed by ether and dried over P₄O₁₀ *in vacuo*. Elemental Anal. Found (Calcd.) (%): C, 59.18 (59.34); H, 3.85 (4.38); N, 11.40 (11.07).

[Cu(hmab)phen] (25): Methanolic solutions of the ligand, H₂hmab (0.284 g, 1 mmol) 1,10-phenanthroline (0.198 g, 1 mmol) and Cu(OAc)₂·H₂O (0.199 g, 1 mmol) were mixed and refluxed for about 4 hours. The dark green crystalline product obtained was filtered, washed with methanol followed by ether and dried over P₄O₁₀ *in vacuo*. Elemental Anal. Found (Calcd.) (%): C, 63.37 (63.93); H, 3.87 (4.22); N, 10.74 (10.65).

5.3 Results and discussion

Six copper complexes were prepared and they are found to be stable in air. They are soluble in organic solvents like acetonitrile and DMF. The elemental analyses values show that the found and calculated values are in good agreement with the general formula of the complexes. Complexes **20**, **21** and **22** show substantial low magnetic moment in the range of 1.05 -1.35 B. M. may be due to the coupling of two magnetic centers suggesting dimeric nature to these complexes [15]. The observed magnetic susceptibility values of the complexes

23, **24** and **25** are in close agreement with the spin only value for a d^9 copper system. The conductance measurements confirm the non-electrolytic nature of the complexes. The magnetic susceptibility and molar conductivity values of the complexes are presented in Table 5.1. X-ray quality single crystals of one of the compounds, [Cu(hmab)phen] (**25**) were obtained by slow evaporation of the solution of compound in CH₃OH over two days.

Table 5.1 Molar conductivities and magnetic susceptibilities of copper(II) complexes

Compound	$\lambda_m^{\#}$	μ_{eff} (B. M.)
[Cu(hmbn)] ₂ ·2H ₂ O (20)	9	1.27
[Cu(hman)] ₂ (21)	6	1.34
[Cu(hmbb)] ₂ ·2H ₂ O (22)	8	1.05
[Cu(hmbb)phen]·1 ¹ / ₂ H ₂ O (23)	4	1.90
[Cu(hmbb)(bipy) H ₂ O] (24)	5	1.95
[Cu(hmab)phen] (25)	6	1.96

[#]molar conductivity (in mho cm² mol⁻¹) taken in 10⁻³ M DMF.

5.3.1 Crystal structure of the compound [Cu(hmab)phen] (**25**)

The crystal structure of the compound along with atom numbering scheme is given in Fig. 5.1. A summary of the key crystallographic information is given in Table 5.2. The complex is crystallized into a monoclinic space group $P2_1/c$. In this complex, the dinegative ligand, 2-hydroxy-4-methoxyacetophenone benzoylhydrazone is coordinated to Cu(II) through the phenolic oxygen O2, azomethine nitrogen N1 and deprotonated enolate oxygen O3, forming five and six membered chelate rings. The heterocyclic base phenanthroline is coordinated to the central metal Cu through two nitrogen atoms N3 and N4 and forms a five membered chelate ring.

The five coordinated complex adopts a square pyramidal geometry, and the basal coordination positions are occupied by O2, N1, O3 and N3 and the apical position by N4. The Cu–N4 bond distance is larger when compared with others. The angular structural parameter $\tau = 0.1366$, is an evidence for the distorted square pyramidal geometry of the complex [16]. The mean plane deviation calculation shows that the atoms O2, N1, O3 and N3 are nearly planar with a mean plane deviation of 0.2059 Å. The significant deviation from regular square pyramidal geometry is evident from the observed values of bond angles and bond lengths summarized in Table 5.3.

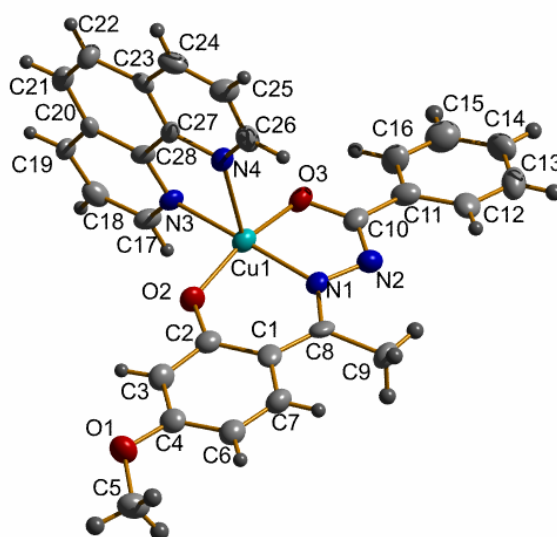


Fig. 5.1. Structure and labeling scheme for [Cu(hmab)phen].

Fig. 5.2 illustrates the packing of the compound in crystal lattice. A beautiful arrangement of molecules in the crystal system in a quadruple cell along *b* axis is shown in Fig. 5.3. The π - π interactions play an important role in controlling the packing or assembly of compounds. Analysis of complexes with nitrogen containing heterocyclic compounds reveals that π - π stacking is usually an offset or slipped facial arrangement of the ring, *ie* the rings are parallel

displaced. Here packing of the compound is stabilized by π - π stacking interactions and C-H \cdots π interactions. The interchain stacking interaction between the phenanthroline rings in the compound is remarkably strong and it may be due to larger π system in phenanthroline ligand [17]. In this compound all the phenanthroline rings are arranged parallel to each other within the unit cell and the phenanthroline rings Cg[5] and Cg[8] are involved in π - π stacking with a distance of 3.507 Å. Fig. 5.4 shows the π - π stacking in [Cu(hmab)phen]. In addition to the π - π stacking interactions significant C-H \cdots π interactions are also present in the unit cell, they are C15-H15 \cdots Cg(3) and C21-H21 \cdots Cg(6). These interaction parameters are listed in Table 5.4. Weak intramolecular hydrogen bonding is observed between C(9)-H(9C) \cdots N(2) [with a H \cdots N distance of 2.19 Å and an angle of 111°]. Intermolecular hydrogen bonding interactions are C(17)-H(17) \cdots O(1) [with a H \cdots O distance of 2.51 Å and an angle of 120°] and C(19)-H(19) \cdots O(2) [with a H \cdots O distance of 2.58 Å and an angle of 167°]. Hydrogen bonding interactions of the compound is shown in Fig. 5.5.

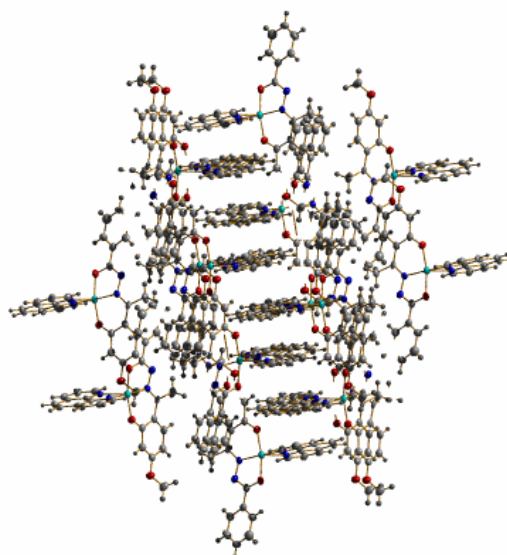


Fig. 5.2. Unit cell packing diagram of the compound [Cu(hmab)phen] viewed along the *b* axis.

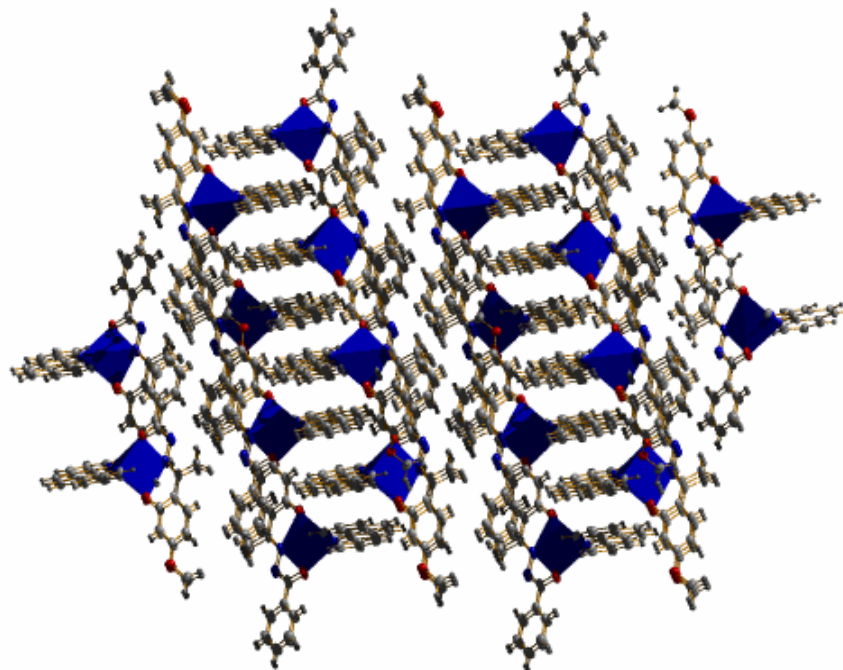


Fig. 5.3. Quadruple cell packing of the compound [Cu(hmab)phen] (6) viewed along the *b* axis.

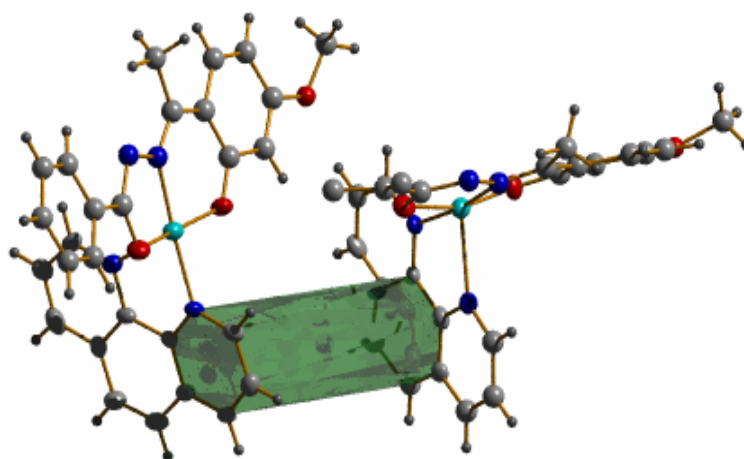


Fig. 5.4. π - π stacking of [Cu(hmab)phen].

Table 5.2 Crystal data and structure refinement parameters for [Cu(hmab)phen]

CCDC No.	696921
Empirical formula	C ₂₈ H ₂₂ CuN ₄ O ₃
Formula weight	526.04
Temperature	100(2) K
Wavelength	0.71073 Å
Crystal system	Monoclinic
Space group	<i>P2₁/c</i>
Unit cell dimensions	a = 16.0239(14) Å b = 10.4971(6) Å c = 14.4246(12) Å α = 90° β = 106.347(9)° γ = 90°
Volume	2328.2(3) Å ³
Z	4
Density (calculated)	1.501 Mg/m ³
Absorption coefficient	0.978 mm ⁻¹
F(000)	1084
Crystal size	0.11 x 0.08 x 0.05 mm ³
θ range for data collection Index ranges	2.94 to 25.00° -19 ≤ h ≤ 19, -12 ≤ k ≤ 12, -17 ≤ l ≤ 17
Reflections collected	19930
Independent reflections	4100 [R(int) = 0.1638]
Refinement method	Full-matrix least-squares on F ²
Data / restraints / parameters	4100 / 0 / 327
Goodness-of-fit on F ²	1.020
Final R indices [I > 2σ(I)]	R ₁ = 0.0832, wR ₂ = 0.1611
R indices (all data)	R ₁ = 0.1633, wR ₂ = 0.2004
Largest diff. peak and hole	1.374 and -0.521 e.Å ⁻³

$$R_1 = \frac{\sum ||F_o| - |F_c||}{\sum |F_o|}$$

$$wR_2 = [\frac{\sum w(F_o^2 - F_c^2)^2}{\sum w(F_o^2)^2}]^{1/2}$$

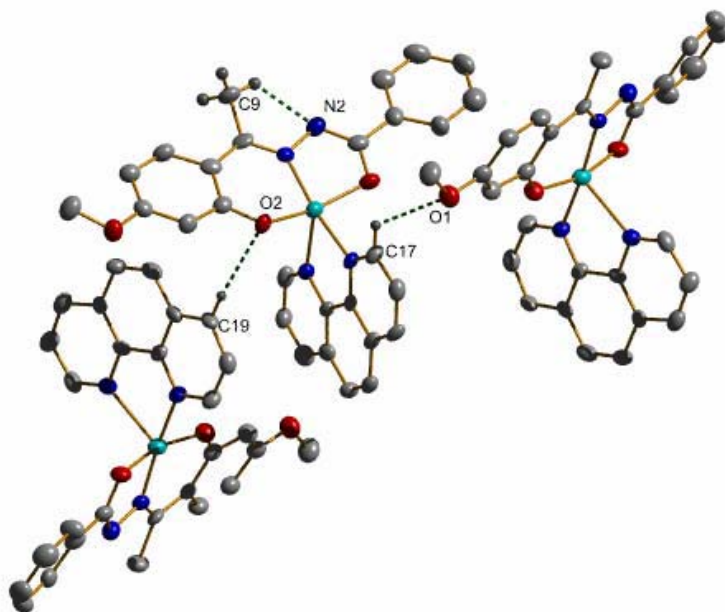


Fig. 5.5. Hydrogen bonding interactions of the compound [Cu(hmab)phen] (6).

Table 5.3 Selected bond lengths (Å) and bond angles (°) for the compound [Cu(hmab)phen]

Bond lengths		Bond angles		Bond angles	
Cu(1)–O(2)	1.902(5)	O(2)–Cu(1)–N(1)	92.6(2)	C(2)–O(2)–Cu(1)	127.2(5)
Cu(1)–N(1)	1.940(6)	O(2)–Cu(1)–O(3)	163.5(2)	C(10)–O(3)–Cu(1)	109.5(5)
Cu(1)–O(3)	1.950(5)	N(1)–Cu(1)–O(3)	82.7(2)	C(8)–N(1)–Cu(1)	128.1(5)
Cu(1)–N(3)	2.012(6)	O(2)–Cu(1)–N(3)	90.4(2)	N(2)–N(1)–Cu(1)	112.8(4)
Cu(1)–N(4)	2.350(6)	N(1)–Cu(1)–N(3)	171.7(2)	C(10)–N(2)–N(1)	111.0(6)
O(2)–C(2)	1.300(8)	O(3)–Cu(1)–N(3)	92.3(2)	C(28)–N(3)–Cu(1)	120.0(5)
O(3)–C(10)	1.308(9)	O(2)–Cu(1)–N(4)	97.3(2)	C(17)–N(3)–Cu(1)	122.3(5)
N(1)–C(8)	1.306(9)	N(1)–Cu(1)–N(4)	111.0(2)	C(26)–N(4)–Cu(1)	134.3(5)
N(1)–N(2)	1.400(8)	O(3)–Cu(1)–N(4)	99.2(2)	C(27)–N(4)–Cu(1)	107.9(5)
N(2)–C(10)	1.327(9)	N(3)–Cu(1)–N(4)	76.2(2)	C(8)–C(1)–C(2)	125.0(7)
C(1)–C(8)	1.425(10)	C(4)–O(1)–C(5)	117.6(6)	O(2)–C(2)–C(1)	124.0(7)

Table 5.4 Interaction parameters of the compound [Cu(hmab)phen]

π-π interactions						
Cg(I)···Cg(J)	Cg···Cg (Å)	α (°)	β (°)	γ (°)	Cg(I) _⊥ (Å)	Cg(J) _⊥ (Å)
Cg(2)···Cg(5) ^a	3.981(4)	2.21	32.53	31.42	3.397	3.356
Cg(4)···Cg(5) ^b	3.676(4)	17.11	27.76	11.70	3.600	3.253
Cg(5)···Cg(5) ^a	3.738(4)	0.00	24.50	24.50	3.402	3.401
Cg(5)···Cg(8) ^a	3.507(4)	0.85	14.21	14.16	3.401	3.400

Equivalent position codes: ^a = 1-x,-y,-z; ^b = 1-x,1/2+y,1/2-z

Cg(2) = Cu(1) N(3), C(28), C(27), N(4); Cg(4) = N(3), C(17), C(18), C(19), C(20), C(28)

Cg(5) = N(4), C(26), C(25), C(24), C(23), C(27); Cg(8) = C(20), C(21), C(22), C(23),

C(27), C(28)

α (°) = Dihedral angle between planes I and J;

β (°) = Angle between Cg(I)-Cg(J) vector and normal to plane I;

γ (°) = Angle between Cg(I)-Cg(J) vector and normal to plane J;

Cg(I)_⊥ (Å) = Perpendicular distance of Cg(I) on ring J;

Cg(J)_⊥ (Å) = Perpendicular distance of Cg(J) on ring I.

C-H···π interactions			
C-H(I)···Cg(J)	H···Cg (Å)	C-H···Cg (°)	C···Cg (Å)
C(15)-H(15)···Cg(3) ^c	2.90	141	3.666
C(21)-H(21)···Cg(6) ^d	2.65	157	3.526

Equivalent position codes: ^c = x,1/2-y,-1/2+z; ^d = 1-x,1/2+y,1/2-z

Cg(3) = Cu(1), O(2), C(2), C(1), C(8), N(1); Cg(6) = C(1), C(2), C(3), C(4), C(6), C(7)

5.3.2 EPR spectra

The Electron Paramagnetic Resonance spectroscopy provides a wealth of information regarding the electronic structure of paramagnetic compounds. In the case copper(II) complexes the doubly degenerate spin states associated with copper(II) ion with a spin angular momentum, $M_s = \pm 1/2$, has been lifted in presence of a magnetic field and the energy difference between them is given by

$$\Delta E = h\nu = g\beta B$$

where h is Planck's constant, ν is the microwave frequency for transition from $M_s = +1/2$ to $M_s = -1/2$, g is the Lande splitting factor (equal to 2.0023 for a free electron), β is the Bohr magneton and B is the magnetic field.

The factors which determine the type of EPR spectrum observed are: (a) the nature of the electronic ground state (b) the symmetry of the effective ligand-field about the copper ion and (c) the mutual orientations of the local molecular axes of the separate copper chromophores in the unit cell which determines the amount of exchange coupling [18].

The electronic properties of the Cu(II) ion are being affected by its geometry, establishes the order of the energy levels of the d orbitals, and accordingly, the ground state for a particular arrangement. For coordination geometries having an elongated octahedron or a square pyramid or square planar, the ground state is $d_{x^2-y^2}$ and when it is a compressed octahedron or a trigonal bipyramid, the ground state is d_{z^2} . EPR spectroscopy helps to differentiate the ground states on the basis of the principal values of the g tensor [19].

The EPR spectra of the complexes in the solid state at 298 K, in DMF at 298 K and at 77 K were recorded using TCNE as the standard, with 100 kHz modulation frequency, modulation amplitude 2 G and 9.1 GHz microwave frequency.

The EPR spectra of the compounds recorded in polycrystalline state at room temperature provide information about the coordination environment of the Cu(II) species in these complexes. The X-band EPR spectrum of compound **20** (Fig. 5.6) gave three g values $g_1 = 2.050$, $g_2 = 2.089$ and $g_3 = 2.187$ which indicate rhombic distortion in its geometry. Since the lowest $g > 2.04$ such a spectrum can

be observed for a copper(II) ion in elongated rhombic symmetry with all the axes aligned parallel and would be consistent with rhombic square-coplanar stereochemistry [20]. In polynuclear Cu(II) complexes, the zero-field splitting parameter D gives rise to transitions corresponding to $\Delta M_s = \pm 2$ which is due to Cu-Cu dipolar interaction. In X-band spectra transitions due to $\Delta M_s = \pm 1$ were observed at magnetic field of 300 mT while transitions due to $\Delta M_s = \pm 2$ were observed at half of this field *ie.* at 150 mT. For compound **20** we got a half field signal at 160 mT with $g = 4.074$, indicating dimeric species, and the copper-copper distance is likely to be less than 3.5 Å [21]. The geometric parameter G , which is a measure of exchange interaction between copper centers, is calculated using the equation

$$G = (g_3 - 2.0023) / (g_{\perp} - 2.0023)$$

where $g_{\perp} = (g_1 + g_2)/2$ [22] is 2.748 and it is less than 4.4 indicates considerable exchange interaction [23].

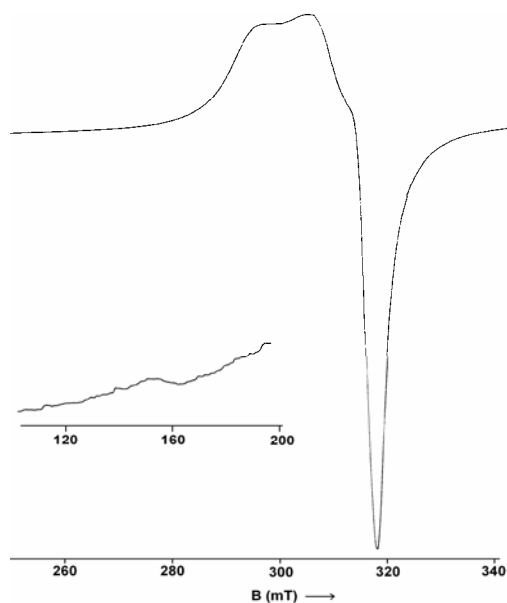


Fig. 5.6. EPR spectrum of compound **20** in polycrystalline state at 298 K.

The solution spectra of all complexes were recorded in DMF at 298 K. An isotropic spectrum is obtained for compound **20** (Fig. 5.7) with g_{iso} 2.115 and A_{iso} $73 \times 10^{-4} \text{ cm}^{-1}$, and this is due to the tumbling motion of molecules in DMF.

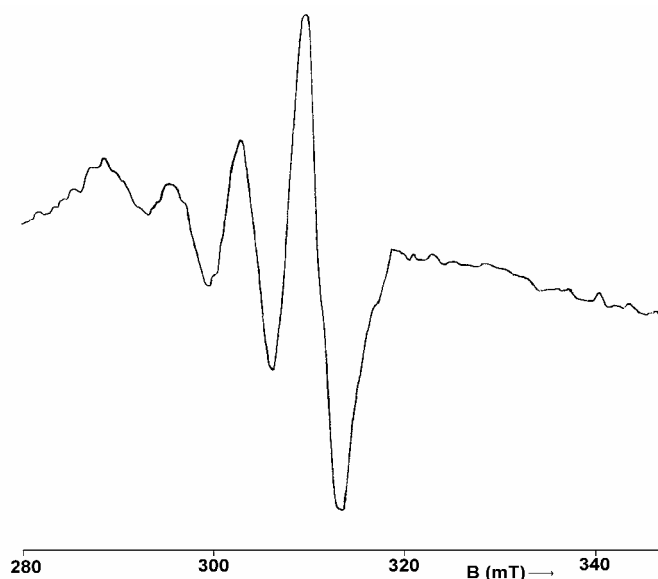


Fig. 5.7. EPR spectrum of compound 20 in DMF at 298 K.

The EPR spectrum obtained in frozen DMF for the same compound is a typical axial spectrum with $g_{\parallel} = 2.235$ and $g_{\perp} = 2.055$, $g_{\parallel} > g_{\perp} > 2.0023$ indicating the presence of $d_{x^2-y^2}$ ground state. Kivelson and Nieman have reported that g_{\parallel} values less than 2.3 indicate considerable covalent character to M–L bonds, while a value greater than 2.3 indicate ionic character. Here it is found that $g_{\parallel} < 2.3$ showing significant covalent character to M–L bond [24]. The A_{\parallel} value is found to be $198 \times 10^{-4} \text{ cm}^{-1}$ and there are no hyperfine lines in the perpendicular region. The expected half field signal is not obtained in the frozen state. However a four fold splitting in the parallel region is obtained. The spectrum of the complex was simulated using Easy Spin package [25] and shown in Fig. 5.8.

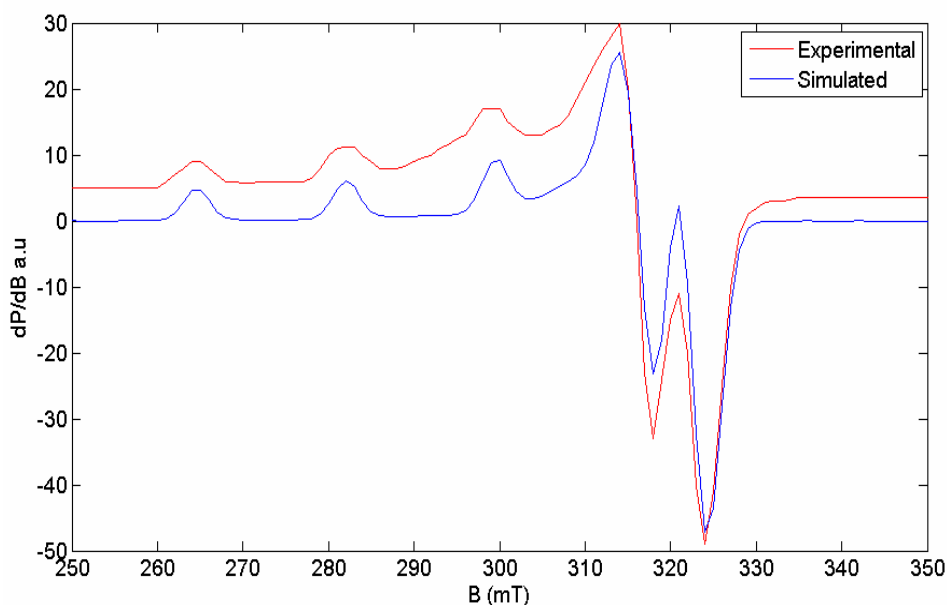


Fig. 5.8. Experimental and simulated best fit EPR spectra of the compound 20 in DMF at 77 K.

Compound **21** in polycrystalline state at 298 K displayed a typical axial spectrum with $g_{\parallel} = 2.192$ and $g_{\perp} = 2.060$ (Fig. 5.9). In this case also $g_{\parallel} > g_{\perp} > 2.0023$, which is consistent with $d_{x^2-y^2}$ ground state. The geometric parameter G for axial spectra, which is a measure of exchange interaction between copper centers, is calculated using the equation,

$$G = (g_{\parallel} - 2.0023) / (g_{\perp} - 2.0023)$$

is found to be 3.288 and it is less than 4.4 indicate considerable exchange interaction in the complex. For this compound we got a half field signal at 157 mT with $g = 4.139$, indicating dimeric species.

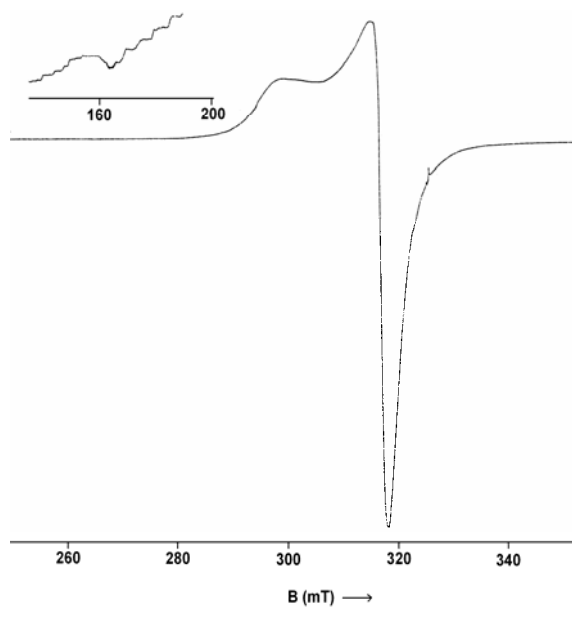


Fig. 5.9. EPR spectrum of compound 21 in polycrystalline state at 298 K.

The spectra obtained for compound **21** in DMF at 298 K and at 77 K were not good to interpret.

Compound **22** is EPR silent in polycrystalline state at room temperature due to strong antiferromagnetic interactions. However in DMF at 298 K, an isotropic spectrum is obtained (Fig. 5.10) due to the cleavage of the molecule with g_{iso} 2.117 and A_{iso} $83 \times 10^{-4} \text{ cm}^{-1}$. In this compound signal corresponding to $M_I = +3/2$ is split into three with superhyperfine coupling constant $A_N = 12 \times 10^{-4} \text{ cm}^{-1}$ indicating that the azomethine nitrogen dominates the bonding.

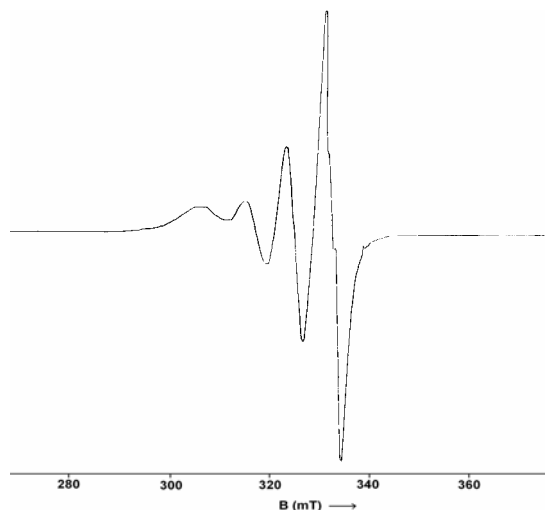


Fig. 5.10. EPR spectrum of compound 22 in DMF at 298 K.

The EPR spectrum of compound **22** in DMF (Fig. 5.11) shows the presence of two copper species in the system and we are unable to simulate this spectrum. This may be due to the cleavage of the compound in DMF and the coordination of solvent molecule to some copper centers [26].

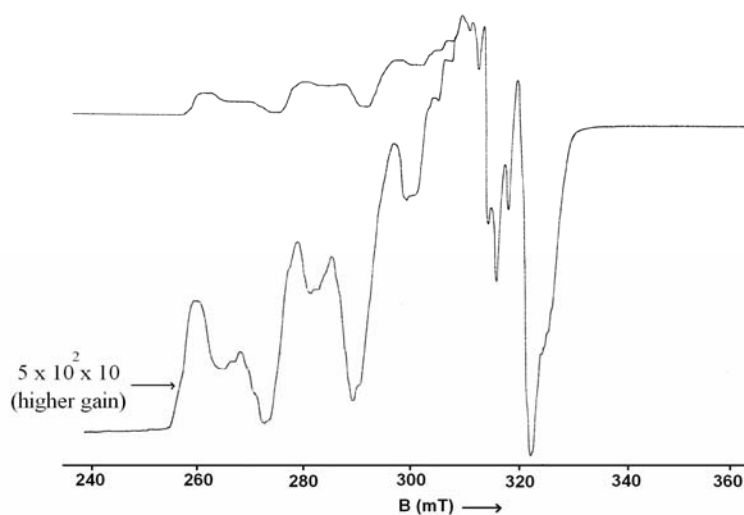


Fig. 5.11. EPR spectrum of compound 22 in DMF at 77 K.

Compound **23** in polycrystalline state at 298 K (Fig. 5.12) displayed a typical axial spectrum with $g_{\parallel} = 2.146$ and $g_{\perp} = 2.080$. Here also $g_{\parallel} > g_{\perp} > 2.0023$ suggests the presence of unpaired electron in $d_{x^2-y^2}$ orbital. $G < 4.4$ indicates the presence of exchange interactions.

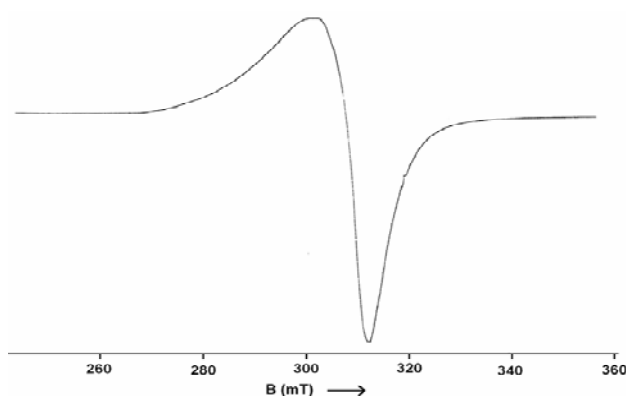


Fig. 5.12. EPR spectrum of compound **23** in polycrystalline state at RT.

The EPR spectrum of compound **23** in DMF at 298 K is an isotropic one with $g_{\text{iso}} = 2.118$ and $A_{\text{iso}} = 75 \times 10^{-4} \text{ cm}^{-1}$. The four hyperfine lines can be clearly resolved from the spectrum and the spectrum is shown in Fig. 5.13.

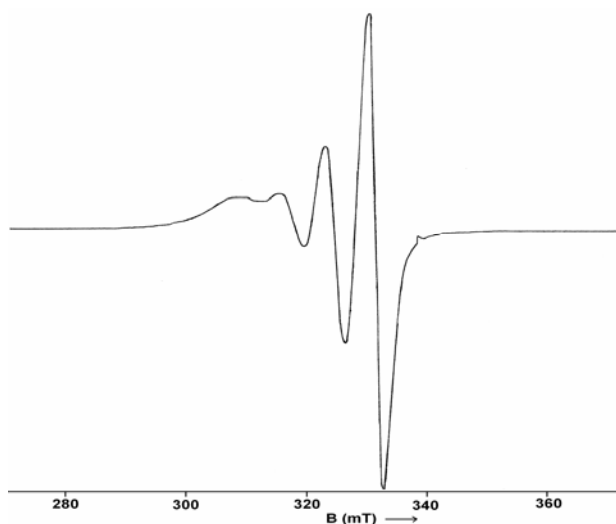


Fig. 5.13. EPR spectrum of compound **23** in DMF at 298 K.

Compound **23** in DMF at 77 K (Fig. 5.14) exhibit an axial spectrum with $g_{\parallel} = 2.256$ and $g_{\perp} = 2.074$ and $A_{\parallel} = 200 \times 10^{-4} \text{ cm}^{-1}$. In this compound expected superhyperfine splitting due to three nitrogen atoms is missing. But $g_{\parallel} > g_{\perp}$ suggest a distorted square pyramidal geometry and rules out the possibility of a trigonal bipyramidal structure.

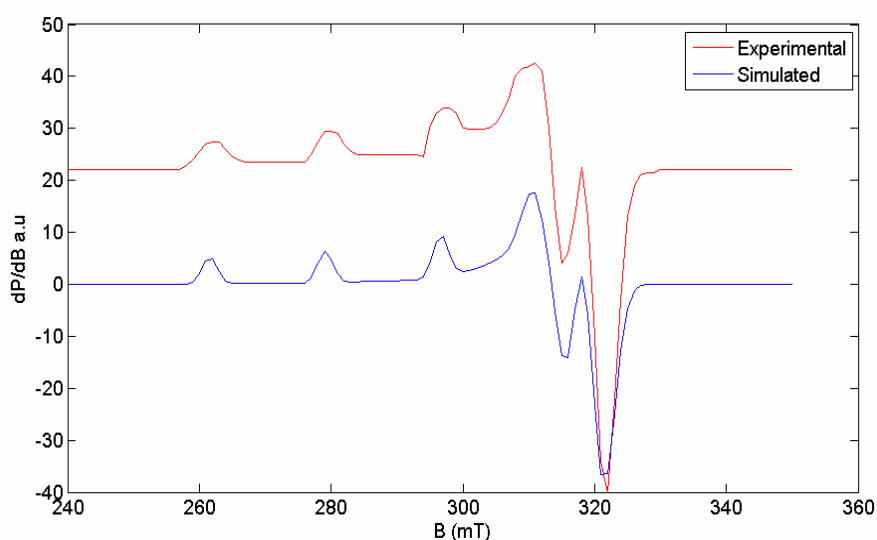


Fig. 5.14. EPR spectrum of compound 23 in DMF at 77 K.

Compound **24** in polycrystalline state at 298 K (Fig. 5.15) exhibits a rhombic spectrum with three g values $g_1 = 2.047$, $g_2 = 2.117$ and $g_3 = 2.163$. Since it is a six coordinated complex, the lowest $g > 2.04$ indicates copper(II) ion in elongated rhombic symmetry with all the axes aligned parallel and would be consistent with elongated rhombic octahedral stereochemistry [20]. Here also the EPR spectrum of compound in DMF at 298 K (Fig. 5.16) is an isotropic one with $g_{\text{iso}} = 2.117$ and $A_{\text{iso}} = 80 \times 10^{-4} \text{ cm}^{-1}$. The azomethine nitrogen dominates in bonding and it is evident from superhyperfine coupling constant $A_{\text{N}} = 15 \times 10^{-4} \text{ cm}^{-1}$.

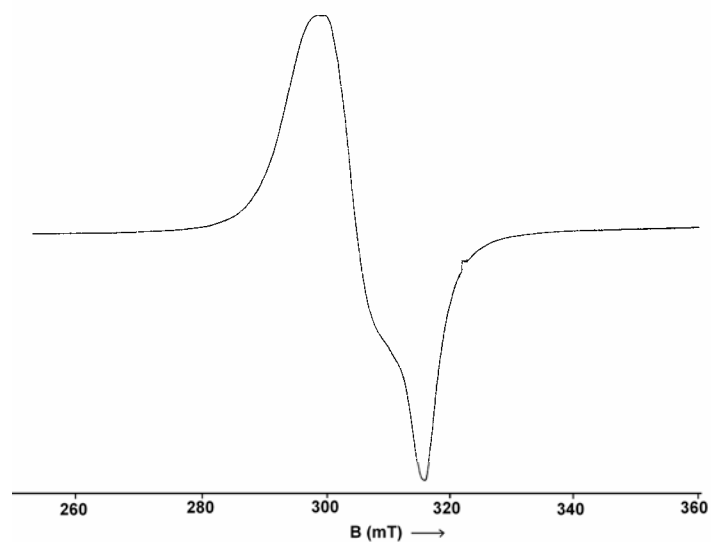


Fig. 5.15. EPR spectrum of compound 24 in polycrystalline state at RT.

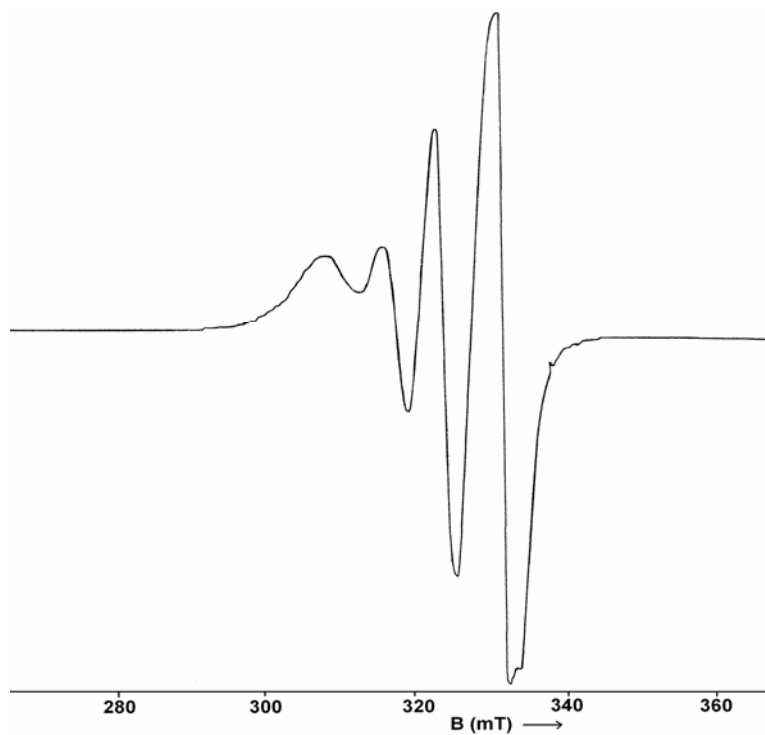


Fig. 5.16. EPR spectrum of compound 24 in DMF at 298 K.

The EPR spectrum of the compound in DMF at 77 K (Fig. 5.17) is axial with well defined $g_{\parallel} = 2.223$ and $g_{\perp} = 2.058$. The g_{av} values obtained from the solid state spectrum and from DMF at 77 K are very close to each other. From this it is evident that the compound retained its geometry in solution state also.

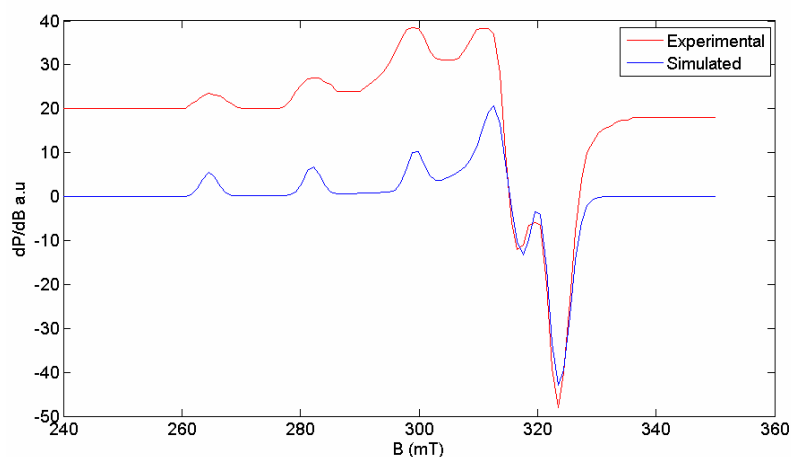


Fig. 5.17. EPR spectrum of compound **24** in DMF at 77 K.

The EPR spectrum of the compound **25** in polycrystalline state at 298 K (Fig. 5.18) is axial with $g_{\parallel} = 2.358$ and $g_{\perp} = 2.066$.

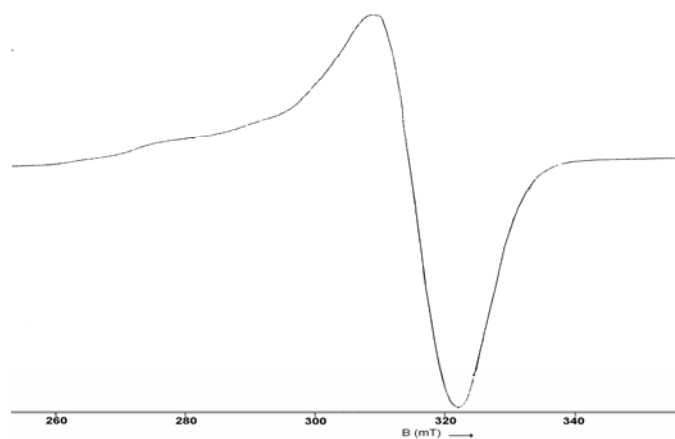


Fig. 5.18. EPR spectrum of compound **25** in polycrystalline state at 298 K.

And in DMF at 298 K (Fig. 5.19) an isotropic spectrum is obtained with $g_{\text{iso}} = 2.109$ and $A_{\text{iso}} = 76 \times 10^{-4} \text{ cm}^{-1}$.

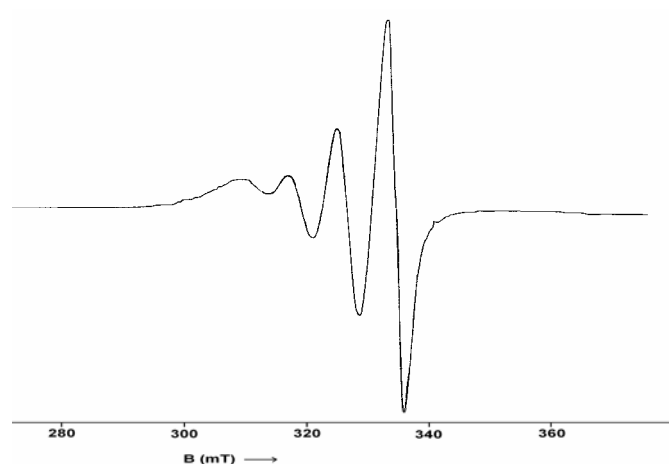


Fig. 5.19. EPR spectrum of compound **25** in DMF at RT.

The frozen solution EPR spectrum of **25** in DMF (Fig. 5.20) at 77 K is axial in nature with $g_{\parallel} = 2.146$ and $g_{\perp} = 2.012$. The pattern observed for g values, $g_{\parallel} > g_{\perp}$ suggest square pyramidal geometry with unpaired electron in $d_{x^2-y^2}$ orbital. This is confirmed by the crystal structure of compound [Cu(hmab)phen].

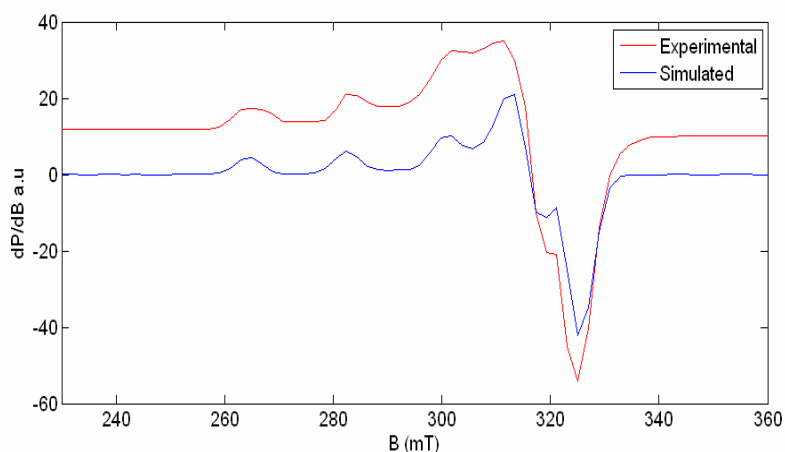


Fig. 5.20. EPR spectrum of compound **25** in DMF at 77 K.

The empirical factor, $f = g_{\parallel} / A_{\parallel}$, is an index of tetragonal distortion and it may vary from 105 to 135. In all the compounds except **21** f falls in the range 105–135 which show small to medium distortion from planarity [27].

The EPR parameters g_{\parallel} , g_{\perp} , A_{\parallel} and the energies of $d-d$ transitions were used to evaluate the bonding parameters α^2 , β^2 and γ^2 which may be regarded as a measure of covalency in the in-plane σ -bonds, in-plane π -bonds and out-of-plane π -bonds. The orbital reduction factors K_{\parallel} and K_{\perp} were also used to calculate these bonding parameters. The following expressions are used to calculate these parameters.

$$\alpha^2 = -\frac{A_{\parallel}}{0.036} + (g_{\parallel} - 2.0023) + \frac{3(g_{\perp} - 2.0023)}{7} + 0.04$$

$$K_{\parallel}^2 = (g_{\parallel} - 2.0023) \frac{\Delta E(d_{xy} \rightarrow d_{x^2-y^2})}{8\lambda_0}$$

$$K_{\perp}^2 = (g_{\perp} - 2.0023) \frac{\Delta E(d_{xz}, d_{yz} \rightarrow d_{x^2-y^2})}{2\lambda_0}$$

$$K_{\parallel} = \alpha^2 \beta^2$$

$$K_{\perp} = \alpha^2 \gamma^2$$

where λ_0 is the spin-orbit coupling constant and has a value -828 cm^{-1} for Cu(II) d^9 system. The value of α^2 indicates the extent of covalent nature, where the value of 1.0 corresponds to a purely ionic nature.

According to Hathaway [28], for pure σ -bonding $K_{\parallel} \approx K_{\perp} \approx 0.77$ and for in-plane π -bonding $K_{\parallel} < K_{\perp}$, while for out-of-plane π -bonding $K_{\perp} < K_{\parallel}$. Here in compounds **22** and **25**, $K_{\perp} < K_{\parallel}$ indicates the presence of out-of-plane π -bonding and in compounds **23** and **24**, $K_{\parallel} < K_{\perp}$ *ie.* in-plane π -bonding is present. The value

of bonding parameters α^2 , β^2 and $\gamma^2 < 1$ confirms the covalent nature of complexes. EPR spectral data and the bonding parameters are summarized in Table 5.5.

Table 5.5 EPR spectral assignments and bonding parameters of copper(II) complexes in polycrystalline state at 298 K, in DMF solution at 298 K and in DMF solution at 77 K.

	20	21	22	23	24	25
Polycrystalline (298 K)						
$g_{ }$	$g_1 = 2.050$ $g_2 = 2.089$ $g_3 = 2.187$	2.192	---	2.146	$g_1 = 2.047$ $g_2 = 2.117$ $g_3 = 2.163$	2.221
g_{\perp}		2.060	---	2.080		2.066
g_{iso}/g_{av}	2.108	2.104	---	2.102	2.109	2.163
G	2.748	3.288	---	1.849	2.016	5.584
DMF (298 K)						
g_{iso}	2.115	---	2.117	2.118	2.117	2.109
A_{iso}^a	73	---	83	75	80	76
A_N^a	---	---	12	---	15	---
DMF (77 K)						
$g_{ }$	2.235	---	2.209	2.256	2.223	2.146
g_{\perp}	2.055	---	2.038	2.074	2.058	2.012
g_{av}	2.115		2.095	2.135	2.113	2.056
$A_{ }^a$	198	---	210	200	195	163
f	113.0		105.0	113.0	114.0	132.0
α^2	0.817	---	0.845	0.879	0.826	0.641
β^2	---	---	0.841	0.881	0.879	0.914
γ^2	---	---	0.782	0.937	0.883	0.475
$K_{ }$	---	---	0.711	0.775	0.727	0.585
K_{\perp}	---	---	0.661	0.824	0.730	0.304

^a Expressed in units of cm^{-1} multiplied by a factor of 10^{-4} .

5.3.3 Infrared spectra

IR spectra in the range 4000-400 cm^{-1} were recorded for all the six complexes and the vibrational bands which are useful for determining the mode of coordination of the ligands, are given in Table 5.6. The broad bands observed around 3400 cm^{-1} in all complexes except **21** and **25** indicate the presence of water in structures. In the case of free acylhydrazones, bands due O–H and N–H were appeared around 3220 and 3035 cm^{-1} and these bands are found to be absent in copper(II) complexes, which is a clear evidence for the coordination of ligands in the dideprotonated form. In the IR spectra of the metal free ligands, the carbonyl and azomethine bands are observed in the regions 1630-1650 and 1600-1605 cm^{-1} respectively. In the infrared spectra of all six complexes, there are no bands due to carbonyl group. Upon complexation, the stretching vibrations of azomethine bond are found to be weakened due to coordination with copper centre. This results a negative shift in azomethine stretching frequencies in comparison with free hydrazones. Here in all compounds the azomethine bands are shifted to lower wavenumbers and the newly formed $-\text{C}=\text{N}-\text{N}=\text{C}-$ moiety gave bands in between 1520-1550 cm^{-1} . The bands around 415 cm^{-1} indicate the coordination of azomethine nitrogen to copper centre. The $\nu(\text{C}-\text{O})$ bands present in ligands are shifted to lower frequencies in complexes suggesting the coordination of the phenolic oxygen. The increase in $\nu(\text{N}-\text{N})$ bands in complexes, due to the increase in double bond character is another proof for the coordination of the ligands through the azomethine nitrogen [29]. There are broad bands observed around 3400 cm^{-1} in all complexes except **21** and **25** indicates the presence of water in structures. In compounds **23**, **24** and **25** bands due to heterocyclic breathing are observed in the region 750-1450 cm^{-1} [29,30]. The spectra of the compounds are shown in Figs. 5.21 – 5.26.

Table 5.6 Selected IR bands (cm^{-1}) with tentative assignments of copper(II) complexes

Compound	$\nu(\text{C}=\text{O})$	$\nu(\text{C}=\text{N})$	$\nu(\text{C}=\text{N})^a$	$\nu(\text{Cu}-\text{N})$	$\nu(\text{N}-\text{N})$	Heterocyclic breathing	$\nu(\text{C}-\text{O})$
Hzhmbn·H ₂ O	1643	1604	----	----	1110	----	1284
[Cu(hmbn)] ₂ ·2H ₂ O (20)	----	1594	1525	420	1140	----	1233
Hzhman	1638	1602	----	----	1135	----	1262
[Cu(hman)] ₂ (21)	----	1591	1531	419	1155	----	1244
Hzhmbb	1630	1600	----	----	1130	----	1286
[Cu(hmbb)] ₂ ·2H ₂ O (22)	----	1588	1547	419	1172	----	1225
[Cu(hmbb)phen]·1½H ₂ O (23)	----	1589	1532	420	1155	1428, 728	1214
[Cu(hmbb)(bipy)H ₂ O] (24)	----	1588	1529	407	1155	1438, 774	1214
Hzhmab	1650	1600	----	----	1127	----	1265
[Cu(hmab)phen] (25)	----	1590	1524	420	1153	1425, 726	1246

^a newly formed

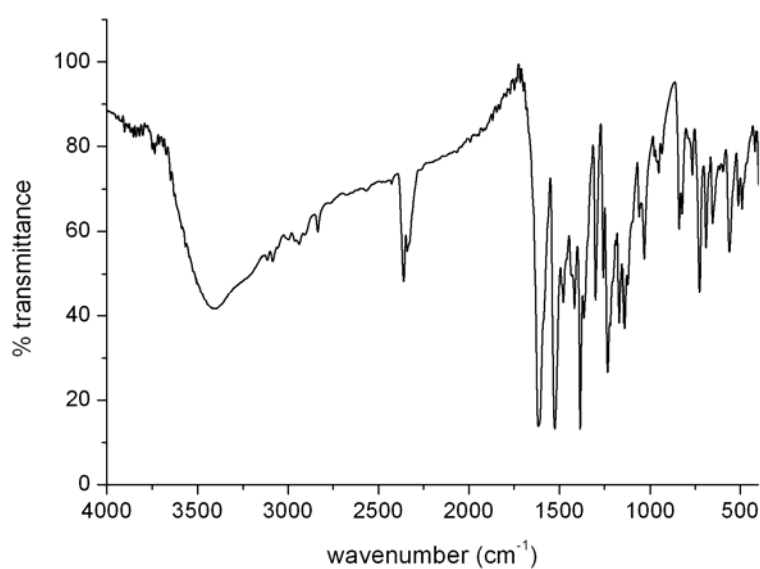


Fig. 5.21. Infrared spectrum of compound 20.

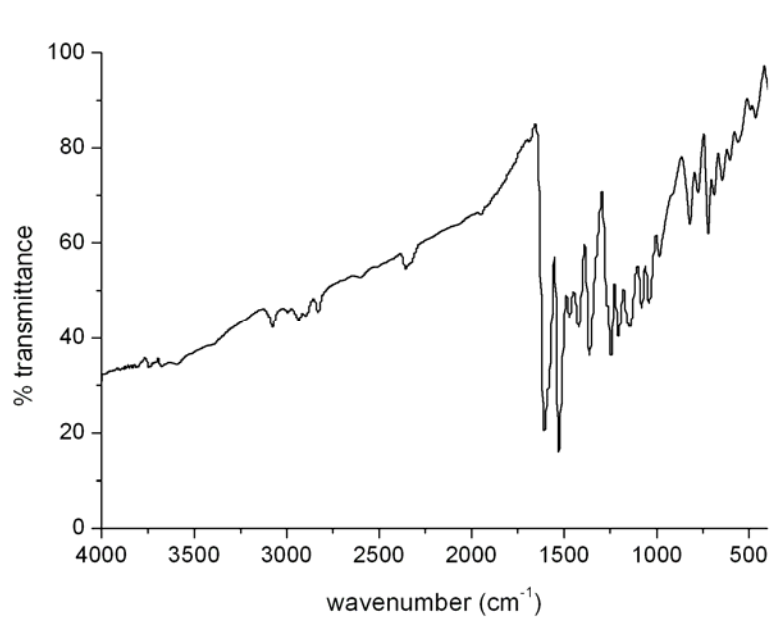


Fig. 5.22. Infrared spectrum of compound 21.

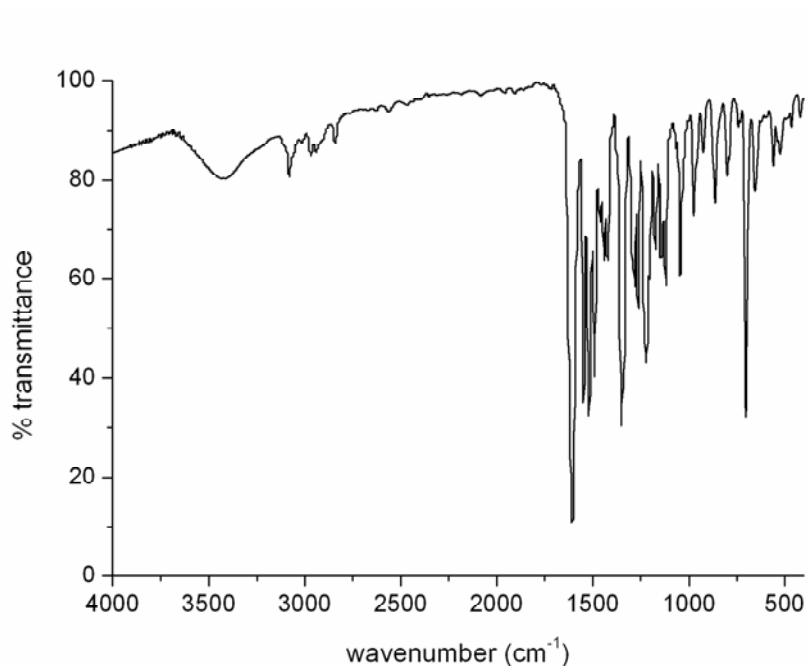


Fig. 5.23. Infrared spectrum of compound 22.

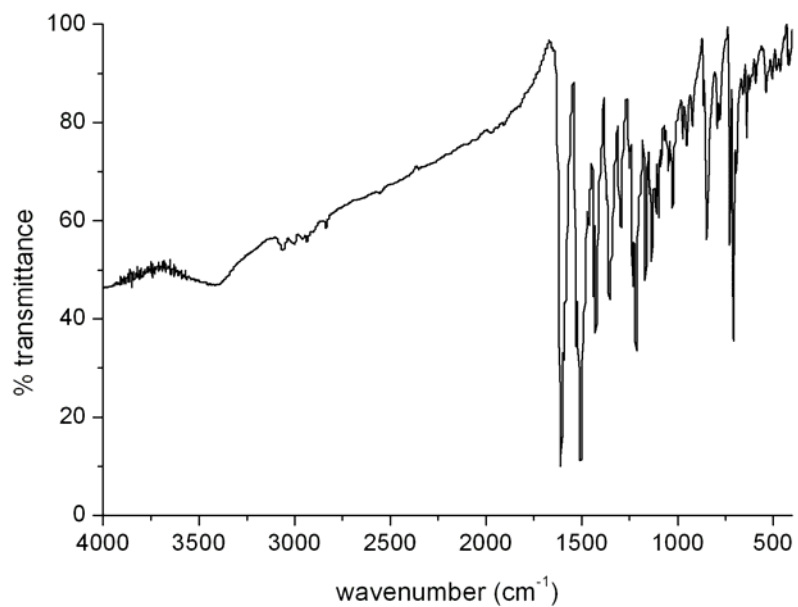


Fig. 5.24. Infrared spectrum of compound 23.

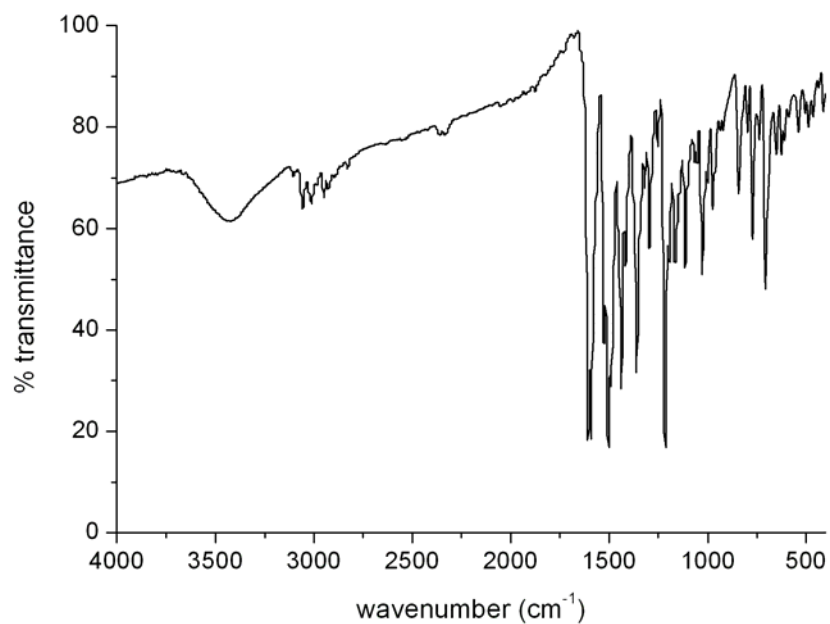


Fig. 5.25. Infrared spectrum of compound 24.

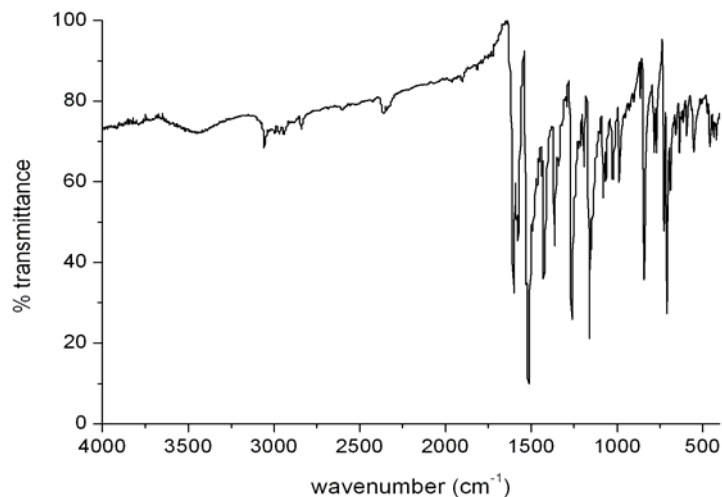


Fig. 5.26. Infrared spectrum of compound 25.

5.3.4 Electronic spectra

Cu(II) ion is one of the transition metal ions which forms complexes having different stereochemistries. For copper(II) ion outer electronic configuration is $3d^9$ with 2D as ground state term, lacks cubic symmetry and it yields other distorted forms of basic stereochemistries. In an octahedral d^9 system expected excitation is from 2E_g to $^2T_{2g}$ results a single absorption band. But the tetragonal distortion results further splitting, so the possible spin allowed excitations are $^2A_{1g} \leftarrow ^2B_{1g}$, $^2B_{2g} \leftarrow ^2B_{1g}$ and $^2E_g \leftarrow ^2B_{1g}$. But in practice it is difficult to resolve them into separate bands due to the low energy difference between these energy levels.

The electronic absorption spectral data of the complexes recorded in acetonitrile (Figs. 5.27-5.31) are summarized in Table 5.7. The electronic spectra of all the four acylhydrazones show bands in the region $30400\text{--}46000\text{ cm}^{-1}$ due to $\pi\text{-}\pi^*$ transitions. The conjugation of azomethine chromophore with olefinic or aryl groups change the spectrum significantly, since rather weak bands due to $n\text{-}\pi^*$ transitions are submerged by strong absorptions associated with $\pi\text{-}\pi^*$

transitions [31]. These intraligand transitions were slightly shifted up on complexation. In all the complexes intense bands were observed near 25670 cm^{-1} . It may be due to electronic transitions essentially from ligand based orbital to metal based orbital (here phenolic oxygen $\rightarrow\text{Cu}_{(d\pi)}$). When this happens charge is transferred from one part of the coordination sphere to other part or in other words charge transfer transition occurs. In all complexes except compound **20**, $d-d$ bands were observed in the low energy region of the spectra as weak bands around 15700 cm^{-1} [32]. In compound **20**, $d-d$ bands are probably masked by intense charge transfer transitions.

Table. 5.7 Electronic spectral assignments (cm^{-1}) of Cu(II) complexes

Compound	Intraligand transitions	LMCT	$d-d$
[Cu(hmbn)] ₂ ·2H ₂ O (20)	30350 (sh), 33260 (sh), 37680, 43520	25310	----
[Cu(hman)] ₂ (21)	30488, 38020, 44150	24630	14990
[Cu(hmbb)] ₂ ·2H ₂ O (22)	32530, 37310, 42980	26150	16210
[Cu(hmbb)phen]·1½H ₂ O (23)	32125, 37490, 43320	25870	15700
[Cu(hmbb)(bipy)H ₂ O] (24)	31363 (sh), 36310, 42290	26010	15850
[Cu(hmab)phen] (25)	32180 (sh), 37490, 43460	26280	15800

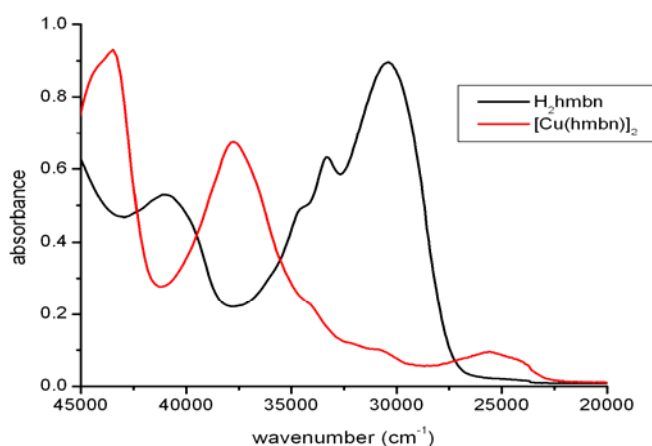


Fig. 5.27. Electronic spectra of H₂hmbn and its copper(II) complex in acetonitrile solution in the region $45000\text{-}20000\text{ cm}^{-1}$.

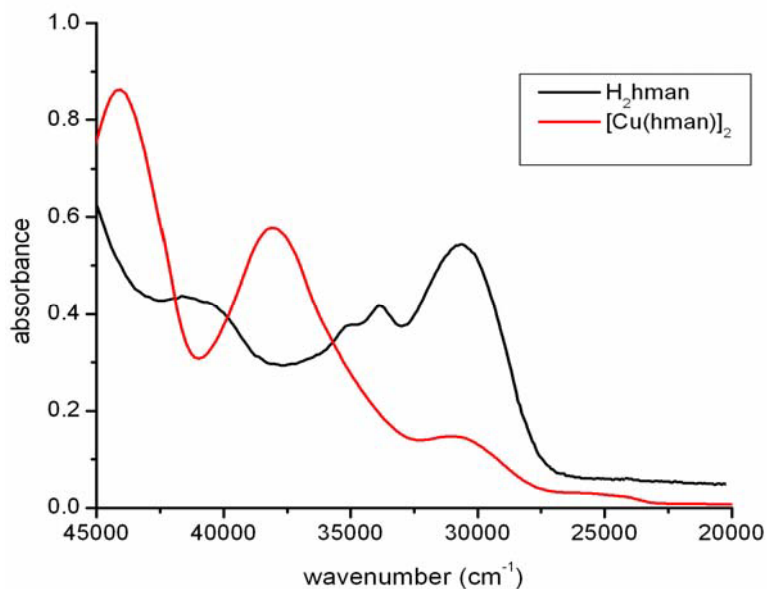


Fig. 5.28. Electronic spectra of H₂hman and its copper(II) complex in acetonitrile solution in the region 45000-20000 cm⁻¹.

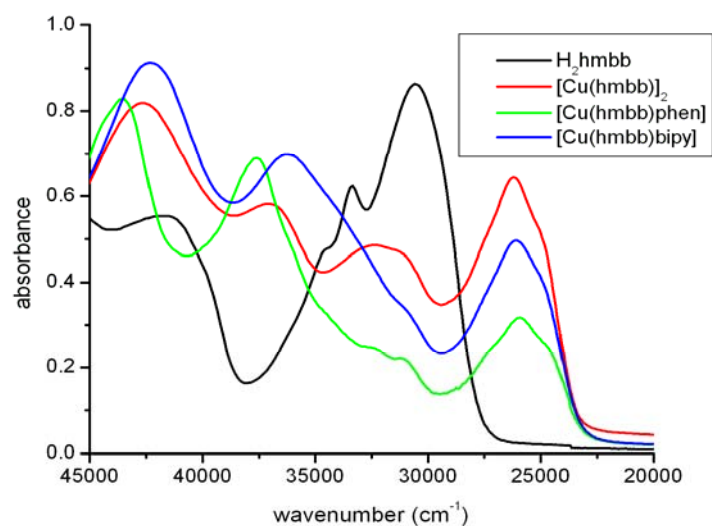


Fig. 5.29. Electronic spectra of H₂hmbb and its copper(II) complexes in acetonitrile solution in the region 45000-20000 cm⁻¹.

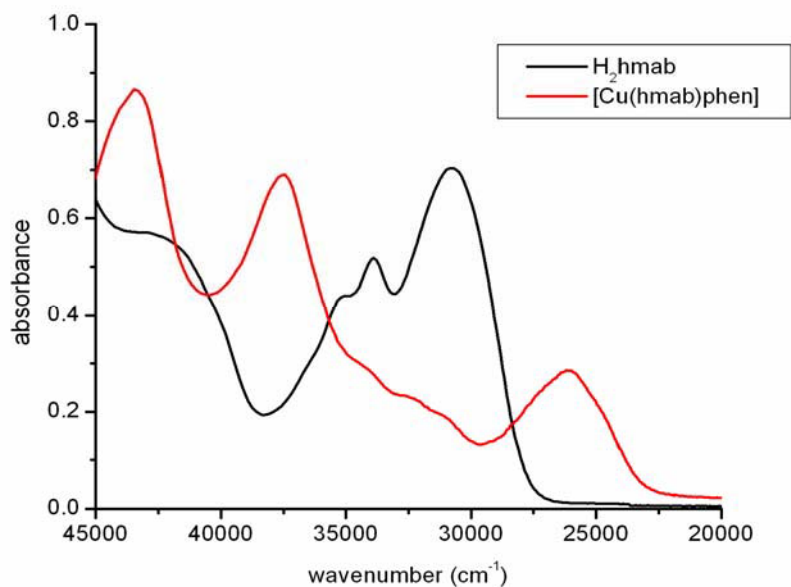


Fig. 5.30. Electronic spectra of H_2hmab and its copper(II) complex in acetonitrile solution in the region 45000-20000 cm^{-1} .

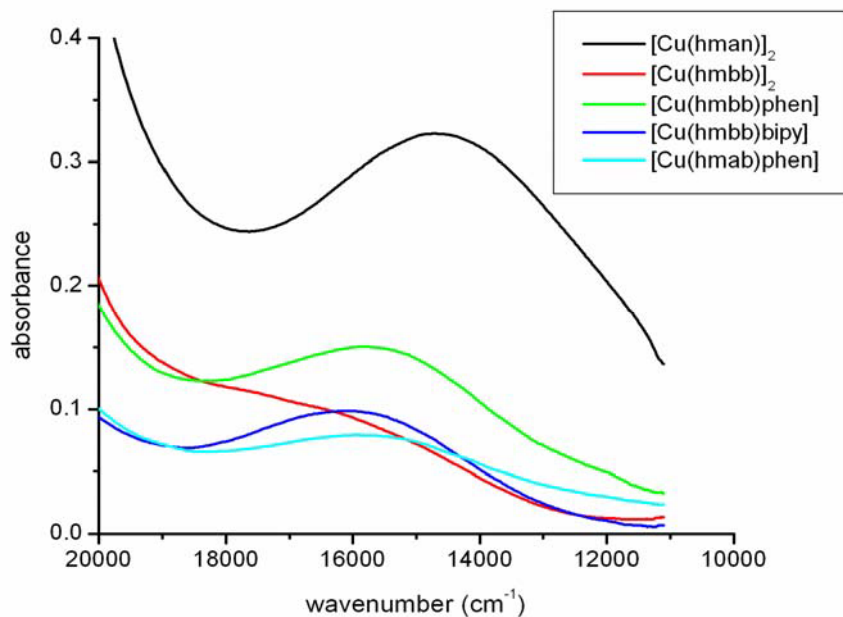


Fig. 5.31. Electronic spectra of complexes 21, 22, 23, 24 and 25 in acetonitrile solution in the region 20000-10000 cm^{-1} .

5.3.5 Thermal analyses

Thermal analyses provide valuable information regarding the thermal stability and nature of water molecules in complexes. It helps us to distinguish the lattice water molecules and coordinated water molecules present in the compound. Reports show that the weight losses for lattice water are in the range of 50-130 °C and weight loss due to coordinated water molecules are in the range of 130-250 °C [33,34]. Here in complexes **20**, **22** and **23** there are weight losses in the region 90-130 °C indicating the presence of lattice water molecules and in compound **24** weight loss is observed in between 160 °C and 210 °C indicating the presence of coordinated water molecule in structure. In compounds **21** and **25** there are no weight loss in these regions indicating the absence of water molecules. All the complexes decompose in the temperature range 250-550 °C. Above 550 °C a plateau is observed which corresponds to the formation of CuO. TG-DTG curves of complexes **22** and **24** are shown in Figs. 5.32 and 5.33.

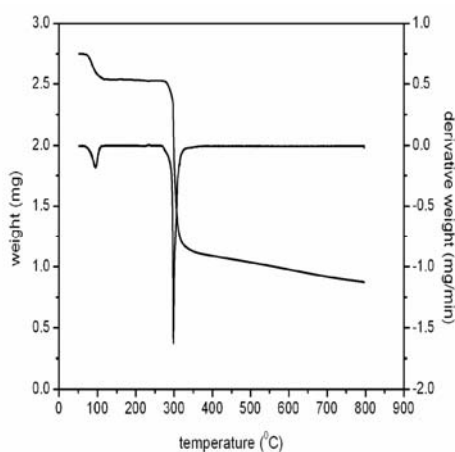


Fig. 5.32. TG-DTG plots of compound **22**.

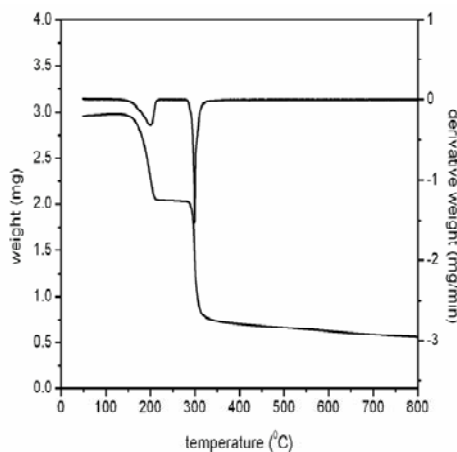


Fig. 5.33. TG-DTG plots of compound **24**.

References

1. E.I. Solomon, K.W. Penfield, D.E. Wilcox, *Struct. Bonding* (Berlin) 53 (1983) 1-57.
2. E.I. Solomon, L.B. LaCroix, D.W. Randall, *Pure Appl. Chem.* 70 (1998) 799-808.
3. I. S. MacPherson, M.E.P. Murphy, *Cell. Mol. Life Sci.* 64 (2007) 2887-2899.
4. D.J. Kosman, *J. Biol. Inorg. Chem.* 15 (2010) 15–28.
5. T. Ito, S. Thyagarajan, K.D. Karlin, S.E. Rokita, *Chem. Commun.* (2005) 4812-4814.
6. L. Li, K.D. Karlin, S.E. Rokita, *J. Am. Chem. Soc.* 127 (2005) 520-521.
7. J.P. Holland, J.C. Green, J.R. Dilworth, *Dalton Trans.* (2006) 783-794.
8. Z.F. Chen, M.X. Tan, L.M. Liu, Y.C. Liu, H.S. Wang, B. Yang, Y. Peng, H.G. Liu, H. Liang, C. Orvig, *Dalton Trans.* (2009) 10824-10833.
9. A.L. Motaleb, M. Ramadan, *Trans. Met. Chem.* 30 (2005) 471-480.
10. F.G. Mutti, R. Pievo, M. Sgobba, M. Gullotti, L. Santagostini, *Bioinorg. Chem. Appl.* 2008 (2008), Article ID 762029, 9 pages.
11. D.K. Johnson, T.B. Murphy, N.J. Rose, W.H. Goodwin, L. Pickart, *Inorg. Chim. Acta* 67 (1982) 159-165.
12. M. Shebl, *Spectrochim. Acta Part A* 73 (2009) 313-323.
13. A.R. Cowley, J.R. Dilworth, P.S. Donnelly, J.M. White, *Inorg. Chem.* 45 (2006) 496–498.
14. E. Manoj, M.R.P. Kurup, A. Punnoose, *Spectrochim. Acta Part A* 72 (2009) 474-483.

15. M. Kato, H.B. Jonassen, J.C. Fanning, *Chem. Rev.* 64 (1964) 99-128.
16. A.W. Addison, T.N. Rao, R. Reedijk, J.V. Rigin, G.C. Verschoor, *J. Chem. Soc., Dalton Trans.* (1984) 1349-1356.
17. B.H. Ye, X.M. Chen, G.Q. Xne, L.N. Ji, *J. Chem. Soc., Dalton Trans.* (1998) 2827-2832.
18. B.J. Hathaway, *Coord. Chem. Rev.* 52 (1983) 87-169.
19. E. Garribba, G. Micera, *J. Chem. Educ.* 83 (2006) 1229-1232.
20. B.J. Hathaway, D.E. Billing, *Coord. Chem. Rev.* 5 (1970) 143-207.
21. U.L. Kala, S.Suma, S. Krishnan, M.R.P. Kurup, R.P. John, *Polyhedron* 26 (2007) 1427-1435.
22. L. Latheef, M.R.P Kurup, *Spectrochim. Acta A* 70 (2008) 86-93.
23. J. R. Wasson, C.Trapp, *J. Phys. Chem.* 73 (1969) 3763-3772.
24. D. Kivelson, R. Nieman, *J. Chem. Soc., Dalton Trans.* 35 (1961) 149.
25. St. Stoll, *Spectral Simulations in Solid-state EPR*, PhD thesis, ETH, Zurich, 2003.
26. R. Pogni, M.C. Baratto, A. Diaz, R. Basosi, *J. Inorg. Biochem.* 79 (2000) 333-337.
27. S.I. Findone, K.W.H. Stevens, *Proc. Phys. Soc.* 73 (1959) 116-117.
28. B.J. Hathaway, *J. Chem. Soc., Dalton Trans.* (1972) 1196-1199.
29. P.B. Sreeja, M.R.P. Kurup, *Polyhedron* 23 (2004) 575-581.
30. B.A. Reddy, *J. Biomed. Sci. Res.* 1 (2009) 27-32.
31. S. Patai, *The Chemistry of Carbon-Nitrogen Double Bond*, Interscience publishers, John Wiley & Sons, London (1970).

Chapter 5

32. A.B.P. Lever, *Inorganic Electronic Spectroscopy*, 2nd Edition, Elsevier, Amsterdam 1984.
33. M.R. Maurya, N. Bharti, *Trans. Met. Chem.* 24 (1999) 389-393.
34. S.M. Abdallah, G.G. Mohamed, M.A. Zayed, M.S. Abou El-Ela, *Spectrochim. Acta Part A* 73 (2009) 833–840.

**********

SYNTHESES AND CHARACTERIZATION OF Zn(II) COMPLEXES DERIVED FROM ONO DONOR ACYLHYDRAZONES

- 6.1 Introduction
- 6.2 Experimental
- 6.3 Results and discussion
- References

6.1 Introduction

Zinc is an essential element for normal functioning of most organisms and is the main constituent in a number of metallo-enzymes like carbonic anhydrase and alcohol dehydrogenase [1,2]. Zinc functions as an antioxidant and is participated in many serious biochemical reactions [3]. It is the second most abundant transition metal ion in human body after iron. It is essential for protein synthesis and which helps to regulate the production of cells in the body's immune system.

Zinc complex of L-carnosine is an anti-ulcer drug in which zinc plays an essential role [4]. More than 1000 enzymes contain zinc in the active centers, and in brief no other metal has as many functions in living organisms as zinc [5]. Yet today the role of zinc in various biological processes is not fully revealed. According to Vahrenkamp [6] may be the 'non-properties' of zinc are the basis of this uniqueness, *ie.* unlike other transition metals zinc has no redox chemistry, no ligand field effects, no typical coordination numbers or geometries, no stability or inertness of its complexes, no typical "hard" or "soft" characteristics.

Reports showed that the salen complexes of zinc can be used as sensing materials for different ions and molecules, emissive materials for organic light emitting diodes and building blocks for various supramolecular architectures [7-9]. Zn(II) ions have a high affinity towards nitrogen, oxygen and sulfur donor ligands [10,11].

Zinc(II) ion provides a number of coordination compounds because of its affinity towards different types of ligands and flexible coordination number ranging from two to eight. The filled *d* shell does not offer crystal field stabilization on Zn²⁺ hence coordination number and stereochemistry are determined by the size of the Zn(II) cation and the steric requirements of the ligands. In zinc complexes commonly found geometries are tetrahedral and octahedral. Among these tetrahedral geometry predominates. Six coordinate complexes may be octahedral or trigonal prismatic. Among the less common five coordinate complexes trigonal bipyramidal geometry predominates over square pyramidal geometry.

This chapter deals with the syntheses and characterization of Zn(II) complexes derived from different ONO donor hydrazones.

6.2 Experimental

6.2.1 Materials

2-Hydroxy-4-methoxyacetophenone (Aldrich), 2-hydroxy-4-methoxybenzaldehyde (Aldrich), nicotinic acid hydrazide (Aldrich), benzhydrazide (Aldrich), Zn(CH₃COO)₂·2H₂O (S.D.Fine) were used without further purification. Solvent used was methanol.

6.2.2 Syntheses of acylhydrazones

The syntheses of acylhydrazones were done as described in Chapter 2.

6.2.3 Syntheses of Zn(II) complexes

[Zn(hmbn)]₂·H₂O (26) : To a methanolic solution of H₂hmbn·H₂O (0.289 g, 1 mmol), Zn(CH₃COO)₂·2H₂O (0.219 g, 1 mmol) in methanol was added and stirred for two hours. The yellow colored product formed was filtered, washed with methanol, followed by ether and dried over P₄O₁₀ *in vacuo*. Elemental Anal. Found (Calcd.) (%): C, 49.05 (48.93); H, 3.01 (3.52); N, 12.50 (12.23).

[Zn(hman)]₂·H₂O (27) : Zn(CH₃COO)₂·2H₂O (0.219 g, 1 mmol) in methanol was added to the H₂hman solution in methanol (0.285 g, 1 mmol) and stirred for about two hours. The yellow product formed was filtered, washed with methanol, followed by ether and dried over P₄O₁₀ *in vacuo*. Elemental Anal. Found (Calcd.) (%): C, 50.90 (50.37); H, 3.58 (3.94); N, 11.75 (11.75).

[Zn(Hhmbb)OAc] (28) : To a methanolic solution of H₂hmbb (0.270 g, 1 mmol), Zn(CH₃COO)₂·2H₂O (0.219 g, 1 mmol) in methanol was added. The yellow colored product formed was filtered washed with methanol, followed by ether and dried over P₄O₁₀ *in vacuo*. Elemental Anal. Found (Calcd.) (%): C, 52.04 (51.86); H, 3.83 (4.10); N, 7.18 (7.11).

[Zn(hmab)]₂ (29) : Methanolic solutions of the H₂hmab (0.284 g, 1 mmol) and Zn(CH₃COO)₂·2H₂O (0.219 g, 1 mmol) were mixed and stirred for about 2 hours. The product separated was yellow colored and it was filtered, washed with methanol, followed by ether and dried over P₄O₁₀ *in vacuo*. Elemental Anal. Found (Calcd.) (%): C, 54.89 (55.27); H, 3.59 (4.06); N, 7.99 (8.06).

6.3 Results and discussion

In the case of all the four complexes, experimental and calculated analytical data are in very close agreement. Magnetic susceptibility studies indicate diamagnetic nature of these complexes and it indicates the *d*¹⁰ outer electronic

configuration of zinc. The molar conductivity measured for all the four complexes in 10^{-3} M DMF solution is found to be below $15 \text{ ohm}^{-1} \text{ cm}^2 \text{ mol}^{-1}$ which is much less than the value of $65\text{-}90 \text{ ohm}^{-1} \text{ cm}^2 \text{ mol}^{-1}$ obtained for a 1:1 electrolyte in the same solvent [12]. So the conductance measurements in DMF suggest that they are non-electrolytes, the conductivity values are tabulated in Table 6.1.

Table 6.1 Molar conductivity measurements

Compound	$\lambda_m^{\#}$
[Zn(hmbn)] ₂ ·H ₂ O (26)	11
[Zn(hman)] ₂ ·H ₂ O (27)	10
[Zn(Hhmbb)OAc] (28)	12
[Zn(hmab)] ₂ (29)	9

[#]molar conductivity (in $\text{mho cm}^2 \text{ mol}^{-1}$) taken in 10^{-3} M DMF.

6.3.1 ¹H NMR spectral studies

Proton Nuclear Magnetic Resonance (¹H NMR) Spectroscopy is a powerful tool used for the determination of the structure of compounds. Because of their diamagnetic nature, the Zn(II) complexes were studied by NMR spectroscopy. The ¹H NMR spectra of the acylhydrazones and complexes have been recorded with DMSO as solvent. The comparison of the NMR spectra of the complexes with the spectra of ligands gave valuable informations regarding the coordination mode of ligands during complexation. The ¹H NMR spectrum obtained for compound **27** was not good due to the poor solubility of the compound. In the spectra of the free hydrazones there are sharp singlets in the range of 12-14 ppm showing the existence of iminol form in solution. They also gave singlets in the range of 11-12 ppm with an area integral of one which is due to phenolic OH protons. Large δ values of these protons may be due to intramolecular hydrogen bonding. Upon D₂O exchange, the intensity of these signals significantly

decreases, which suggests that these protons are easily exchangeable and confirm the assignment. The singlets with an area integral of three in the range of 3-3.8 ppm indicate the presence of three methoxy hydrogens. Peaks for aromatic protons were found in the region 6-8 ppm. In the spectra of the complexes, there are no peaks in the region 11-12 ppm, which is an evidence for the coordination of phenolic oxygen to the metal centre. Similarly peaks corresponds to iminol protons found in the spectra of free hydrazones were absent in the spectra of complexes indicating the coordination of iminol oxygen to zinc. In the spectrum of compound **28**, a singlet with an area integral of three is found at 2.086 ppm and it is assigned to the methyl group present in acetate which is coordinated to zinc. Also a singlet with area integral one is appeared at 8.524 ppm may indicate the presence of NH proton suggests the coordination of ligand in the amido form. All other peaks observed in the spectra of free hydrazones are slightly shifted. The ^1H NMR spectra of complexes **26** and **28** are shown in the Figs. 6.1 and 6.2.

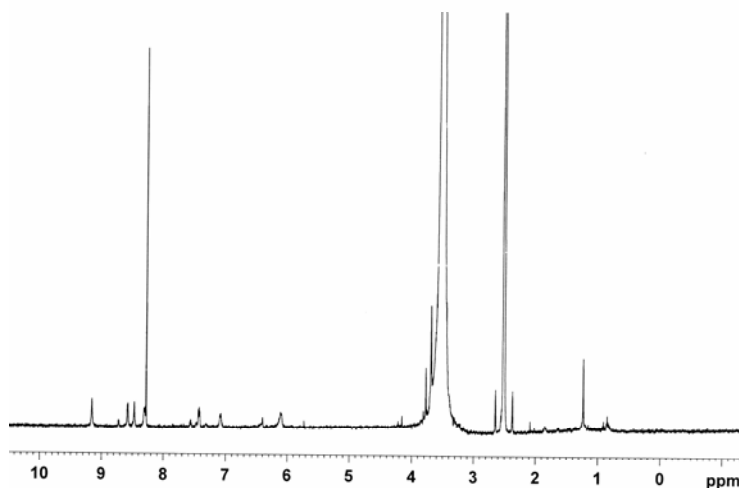


Fig. 6.1. ^1H NMR spectrum of $[\text{Zn}(\text{hmbn})]_2 \cdot \text{H}_2\text{O}$ (**26**).

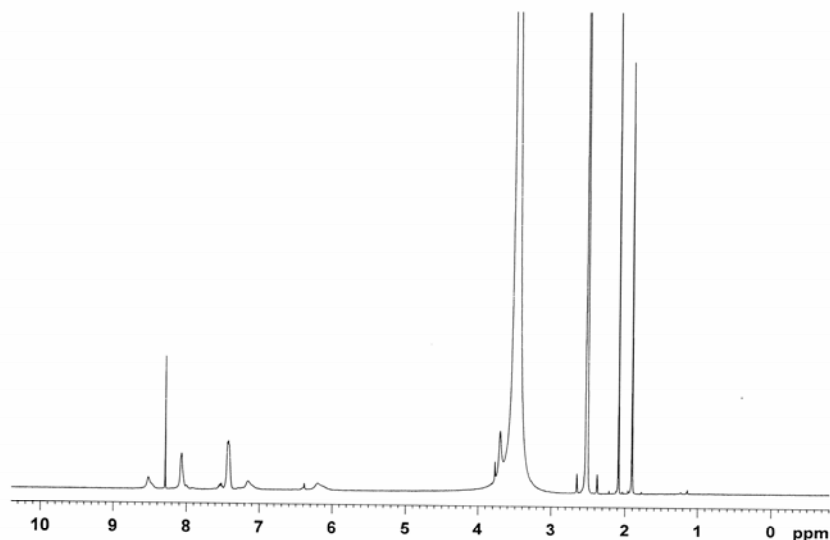


Fig. 6.2. ^1H NMR spectrum of $[\text{Zn}(\text{Hhmbb})\text{OAc}]$ (**28**).

6.3.2 Infrared spectra

The IR spectra of the complexes, in comparison with those of the free ligands, display certain changes, which give an idea about the type of coordination and their structure. Significant IR spectral bands of the complexes are listed in Table 6.2. Free hydrazones show strong absorptions in the 1630-1650 cm^{-1} region are assigned to carbonyl group, and bands due to azomethine group were observed around 1600 cm^{-1} . In compounds **26** and **27**, broad bands were observed at 3409 and 3417 cm^{-1} due to lattice water. Coordination of hydrazones to the zinc ion through the azomethine nitrogen atom is expected to reduce the electron density in the azomethine link and thus, lower the $\nu(\text{C}=\text{N})$ absorption frequency. Hence this band undergoes a shift to lower wavenumber [13,14]. In complexes **26**, **27** and **29**, a lower shift is observed in $\nu(\text{C}=\text{N})$ absorption frequency indicates coordination of azomethine nitrogen to zinc. Coordination of azomethine nitrogen is also evident from the increase in N-N

stretching frequency in all the complexes. In complexes **26**, **27** and **29**, bands correspond to carbonyl groups are absent suggesting the enolization of ligands during complexation. But in compound **28** bands observed around 1645 and 3000 cm^{-1} are assigned to carbonyl group and NH group respectively, *ie.* in this complex, ligand is in the amido form. For the compound **28**, bands at 1600 and 1386 cm^{-1} correspond to symmetric and asymmetric vibrations of the acetate group are consistent with the presence of a unidentate acetate group [15,16]. In compound **28**, a very intense band is observed at 1600 cm^{-1} , is a combination band of $\nu(\text{C}=\text{N})$ and $\nu_{\text{a}}(\text{CH}_3\text{COO})$ stretching frequencies. For all the complexes, phenolic C–O stretching occurs at lower wavenumber when compared to that of the ligands indicating the deprotonation and coordination of phenolic OH. Appearance of new bands in the regions of 525-560 and 440-460 cm^{-1} are assignable to $\nu(\text{Zn}-\text{O})$ and $\nu(\text{Zn}-\text{N})$ respectively. The IR spectra of the complexes are shown in the Figs. 6.3-6.6.

Table 6.2 Selected IR bands (cm^{-1}) with tentative assignments of Zn(II) complexes

Compound	$\nu(\text{C}=\text{N})$	$\nu(\text{C}=\text{N})^{\text{a}}$	$\nu(\text{N}-\text{N})$	$\nu(\text{C}-\text{O})$	$\nu(\text{Zn}-\text{O})$	$\nu(\text{Zn}-\text{N})$
$[\text{Zn}(\text{hmbn})]_2 \cdot \text{H}_2\text{O}$ (26)	1597	1527	1167	1210	527	454
$[\text{Zn}(\text{hman})]_2 \cdot \text{H}_2\text{O}$ (27)	1596	1524	1161	1244	547	445
$[\text{Zn}(\text{Hhmbb})\text{OAc}]$ (28)	1600	.	1124	1247	560	460
$[\text{Zn}(\text{hmab})]_2$ (29)	1593	1540	1150	1223	540	459

^a newly formed

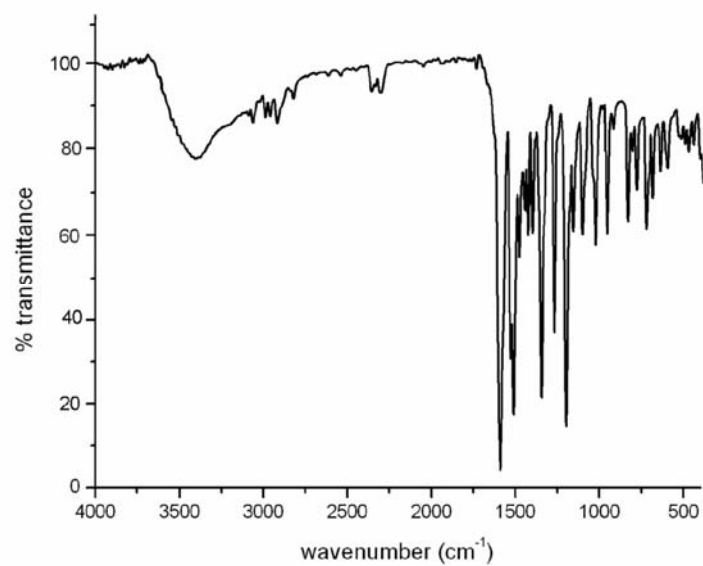


Fig. 6.3. IR spectrum of $[\text{Zn}(\text{hmbn})]_2 \cdot \text{H}_2\text{O}$ (26).

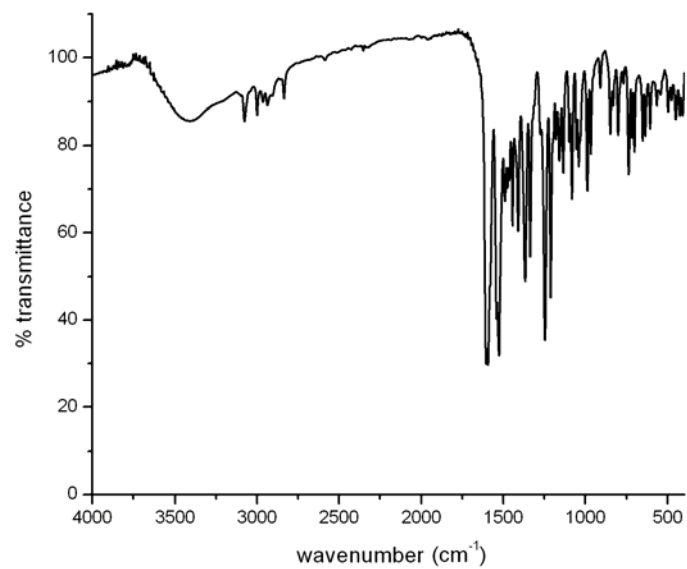


Fig. 6.4. IR spectrum of $[\text{Zn}(\text{hman})]_2 \cdot \text{H}_2\text{O}$ (27).

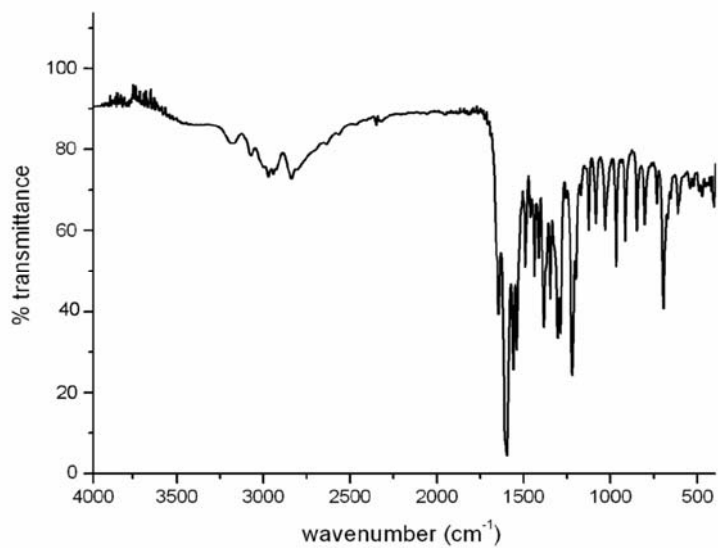


Fig. 6.5. IR spectrum of [Zn(Hhmbb)OAc] (28).

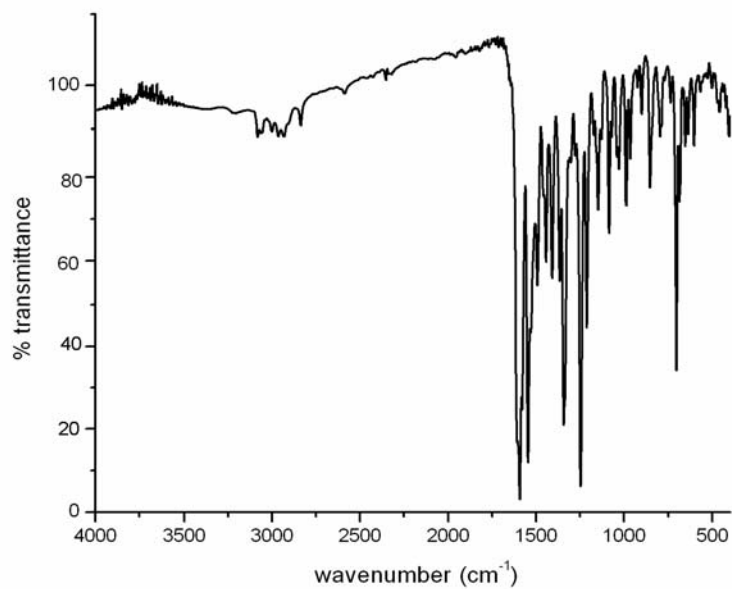


Fig. 6.6. IR spectrum of [Zn(hmab)]₂ (29).

6.3.3 Electronic spectra

The electronic spectra of the ligands and complexes were recorded in acetonitrile solutions on a UVD-3500, UV-vis Double Beam Spectrophotometer. Due to filled d orbitals, $d-d$ transitions are not expected in the case of Zn(II) complexes. But these complexes are yellow colored and the colors of the complexes are attributed to metal to ligand charge transfer transitions. Here MLCT bands were observed in the range of 24000-28000 cm^{-1} [17]. The electronic spectra of all the four acylhydrazones showed bands in the region 30400-46000 cm^{-1} due to $\pi-\pi^*$ transitions and $n-\pi^*$ transitions. These intraligand transitions were found to be slightly shifted during complexation. Table 6.3 summarized the electronic absorptions of the complexes and the spectra of the complexes are shown in Figs 6.7-6.10.

Table 6.3 Electronic spectral assignments (cm^{-1}) of Zn(II) complexes

Compound	Intraligand transitions	Charge transfer transition
[Zn(hmbn)] ₂ ·H ₂ O (26)	30880, 36520, 42970	25530
[Zn(hman)] ₂ ·H ₂ O (27)	30130, 35960, 42150	24630
[Zn(Hhmbb)OAc] (28)	30950, 37270, 43740	24280
[Zn(hmab)] ₂ (29)	31570, 39430, 43210	27800

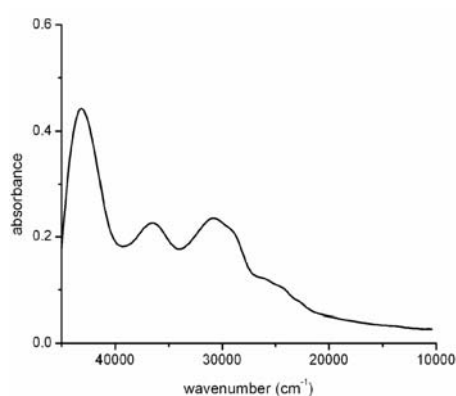


Fig. 6.7. Electronic spectrum of [Zn(hmbn)]₂ (26**).**

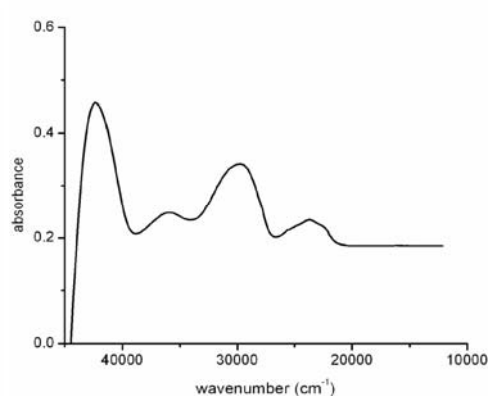


Fig. 6.8. Electronic spectrum of [Zn(hman)]₂ (27**).**

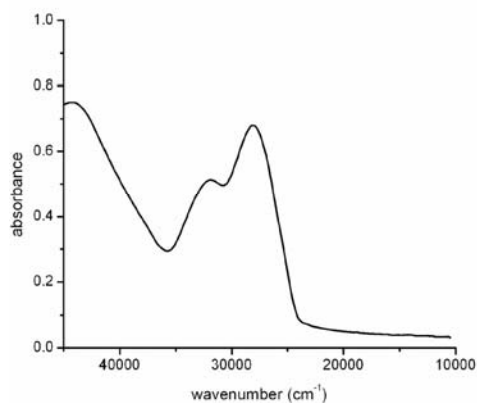


Fig. 6.9. Electronic spectrum of [Zn(Hhmbb)OAc] (28).

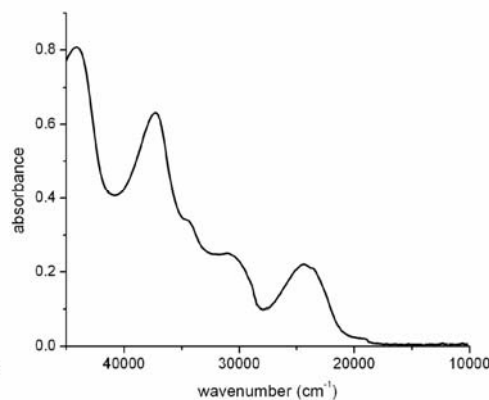


Fig. 6.10. Electronic spectrum of [Zn(hmab)]₂ (29).

6.3.4 Thermal analyses

Thermogravimetric analyses of the complexes will give information concerning the thermal stability of the complex and to decide whether the water molecules are in the inner or outer coordination sphere of the central metal ion [18]. Here Thermogravimetric analyses were carried out from 50 to 1000 °C under nitrogen atmosphere. In complexes **26** and **27**, there is a weight loss below 120 °C indicating the presence of lattice water. In complexes **28** and **29**, no weight loss is observed in between 50-250 °C indicating absence of water molecules in these complexes. Above 400 °C the complexes begin to decompose and the decomposition was not seen to be completed even at 1000 °C. TG – DTG plots of complexes **26** and **28** are shown in Figs. 6.11 and 6.12.

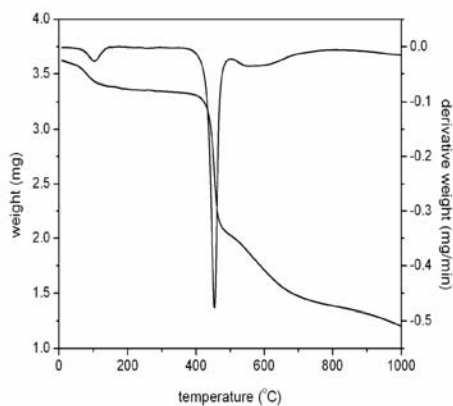


Fig. 6.11. TG-DTG plots of [Zn(hmbn)]₂·H₂O (26).

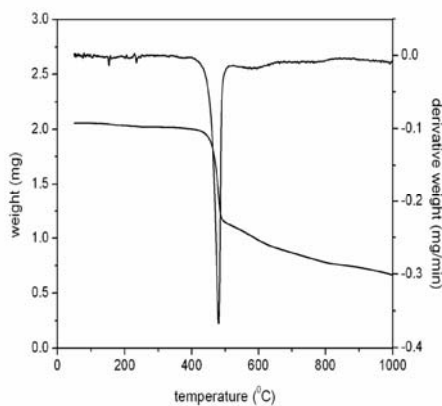


Fig. 6.12. TG-DTG plots of [Zn(Hhmbb)OAc] (28).

References

1. M.R. Badger, G.D. Price, *Annu. Rev. Plant Physiol. Plant Mol. Bio.* 45 (1994) 369–392.
2. P.C. Sanghani, H. Robinson, W.F. Bosron, T.D. Hurley, *Biochemistry* 41 (2002) 10778–10786.
3. G. Kirkil, M.H. Muz, D. Seçkin, K. Şahin, Ö. Küçük, *Resp. Med.* 102 (2008) 840–844.
4. T. Matsukura, H. Tanaka, *Biochemistry (Moscow)* 65 (2000) 817–823.
5. *Encyclopedia of Inorganic Chemistry*, 2nd Edition, R. Bruce King, Wiley (2005).
6. H. Vahrenkamp, *Dalton Trans.* 42 (2007) 4751–4759.
7. M. Cano, L. Rodriguez, J.C. Lima, F. Pina, A.D. Cort, C. Pasquini, L. Schiaffino, *Inorg. Chem.* 48 (2009) 6229–6235.
8. P.I.P. Elliott, *Annu. Rep. Prog. Chem. Sect. A* 106 (2010) 526–552.

9. A.W. Kleij, Dalton Trans. (2009) 4635–4639.
10. A.A.R. Despaigne, J.G.D. Silva, A.C.M. do Carmo, O.E. Piro, E.E. Castellano, H. Beraldo, Inorg. Chim. Acta 362 (2009) 2117-2122.
11. E.B. Seena, M.R.P. Kurup, Spectrochim. Acta A 69 (2008) 726-732.
12. W.J. Geary, Coord. Chem. Rev. 7 (1971) 81-122.
13. M.S. Nair, R.S. Joseyphus, Spectrochim. Acta Part A 70 (2008) 749–753.
14. L. Latheef, E. Manoj, M.R.P. Kurup, Polyhedron 26 (2007) 4107–4113.
15. K. Nakamoto, J. Fujitha, S. Tanaka, M. Kobayashi, J. Am. Chem. Soc. 79 (1957) 4904–4908.
16. K. Nakamoto, Infrared and Raman Spectra of Inorganic and Coordination Compounds, 5th ed., Wiley, New York, 1997.
17. T.A. Reena, E.B. Seena, M.R.P. Kurup, Polyhedron 27 (2008) 3461-3466.
18. A.A.A. Emara, B.A. El-Sayed, E.A.E. Ahmed, Spectrochim. Acta Part A 69 (2008) 757–769.

*****CRS*****

SYNTHESES AND CHARACTERIZATION OF Mo(VI) COMPLEXES DERIVED FROM ONO DONOR ACYLHYDRAZONES

7.1	Introduction
7.2	Experimental
7.3	Results and discussion
	References

7.1 Introduction

Recently molybdenum chemistry gained considerable attention due to their versatile applications in the field of catalysis and biology [1,2]. Among the second series of transition metals, molybdenum is the only biometal, important for living kingdom with a large number of stable and accessible oxidation states. The importance of molybdenum as a biological trace element depends on its contribution in various molybdoenzymes. The dioxomolybdenum complexes have been widely studied, as models for the active sites of oxotransfer molybdoenzymes like sulfite and aldehyde oxidase, xanthine oxidase, xanthine dehydrogenase and nitrate reductase [3-5]. In the catalytic activity of molybdoenzymes the oxidation state of molybdenum varies between VI and IV states and Mo(V) coexists with Mo(VI) and Mo(IV) [6]. The presence of cis-MoO₂²⁺ group in the oxidized form of some molybdoenzymes stimulate the search for new compounds in which this moiety is coordinated to ligands containing heteroatoms like O, N and S. The cofactors of these enzymes are most probably coordinatively unsaturated and this helps the easy binding of substrate. The study of molybdenum complexes with dianionic tridentate ligands are

particularly significant because, the coordination of cis-MoO_2^{2+} with dianionic tridentate ligand systems provides an open active site on molybdenum [7]. The catalytic activity of dioxomolybdenum complexes are proved by several reports [8,9]. Many reports are available for the studies of dioxomolybdenum complexes with O, N and S containing ligands [10-12].

7.2 Experimental

7.2.1 Materials

2-Hydroxy-4-methoxyacetophenone (Aldrich), 2-hydroxy-4-methoxybenzaldehyde (Aldrich), nicotinic acid hydrazide (Aldrich), benzhydrazide (Aldrich), $\text{MoO}_2(\text{acac})_2$ (Aldrich) were used without further purification. Solvent used was methanol.

7.2.2 Syntheses of acylhydrazones

The syntheses of 2-hydroxy-4-methoxybenzaldehyde nicotinoylhydrazone monohydrate ($\text{H}_2\text{hmbn}\cdot\text{H}_2\text{O}$), 2-hydroxy-4-methoxyacetophenone nicotinoylhydrazone (H_2hman), 2-hydroxy-4-methoxybenzaldehyde benzoylhydrazone (H_2hmbb) and 2-hydroxy-4-methoxyacetophenone benzoylhydrazone (H_2hmab) have been described in Chapter 2.

7.2.3 Syntheses of Mo(VI) complexes

$[\text{MoO}_2(\text{hmbn})]_2\cdot\text{H}_2\text{O}$ (30) : To a methanolic solution of $\text{H}_2\text{hmbn}\cdot\text{H}_2\text{O}$ (0.289 g, 1 mmol), $\text{MoO}_2(\text{acac})_2$ (0.326 g, 1 mmol) in methanol was added. The resulting orange color solution was refluxed for four hours. The orange colored product formed was filtered, washed with methanol, followed by ether and dried over P_4O_{10} *in vacuo*. Elemental Anal. Found (Calcd.) (%): C, 41.50 (41.40); H, 2.29 (2.98); N, 10.57 (10.34).

[MoO₂(hman)]₂·H₂O (31) : To the H₂hman solution in methanol (0.285 g, 1 mmol), methanolic solution of MoO₂(acac)₂ (0.326 g, 1 mmol) was added. The resulting solution has an orange color and it was refluxed for four hours. The orange colored product formed was filtered, washed with methanol, followed by ether and dried over P₄O₁₀ *in vacuo*. Elemental Anal. Found (Calcd.) (%): C, 42.85 (42.87); H, 3.20 (3.36); N, 10.17 (10.00).

[MoO₂(hmbb)]₂·H₂O (32) : To a methanolic solution of H₂hmbb (0.270 g, 1 mmol), MoO₂(acac)₂ (0.326 g, 1 mmol) in methanol was added. The solution turns to orange color and it was refluxed for four hours. The orange colored product formed was filtered, washed with methanol, followed by ether and dried over P₄O₁₀ *in vacuo*. Elemental Anal. Found (Calcd.) (%): C, 44.87 (44.46); H, 3.64 (3.23); N, 6.57 (6.91).

[MoO₂(hmab)]₂ (33) : Methanolic solutions of the H₂hmab (0.284 g, 1 mmol) and MoO₂(acac)₂ (0.326 g, 1 mmol) were mixed and refluxed for about 4 hours. The product separated was orange colored and it was filtered, washed with methanol, followed by ether and dried over P₄O₁₀ *in vacuo*. Elemental Anal. Found (Calcd.) (%): C, 46.14 (46.84); H, 3.32 (3.44); N, 6.86 (6.83).

7.3 Results and discussion

All the four complexes were synthesized in an identical way and in all of them hydrazones acts as a tridentate dianionic ONO donor towards MoO₂²⁺ centre. The experimental and calculated analytical data are in very close agreement. Magnetic susceptibility studies indicate diamagnetic nature of these complexes and it is an evidence for Mo is in +6 oxidation state. The molar conductivity values measured for all the four complexes in 10⁻³ M DMF solutions is in the range of 2-5 ohm⁻¹ cm² mol⁻¹ which is much less than the value of 65-90 ohm⁻¹ cm² mol⁻¹ reported for a 1:1 electrolyte in the same solvent [13]. So the

conductance measurements in DMF suggest that they are non-electrolytes. The magnetic susceptibility and molar conductivity values of the complexes are presented in Table 7.1.

The electrochemical behavior of the complexes and free hydrazones were studied in DMF by cyclic voltammetry on a CHI 608D electrochemical analyzer with platinum disc as working electrode. The counter electrode used was platinum wire and reference electrode Ag/Ag⁺ electrode. The supporting electrolyte used was tetrabutylammonium phosphate (TBAP). The cyclic voltammograms of the complexes did not show any redox properties. Reversible one electron reduction of [MoO₂]²⁺ complexes to analogous [MoO₂]⁺ complexes is uncommon and occurs only when aprotic ligands and solvents are used and when the ligand has sufficient steric bulk to prevent dimerization [14]. So the absence of redox behavior is an evidence for the dimeric nature of the compounds.

Table 7.1. Molar conductivity measurements

Compound	$\lambda_m^{\#}$
[MoO ₂ (hmbn)] ₂ ·H ₂ O (30)	3
[MoO ₂ (hman)] ₂ ·H ₂ O (31)	4
[MoO ₂ (hmbb)] ₂ ·H ₂ O (32)	5
[MoO ₂ (hmab)] ₂ (33)	5

[#]molar conductivity (in mho cm² mol⁻¹) taken in 10⁻³ M DMF

7.3.1 ¹H NMR spectral studies

In the case of diamagnetic Mo(VI) complexes the coordination of acylhydrazones to the metal centre is substantiated by ¹H NMR spectral studies of the ligands and complexes, in DMSO solution. Singlets found in the region 12-14 ppm due to iminol protons in free hydrazones were not found in the spectra of complexes indicate the coordination of iminol oxygen to metal centre. Similarly

singlets due to OH proton were found in-between 11 ppm and 12 ppm in free hydrazones were also absent in the spectra of complexes indicate the coordination of phenolic oxygen to metal centre. This leads to the conclusion that the hydrazones are coordinated in all the complexes in a dianionic form suggesting the ONO coordination to molybdenum. The singlets with an area integral of three in the range of 3-3.8 ppm indicate the presence of three methoxy hydrogens in free acylhydrazones were slightly shifted upon complexation. Multiplets for aromatic protons were found in the region 6-8 ppm in ligands do not show much shift in complexes. The ^1H NMR spectra of the complexes are shown in the Figs 7.1-7.4.

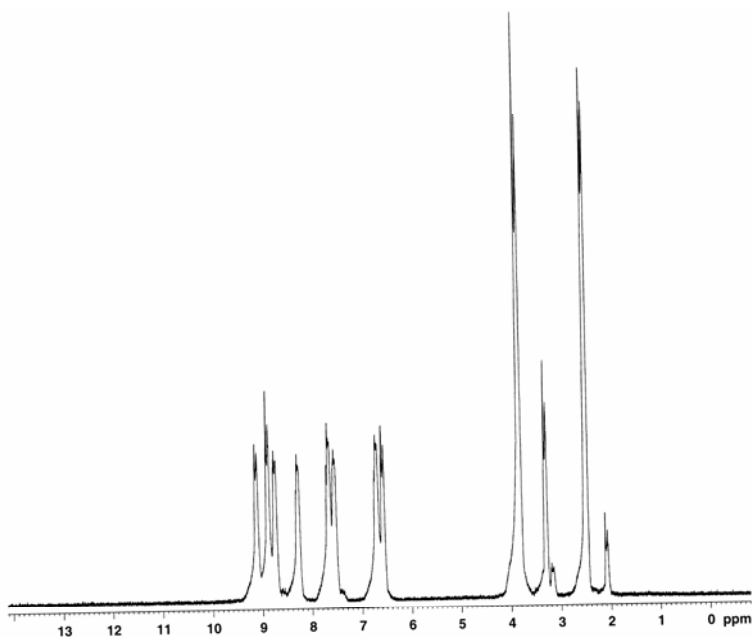


Fig. 7.1. ^1H NMR spectrum of $[\text{MoO}_2(\text{hmbn})]_2 \cdot \text{H}_2\text{O}$.

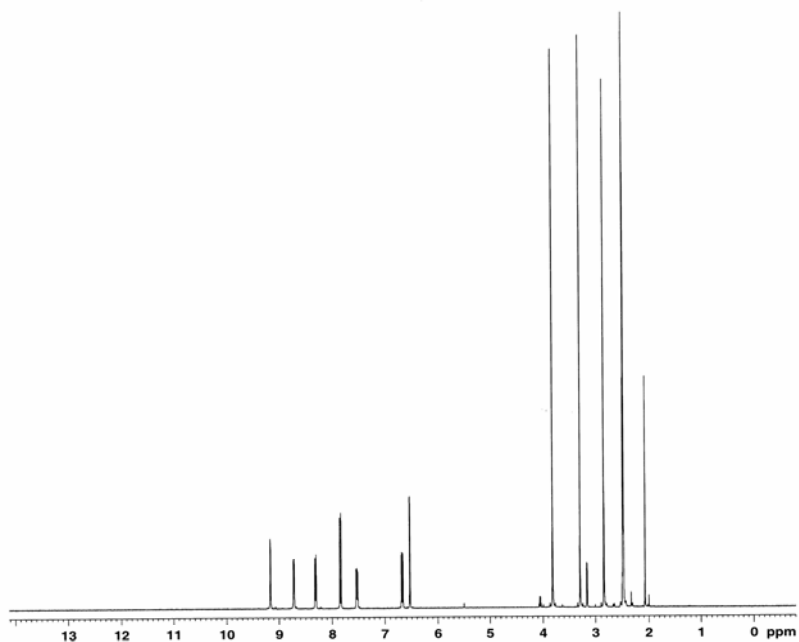


Fig. 7.2. ^1H NMR spectrum of $[\text{MoO}_2(\text{hman})]_2 \cdot \text{H}_2\text{O}$.

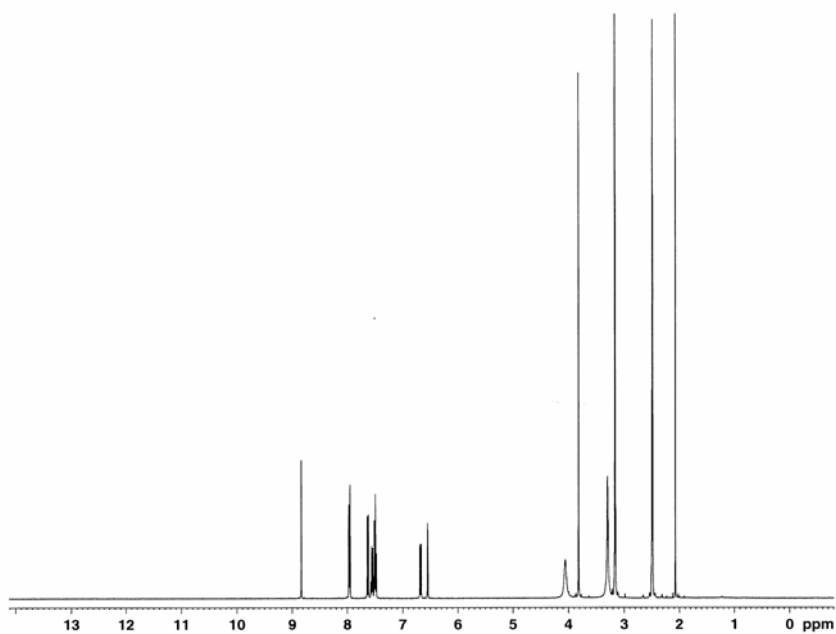


Fig. 7.3. ^1H NMR spectrum of $[\text{MoO}_2(\text{hmbb})]_2 \cdot \text{H}_2\text{O}$.

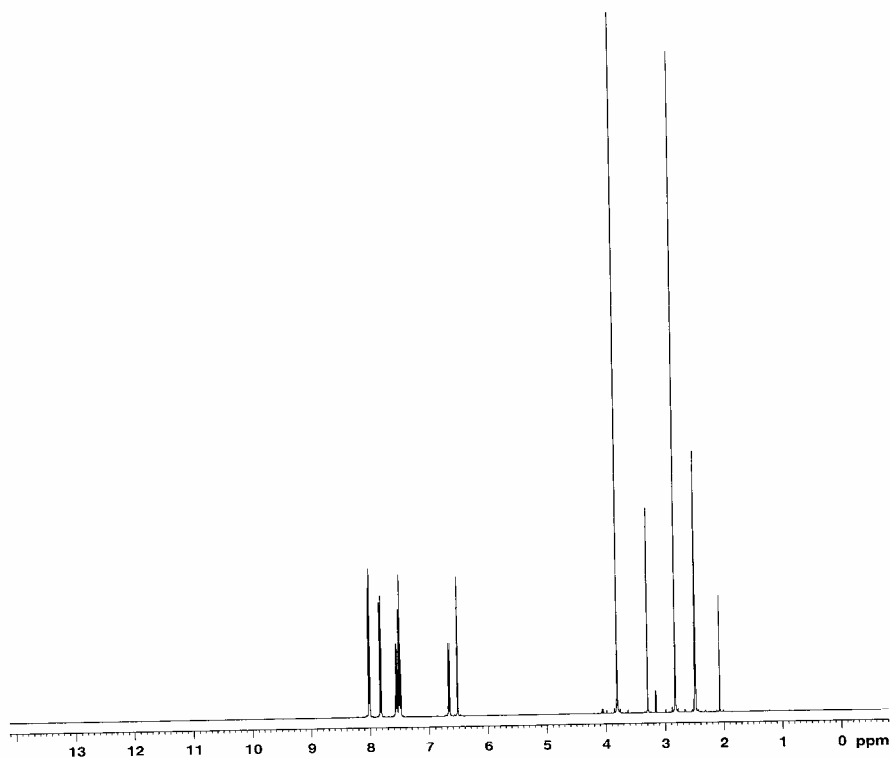


Fig. 7.4. ^1H NMR spectrum of $[\text{MoO}_2(\text{hmab})]_2$.

7.3.2 Infrared spectral studies

The most interesting vibrational frequencies of acyl hydrazones and their molybdenum complexes, which help us to understand the coordination environment of the metal in these complexes, are given in Table 7.2. In the IR spectra of the free hydrazones, the bands due to carbonyl group are observed in the region $1630\text{--}1650\text{ cm}^{-1}$ and these are absent in the spectra of the complexes suggesting enolization and deprotonation of ligands. This is also confirmed from the fact that the O–H and N–H stretching frequencies observed around 3220 and

3035 cm^{-1} in free hydrazones are absent in complexes. Another result obtained from this is that the ligands are coordinated in a dianionic form in these complexes. IR spectra of compounds **30**, **31** and **32**, there are broad bands observed at 3424, 3445 and 3438 cm^{-1} indicating the presence of lattice water. The azomethine bands of the acylhydrazones were appeared at 1600-1605 cm^{-1} and in the spectra of the complexes these bands are shifted to a lower frequency by 4-15 cm^{-1} indicating the coordination of azomethine nitrogen to the metal. The increase in $\nu(\text{N-N})$ bands in complexes, due to the increase in double bond character is another proof for the coordination of the ligands through the azomethine nitrogen. The $\nu(\text{C-O})$ bands present in ligands are shifted to lower frequency in complexes suggests the coordination of the phenolic oxygen. In all complexes two bands are observed in the region 900-950 cm^{-1} , are assigned to symmetric and antisymmetric vibrations of the *cis*- MoO_2^{2+} core [15]. Reports show that structurally characterized dimeric dioxomolybdenum(VI) tridentate complexes have sharp bands in the region 800-850 cm^{-1} [16,17]. Here all the complexes have a band in the above said region indicates the presence of dimeric dioxomolybdenum complexes. IR spectra of compounds are shown in Figs. 7.5-7.8.

Table 7.2 Selected IR bands (cm^{-1}) with tentative assignments of Mo(VI) complexes

Compound	$\nu(\text{C=N})$	$\nu(\text{C=N})^a$	$\nu(\text{N-N})$	$\nu(\text{C-O})$	$\nu(\text{Mo=O})$	$\nu(\text{Mo=O-Mo})$
$[\text{MoO}_2(\text{hmbn})_2 \cdot \text{H}_2\text{O}$ (30)	1589	1540	1129	1225	903, 937	833
$[\text{MoO}_2(\text{hman})_2 \cdot \text{H}_2\text{O}$ (31)	1593	1532	1140	1249	913, 942	854
$[\text{MoO}_2(\text{hmbb})_2 \cdot \text{H}_2\text{O}$ (32)	1596	1535	1138	1230	910, 930	850
$[\text{MoO}_2(\text{hmab})_2$ (33)	1597	1549	1156	1290	913, 942	854

^a newly formed

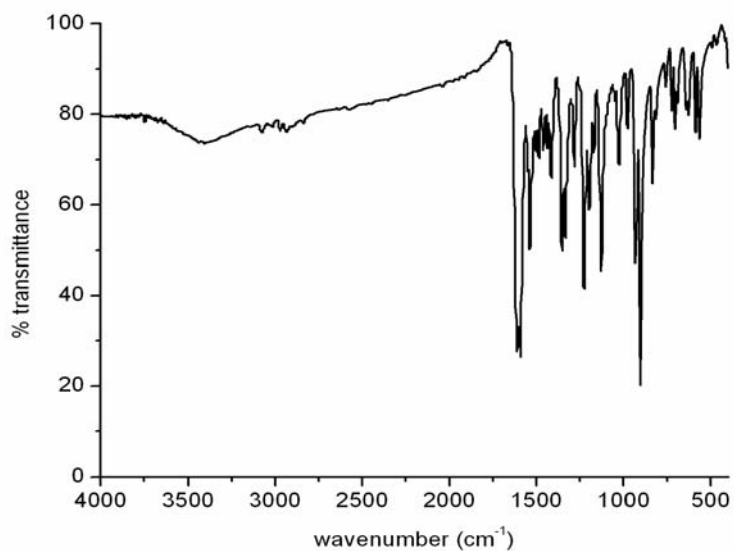


Fig. 7.5. IR spectrum of $[\text{MoO}_2(\text{hmbn})]_2 \cdot \text{H}_2\text{O}$.

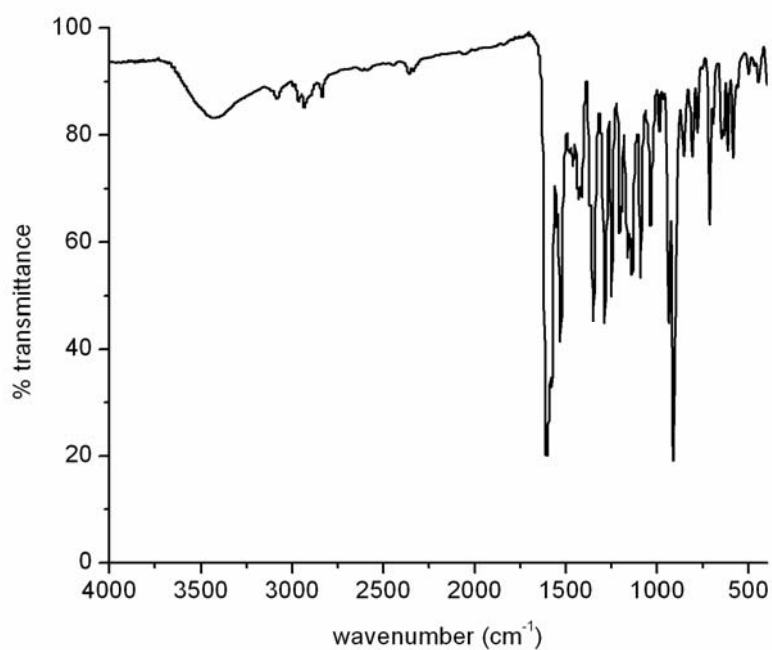


Fig. 7.6. IR spectrum of $[\text{MoO}_2(\text{hman})]_2 \cdot \text{H}_2\text{O}$.

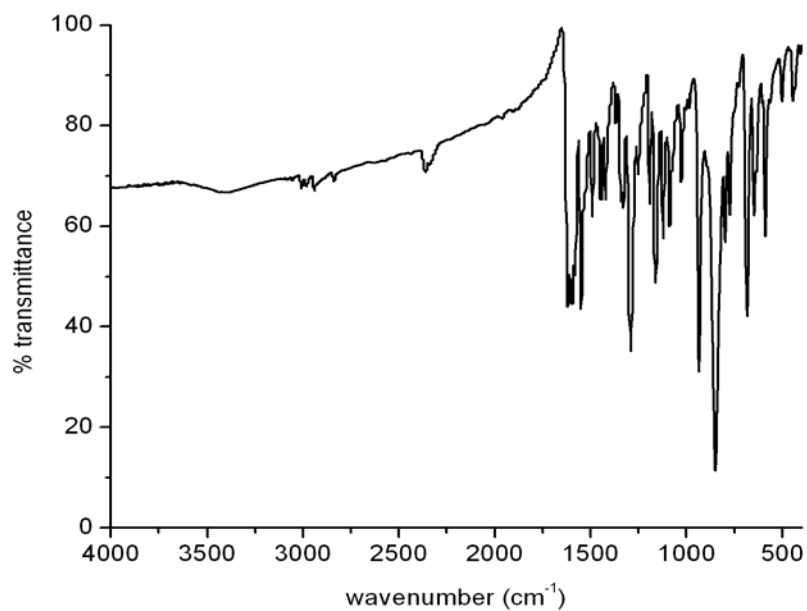


Fig. 7.7. IR spectrum of $[\text{MoO}_2(\text{hmbb})]_2 \cdot \text{H}_2\text{O}$.

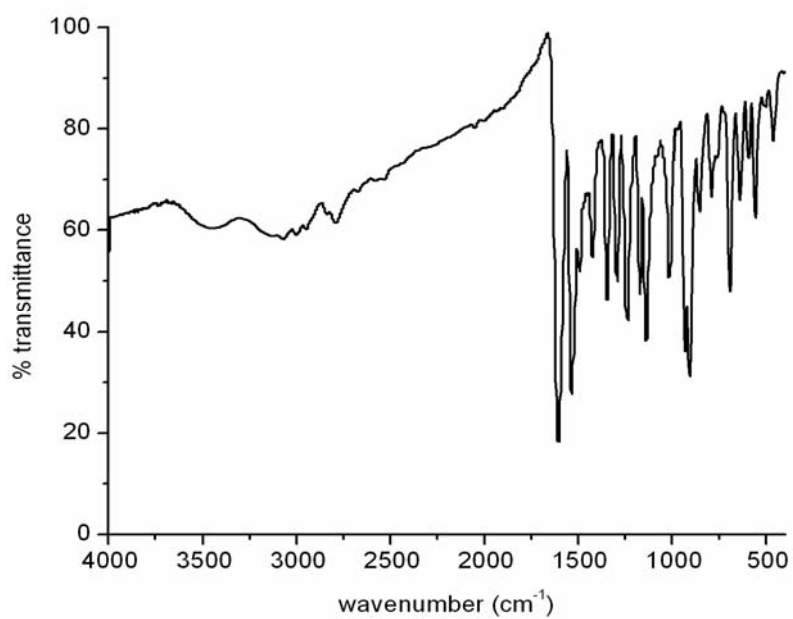


Fig. 7.8. IR spectrum of $[\text{MoO}_2(\text{hmab})]_2$.

7.3.3 Electronic spectral studies

The electronic spectra of all the four acylhydrazones showed bands in the region 30400-46000 cm^{-1} due to $\pi-\pi^*$ transitions. The $n-\pi^*$ transitions that are forbidden by the selection rules are not observed in these compounds. In the electronic spectra of complexes these transitions are slightly shifted. The complexes show strong bands *ca.* 24000 cm^{-1} and are assigned as ligand to metal charge transfer transitions. Electronic spectra of the complexes are presented in Fig. 7.9 and the assignments are listed in Table 7.3.

Table 7.3 Electronic spectral assignments (cm^{-1}) of Mo(VI) complexes

Compound	Intraligand transitions	Charge transfer transition
$[\text{MoO}_2(\text{hmbn})]_2 \cdot \text{H}_2\text{O}$ (30)	31360, 40910	24230
$[\text{MoO}_2(\text{hman})]_2 \cdot \text{H}_2\text{O}$ (31)	31580, 39600, 42840	24150
$[\text{MoO}_2(\text{hmbb})]_2 \cdot \text{H}_2\text{O}$ (32)	31640, 39740, 42830	24230
$[\text{MoO}_2(\text{hmab})]_2$ (33)	31640, 40360, 42550	24970

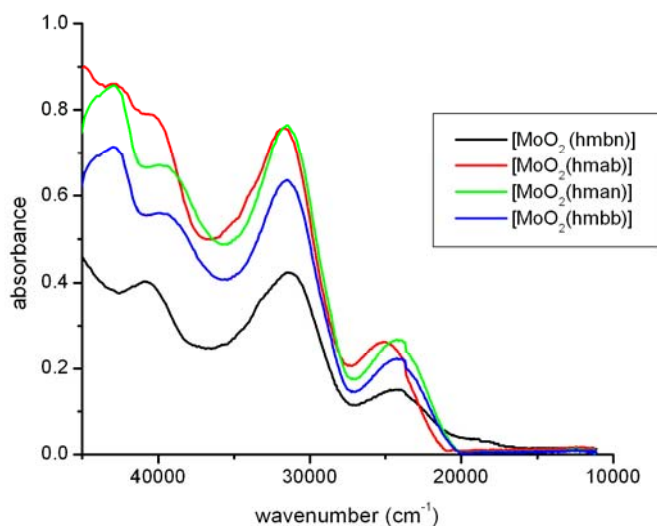


Fig. 7.9. Electronic spectra of the Mo(VI) complexes.

7.3.4 Thermal studies

TG-DTG analyses of the prepared complexes were carried out on a Perkin Elmer, Diamond thermogravimetric analyzer. The heat flow is 10 °C per minute under nitrogen atmosphere over a temperature range of 50-1000 °C. The thermal analyses give information concerning the thermal stability and nature of water molecules in complexes *ie.* whether they are lattice water or coordinated water. Reports show that the weight losses for lattice water are in the range of 50-130 °C [18,19]. The complexes **30**, **31** and **32** showed loss of weight corresponds to one water molecule in the temperature range 80-110 °C indicate the presence of lattice water in these complexes. In complex **33**, there is no weight loss in the region below 250 °C shows the absence of water molecule. All the complexes decompose over 250 °C. TG-DTG curves of the complexes are shown in Figs. 7.10-7.13.

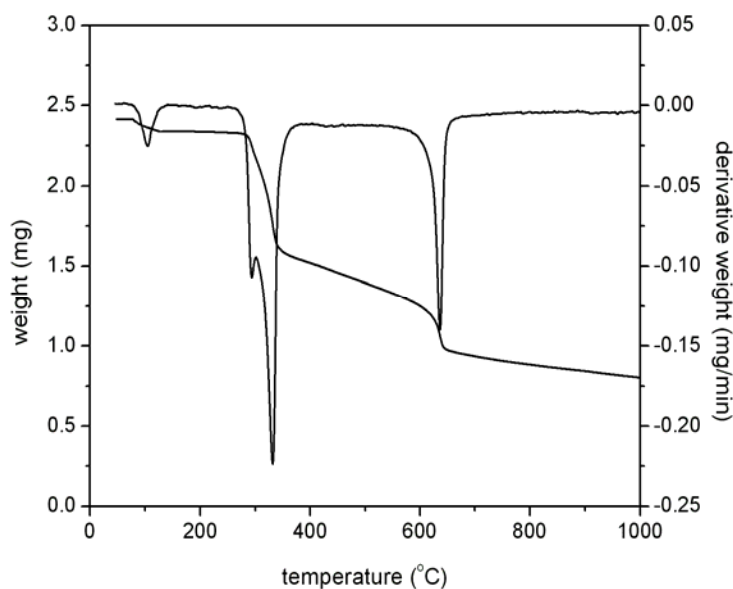


Fig. 7.10. TG-DTG plots of [MoO₂(hmbn)]₂·H₂O (**30**).

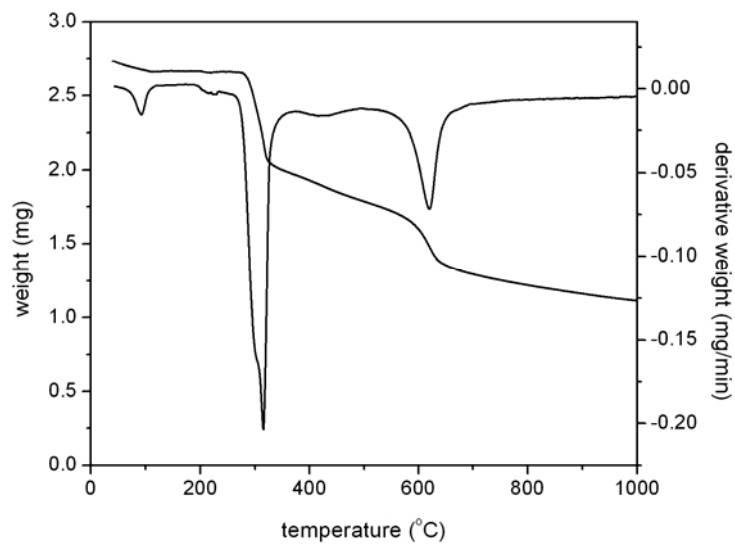


Fig. 7.11. TG-DTG plots of $[\text{MoO}_2(\text{hman})]_2 \cdot \text{H}_2\text{O}$ (31).

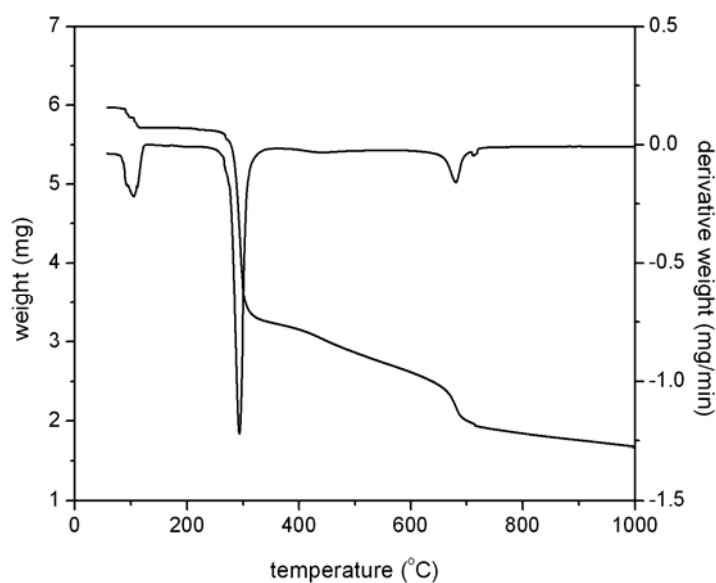


Fig. 7.12. TG-DTG plots of $[\text{MoO}_2(\text{hmbb})]_2 \cdot \text{H}_2\text{O}$ (32).

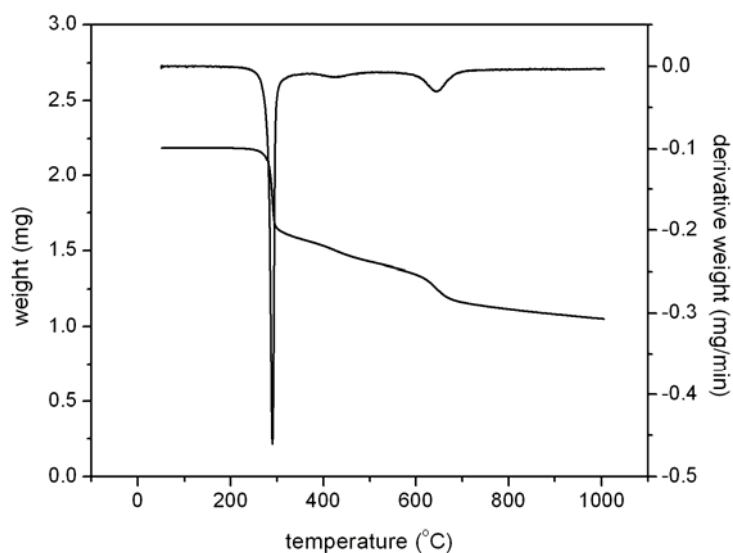


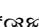
Fig. 7.13. TG-DTG plots of $[\text{MoO}_2(\text{hmab})]_2$ (33).

References

1. D. Eierhoff, W.C. Tung, A. Hammerschmidt, B. Krebs, *Inorg. Chim. Acta* 362 (2009) 915-928.
2. M. Bagherzadeh, R. Latifi, L. Tahsini, V. Amani, A. Ellern, L.K. Woo, *Polyhedron* 28 (2009) 2517-2521.
3. R.C. Bray, *Quart. Rev. Biophys.* 21 (1988) 299-329.
4. J.P.G. Malthouse, R.C. Bray, *Biochem. J.* 191 (1980) 265-267.
5. R.H. Holm, *Chem. Rev.* 87 (1987) 1401-1449.
6. S. Gupta, A.K. Barik, S. Pal, A. Hazra, S. Roy, R.J. Butcher, S.K. Kar, *Polyhedron* 26 (2007) 133-141.

*Syntheses and characterization of Mo(VI) complexes derived from
ONO donor acylhydrazones*

7. K. Andjelković, M. Šumar and I. Ivanović-Burmazović, J. Therm. Anal. Cal. 66 (2001) 759-778.
8. M. Mancka, W. Plass, Inorg. Chem. Commu. 10 (2007) 677-680.
9. Y. Sui, X. Zeng, X. Fang, X. Fu, Y. Xiao, L. Chen, M. Li, S. Cheng, J. Mol. Cat. A: Chem. 270 (2007) 61-67.
10. V. Vrdoljak, J. Pisk, B. Prugovečki, D.M. Čalogović, Inorg. Chim. Acta 362 (2009) 4059-4064.
11. M. Cindrić, V. Vrdoljak, N. Strukan, B. Kamenar, Polyhedron 24 (2005) 369-376.
12. S.N. Rao, K.N. Munshi, N.N. Rao, M.M. Bhadbhade, E. Suresh, Polyhedron 18 (1999) 2491-2497.
13. W.J. Geary, Coord. Chem. Rev. 7 (1971) 81-122.
14. S.A. Roberts, C.G. Young, C.A. Kipke, W.E. Cleland, K. Yamanouchi, M.D. Carducci, J.H. Enemark, Inorg. Chem 29 (1990) 3650-3656.
15. K. Nakamoto, Infrared and Raman Spectra of Inorganic and Coordination Compounds, 5th ed., Wiley, New York, 1997.
16. E.B. Seenaa, M.R.P. Kurup, Polyhedron 26 (2007) 3595–3601.
17. R.A. Lal, D. Basumatary, S. Adhikari, A. Kumar, Spectrochim. Acta Part A 69 (2008) 706–714.
18. M.R. Maurya, N. Bharti, Trans. Met. Chem. 24 (1999) 389-393.
19. S.M. Abdallah, G.G. Mohamed, M.A. Zayed, M.S. Abou El-Ela, Spectrochim. Acta Part A 73 (2009) 833–840.

**********



SUMMARY AND CONCLUSIONS

The study of the synthesis, structures and properties of transition metal complexes is a key line of research in modern coordination chemistry. Hydrazones are an interesting class of ligands in coordination chemistry, and they are obtained by the condensation reaction between a carbonyl compound and a hydrazide. Their coordination capability and binding modes can be altered by the use of suitable substituents both in the carbonyl and hydrazide part. Acting as ligands they easily form mono, bi and polynuclear coordination compounds. The metal complexes derived from hydrazones find applications in many areas such as medicine, biology, catalysis, optics and analytical chemistry. Hence, the knowledge of characteristics of deprotonation, tautomerization and complexation in solution as well as the structural details of coordination with metal ions in solid state is fundamental for forecasting the properties of this class of azomethine compounds.

To explore the coordination properties of acylhydrazones, in this work we have synthesized four different acylhydrazones by the condensation of *o*-hydroxy aromatic aldehyde and ketone with benzhydrazide and nicotinic acid hydrazide. The thesis is divided into seven chapters and **Chapter 1** gives an introduction to acylhydrazones, their mode of bonding in complexes and applications in different areas. The objectives of the present work and the details of different analytical techniques used for characterization are also presented in this chapter. **Chapter 2**

deals with the syntheses and characterization of four different acylhydrazones and they are

1. 2-Hydroxy-4-methoxybenzaldehyde nicotinoylhydrazone monohydrate (**H₂hmbn·H₂O**)
2. 2-Hydroxy-4-methoxyacetophenone nicotinoylhydrazone (**H₂hman**)
3. 2-Hydroxy-4-methoxybenzaldehyde benzoylhydrazone (**H₂hmbb**)
4. 2-Hydroxy-4-methoxyacetophenone benzoylhydrazone (**H₂hmab**).

The acylhydrazones were characterized by elemental analyses, FTIR, ¹H NMR and UV–Vis spectral studies. Single crystal X-ray diffraction studies of one of the hydrazones H₂hmbn·H₂O revealed that the compound is non planar and exist in amido form in solid state. The novelty about this crystal lies in the packing; three molecules are involved in intermolecular hydrogen bonding interactions with one water molecule. The ¹H NMR studies indicate the enolization of these compounds in solution state.

Chapter 3 describes the syntheses and structural characterization of twelve oxovanadium complexes of acylhydrazones. Magnetic susceptibility measurements clearly indicate that, all the compounds except one, are paramagnetic compounds with vanadium is in +4 oxidation state. Some compounds exhibit subnormal magnetic moments due to the strong antiferromagnetic exchange, suggesting dimeric nature to these complexes. The molar conductivity values for all the complexes in 10⁻³ M DMF solution are found to be less than the value of 65-90 ohm⁻¹ cm² mol⁻¹ obtained for a 1:1 electrolyte in the same solvent confirmed the non-electrolytic nature of the complexes. IR spectroscopy gives evidence for the coordination of hydrazones to the metal centre in enolic form and hence act as dideprotonated tridentate ligands. EPR spectra of the compounds in DMF at 77 K displayed axial features with eight

hyperfine splitting and in all complexes except one follows the $g_{\parallel} < g_{\perp}$ and $A_{\parallel} > A_{\perp}$ relationship, is characteristic of an axially compressed d_{xy}^1 configuration. One of the oxovanadium compound is crystallized from methanol and single crystal X-ray diffraction studies showed that the compound is a centrosymmetric bis(μ -methoxy) bridged vanadium(V) dimeric complex.

Chapter 4 depicts the syntheses and characterization of some manganese and iron complexes of acylhydrazones. Two manganese and five iron complexes were prepared by refluxing 1:1 mixture of metal salt and corresponding acylhydrazones in methanol/ethanol for about 4-6 hours. The prepared complexes were characterized by elemental analyses, IR, electronic and EPR spectral studies, thermogravimetric analyses, conductance and magnetic susceptibility measurements. The non-electrolytic nature of the complexes is evident from their low conductivity values. Magnetic susceptibility measurements suggest that all the compounds are paramagnetic with central metal atom has a d^5 high spin configuration. Infrared spectral data suggest that the ligands are coordinated in amido form in complexes. In the EPR spectra of manganese complexes only one sextet is observed due to electron spin-nuclear spin coupling and the g values are close to the g value of a free electron. And the values of hyperfine coupling constants are consistent with an octahedral environment. Single crystals of one of the iron complexes were isolated from ethanol and it is found that in the compound iron is in a distorted octahedral environment.

Chapter 5 deals with the syntheses of six Cu(II) complexes and their characterization by different physicochemical techniques. The magnetic susceptibility measurements suggest that the compounds are paramagnetic and in close agreement with the spin only value for a d^9 copper system. Some complexes show substantial low magnetic moment may be due to the coupling of two magnetic centers suggesting dimeric nature to these complexes. In the IR spectra

of the free ligands, the carbonyl and azomethine bands are observed in the region 1630-1650 cm^{-1} and 1600-1605 cm^{-1} respectively. In the infrared spectra of the all six complexes there are no bands due to carbonyl group. Upon complexation, the stretching vibrations of azomethine bond are found to be weakened due to coordination with copper centre, *ie.* the ligands were coordinated in iminol form. In the electronic spectra of the complexes weak *d-d* bands are observed. EPR spectra of the complexes were taken in polycrystalline state at 298 K, DMF at 298 K and 77 K. The *g* value obtained from EPR spectral assignments are consistent with the single unpaired electron is in the $d_{x^2-y^2}$ orbital. Single crystals of one of the complexes are separated from methanol and the X-ray diffraction studies showed that in the compound, Cu is in a distorted square pyramidal environment. Packing of the compound is stabilized by strong π - π stacking interactions. In addition to the π - π stacking interactions, significant C-H \cdots π interactions and hydrogen bonding are also present.

Chapter 6 describes the syntheses and characterization of four zinc complexes. All the complexes are non-electrolytic as well as diamagnetic compounds. In all the complexes except one, ligands are coordinated in the iminol form.

Chapter 7 explains the syntheses and characterization four dioxomolybdenum complexes. The ^1H NMR and IR spectral data indicate tridentate nature of the ligands through enolization. IR spectra provide information about the dimeric nature of the complexes. The thermal analyses of the complexes showed the presence of lattice water in some of the complexes.

««« Curriculam vitae »»»

Nancy Mathew

Thompikkottu
Nellimattom P.O.
Kothamangalam
Ernakulam-686693
KERALA, INDIA

Email: nancymathew1@gmail.com
nancymathew@cusat.ac.in

Areas of Interest: Teaching and Research

Academic Profile

Pursuing Ph.D. (Inorganic Chemistry)
(2007-present)
Area of research – Coordination Chemistry
Supervising guide – Prof. M.R. Prathapachandra Kurup
Department of Applied Chemistry.
Cochin University of Science & Technology, Kochi

M.Sc. (2001-2003)
Newman College , Thodupuzha
University - Mahatma Gandhi University, Kerala.
Percentage of marks – 75.3%

B.Sc. (1998- 2001)
M.A. College , Kothamangalam
University - Mahatma Gandhi University, Kerala.
Percentage of marks – 79.2%

Pre-Degree (1996- 1998)
M.A. College , Kothamangalam
University - Mahatma Gandhi University, Kerala.
Percentage of marks – 72%

S.S.L.C (1996)
Govt. High School Ayyankavu, Ernakulam, Kerala
Percentage of marks – 86%

Achievements

1. Qualified CSIR-UGC Lectureship NET - 2003 December
2. Qualified CSIR-UGC JRF - 2007 December

Research Experience

- More than four years of research experience in the field of coordination chemistry

Teaching Experience

- October 2004 - August 2006
Organization: Department of Chemistry, Sacred Heart College, Thevara
Designation: FIP substitute lecturer

Professional Skills

- Familiar with MS Office
- Familiar with chemistry software packages like Chemsketch, Origin, EPR simulation packages
- Familiar with crystallographic softwares
- Experienced in using instruments like UV-Vis spectrometer, FTIR spectrometer, Thermogravimetric analyzer, Gouy balance etc.

Personal Profile

Father's name : Mathew T.J.
Husband's name : Eldhose K.V.
Date of Birth : 11th February 1981
Nationality : Indian
Gender : Female
Marital Status : Married

Papers published/communicated

1. 2'-(2-Hydroxy-4-methoxybenzylidene)nicotinohydrazide monohydrate, Nancy Mathew, Mini Kuriakose, E.B. Seena, M.R.P. Kurup, Acta Cryst. E 63 (2007) 2190
2. Synthesis, spectral and EPR studies of oxovanadium(IV) complexes incorporating tridentate ONO donor hydrazone ligands: Structural study of one oxovanadium(V) complex, E. B. Seena, Nancy Mathew, Mini Kuriakose, M.R.P. Kurup, Polyhedron 27 (2008) 1455.
3. Synthesis and characterization of Mo(VI) complexes derived from ONO donor acylhydrazones, Nancy Mathew, M.R.P. Kurup, Spectrochim. Acta A 78 (2011) 1424.
4. Spectral studies of copper(II) complexes of tridentate hydrazone ligands with heterocyclic compounds as coligands: Structure of one copper(II) complex, Nancy Mathew, M. Sithambaresan, M.R.P. Kurup, Spectrochim. Acta A, *in press*.

Papers presented in symposia

1. Participated and presented a poster in the National Conference “MTIC-XII” held at IIT Madras, Chennai during 6-8 December 2007.
2. Participated and presented a paper in the National Conference “CTriC-2008” held at the Department of Applied Chemistry, Cochin University of Science and Technology, Kochi during 18-19 January 2008.